



TECHNISCHE  
UNIVERSITÄT  
WIEN

## DISSERTATION

# Undular hydraulic jumps in plane and axisymmetric free-surface flows

carried out for the purpose of obtaining the degree of  
Doctor technicae (Dr.techn.),  
submitted at TU Wien, Faculty of Mechanical and Industrial Engineering, by

**Dominik MURSCHENHOFER**

Mat.no.: 00927263

under the supervision of  
Dr.techn. Dr.h.c. Wilhelm SCHNEIDER  
Em.O.Univ.Prof.  
Institute of Fluid Mechanics and Heat Transfer, E322

reviewed by

Dr. Robert I. BOWLES	Dr.techn. Herbert STEINRÜCK
Senior Lecturer	Ao.Univ.Prof.
Department of Mathematics, University College London	Institute of Fluid Mechanics and Heat Transfer, TU Wien
Gower Street, London WC1E 6BT, United Kingdom	Getreidemarkt 9, 1060 Vienna, Austria

This work was financially supported by AIC Androsch International Management Consulting GmbH.

I confirm that printing this thesis needs the confirmation of the examination committee.

### *Affidavit*

I declare in lieu of an oath that I wrote this thesis and performed the associated research myself, using only literature cited in this volume. If text passages from sources are used literally, they are marked as such.

I confirm that this work is original and has neither been submitted elsewhere for any examination, nor is it currently under consideration for a thesis elsewhere.

Vienna, April 2021

---

*Dominik Murschenhofer*

A PERSON WHO NEVER MADE A MISTAKE  
NEVER TRIED ANYTHING NEW.

Albert Einstein

# Acknowledgements

First and foremost, I should like to thank Prof. Wilhelm Schneider for his excellent supervision and guidance. His persistent constructive criticism in numerous discussions eventually led to the thesis in its present form. Besides our scientific debates, also our non-scientific conversations were always enormously enriching.

I would also like to thank Dr. Robert I. Bowles and Ao.Prof. Herbert Steinrück for agreeing to act as referees of this thesis. Moreover, Ao.Prof. Herbert Steinrück was always available to answer questions concerning his previous work on undular jumps.

Prof. Hendrik Kuhlmann's weekly seminar provided a great forum to present my thesis's progress once per semester. After one of my presentations, he suggested analysing undular jumps in axisymmetric sink flow, which ultimately led to a whole chapter in this thesis. In stimulating discussions, Priv.-Doz. Bernhard Scheichl brought alternative perspectives to my investigations and drew my attention to valuable literature. As a trained mathematician, Dr. Pierre-Emmanuel des Boscès was always willing to answer questions regarding numerical methods. I am indebted to my colleague and friend Dipl.-Ing. Dominik Kuzdas for encouraging me during times of lacking motivation and countless fruitful discussions about nearly every topic of this thesis.

My predecessor, Dr. Richard Jurisits, kindly shared his knowledge about undular hydraulic jumps in many helpful conversations. I also gratefully acknowledge that Prof. Youichi Yasuda and Prof. Hiroshi Gotoh, both from Nihon University, Japan, provided important information about previously conducted undular jump experiments.

Special thanks go to my parents Sigrid and Michael, and my sister Sonja, who always supported, encouraged and believed in me. Only with the backing of my family, I could come this far.

Thanks to the financial support of AIC Androsch International Management Consulting GmbH, I was able to experience three and a half incredibly inspiring years.

# Kurzfassung

Eine stationäre, turbulente Strömung mit freier Oberfläche bei großen Reynolds-Zahlen und Froude-Zahlen nahe dem kritischen Wert 1 wird betrachtet. Die spezielle Koppelung der beiden Grenzübergänge erlaubt eine Analyse frei von Turbulenzmodellierung.

Im ersten Teil der Dissertation werden wellige Wassersprünge in offener Kanalströmung über horizontalem Boden mittels der Methode der mehrfachen Variablen, angewendet auf die Reynolds-Gleichungen, untersucht. Die Lösung beschreibt die Störung erster Ordnung der freien Oberfläche. Der Vergleich der freien Oberflächenstörung mit der Lösung einer erweiterten stationären Version der Korteweg–de Vries (KdV)-Gleichung bestätigt deren gleichmäßige Gültigkeit. Außerdem wird der Grenzübergang verschwindender Bodenneigung bei fixierter Froude- und Reynolds-Zahl betrachtet. Die resultierende erweiterte KdV-Gleichung wird als Anfangswert- sowie als Zweipunkt-Randwertproblem gelöst. Letzteres entspricht dem Übergang zu voll-ausgebildeter Strömung weit stromab. Der Vergleich mit Experimenten zeigt passable Übereinstimmung.

Im zweiten Teil werden wellige Wassersprünge in turbulenter achsensymmetrischer Strömung mit freier Oberfläche über horizontalem Boden untersucht. Die Oberflächenauslenkung wird durch eine neue Version der erweiterten KdV-Gleichung beschrieben, welche unter der Voraussetzung großer Sprungradien als gleichmäßig gültige Differenzialgleichung hergeleitet wurde. Die Gleichung gilt sowohl für Quell- als auch für Senkenströmung. In beiden Fällen liefert die numerische Lösung der Gleichung als Anfangswertproblem wellige Sprünge. Weit stromab des Sprunges führt jedoch Reibung zum Absturz der Lösung. Die Betrachtung reibungsfreier Quellströmung zeigt, dass wellige Wassersprünge bei großen Radien existieren und erneut durch eine erweiterte KdV-Gleichung beschrieben werden. Verglichen zu turbulenter Strömung ist die Gültigkeit der Lösungen auf einen kleinen Bereich nahe dem Beginn des Sprunges begrenzt. Wellige Wassersprünge in reibungsfreier Senkenströmung sind nicht möglich.

# Abstract

Steady turbulent free-surface flow in the limit of very large Reynolds numbers and Froude numbers close to the critical value 1 is considered. A specific coupling of the two limiting processes assures an analysis free of turbulence modelling.

In part one of the thesis, undular hydraulic jumps in open-channel flow with a horizontal bottom are investigated employing a multiple-scales analysis of the Reynolds equations. The multiple-scales solution describing the first-order perturbation of the free-surface elevation is compared with the numerical solution of an extended steady-state version of the Korteweg–de Vries (KdV) equation, confirming the uniform validity of this non-linear third-order ODE. Furthermore, the limiting process of a vanishing bottom slope is analysed by keeping the Froude and Reynolds numbers fixed. The resulting extended KdV equation is solved as both initial value and two-point boundary-value problem, the latter representing the transition to fully developed flow far downstream. Comparing the theory with experimental data shows reasonable agreement.

In part two, undular hydraulic jumps in turbulent axisymmetric free-surface flow over a horizontal bottom are studied. Provided the jump's origin is located at very large radii, the free surface is described by a new version of an extended KdV equation, derived as a uniformly valid differential equation. The same equation is valid for both turbulent source and sink flow. In both cases, undular solutions of the extended KdV equation are obtained from numerically solving the equation as an initial value problem. However, far downstream of the jump, friction enforces a breakdown of the solutions. By considering inviscid axisymmetric source flow, undular jumps are shown to be possible at large radii, and the surface is described by another version of an extended KdV equation. Compared to turbulent flow, the solution's validity is limited to moderate distances from the origin of the jump. Undular hydraulic jumps in inviscid sink flow are not possible.

# Contents

<b>Acknowledgements</b>	<b>iv</b>
<b>Kurzfassung</b>	<b>v</b>
<b>Abstract</b>	<b>vi</b>
<b>Nomenclature</b>	<b>x</b>
<b>I Undular hydraulic jumps in open-channel flow</b>	<b>1</b>
<b>1 Introduction</b>	<b>2</b>
<b>2 Horizontal bottom</b>	<b>4</b>
2.1 Problem formulation . . . . .	4
2.2 Multiple-scales analysis . . . . .	7
2.3 Uniformly valid differential equation . . . . .	11
2.4 Results and discussion . . . . .	13
2.4.1 Comparison between solutions of the multiple-scales analysis and the extended KdV equation . . . . .	13
2.4.2 Comparison with the theory of inclined bottoms . . . . .	15
2.4.3 Comparison with experimental data . . . . .	16
<b>3 The limiting process of vanishing bottom slope</b>	<b>20</b>
3.1 Problem formulation . . . . .	20
3.2 Asymptotic analysis . . . . .	21
3.3 Hydraulic approximation . . . . .	23

3.4	Results and discussion . . . . .	24
3.4.1	Numerical solutions of the extended KdV equation in the limit of vanishing bottom slope . . . . .	24
3.4.2	Transition to fully developed flow far downstream . . . . .	25
3.4.3	Comparison with experimental data . . . . .	29
<b>4</b>	<b>Conclusions of Part I</b>	<b>32</b>
<b>II</b>	<b>Undular hydraulic jumps in axisymmetric flow</b>	<b>34</b>
<b>5</b>	<b>Introduction</b>	<b>35</b>
<b>6</b>	<b>Hydraulic approximation</b>	<b>39</b>
6.1	Inviscid flow . . . . .	40
6.2	Constant friction coefficient . . . . .	41
6.3	Variable friction coefficient . . . . .	44
<b>7</b>	<b>Near-critical inviscid axisymmetric source flow</b>	<b>47</b>
7.1	Problem formulation . . . . .	47
7.2	Asymptotic analysis . . . . .	49
7.3	Results and discussion . . . . .	51
7.3.1	Undular jumps at a reference radius of $O(\varepsilon^{-5/2})$ . . . . .	52
7.3.2	Undular jumps at a reference radius of $O(\varepsilon^{-2})$ . . . . .	54
<b>8</b>	<b>Near-critical turbulent axisymmetric source flow</b>	<b>57</b>
8.1	Problem formulation . . . . .	57
8.2	Asymptotic analysis . . . . .	58
8.3	Results and discussion . . . . .	62
8.3.1	Undular jumps at a reference radius of $O(\varepsilon^{-5/2})$ . . . . .	63
8.3.2	Undular jumps at a reference radius of $O(\varepsilon^{-2})$ . . . . .	69
8.3.3	Comparison between undular hydraulic jumps in turbulent and inviscid axisymmetric flow . . . . .	72
<b>9</b>	<b>Near-critical turbulent axisymmetric sink flow</b>	<b>76</b>
9.1	Problem formulation and asymptotic analysis . . . . .	76

---

9.2 Results and discussion . . . . .	77
<b>10 Conclusions of Part II</b>	<b>81</b>
<b>Appendix A Algebraic properties of the polynomial <math>p(H_1; R, S)</math></b>	<b>83</b>
<b>Bibliography</b>	<b>85</b>
<b>Curriculum vitae</b>	<b>92</b>

# Nomenclature

## Latin letters

$B$	Coupling parameter, [-], page 7
$b$	Channel width, [m], page 17
$C$	Parameter for the validity of the asymptotic results, [-], page 62
$C^+$	Empirical constant, [-], page 6
$c_1$	Non-dimensional function of integration, [-], page 49
$c_f$	Friction coefficient, [-], page 17
$\text{cn}[\xi m]$	Cnoidal Jacobian elliptic function with the parameter $m$ , [-], page 11
$D$	Empirical constant, [-], page 17
$D_{ae}$	Equivalent diameter, [m], page 44
$\bar{D}$	Discriminant of the polynomial $p(H_1; R, S)$ defined in (A.1), [-], page 83
$D_h$	Hydraulic diameter, [m], page 17
$E(m)$	Complete elliptic integral of the second kind with the parameter $m$ , [-], page 10
$f(\eta; n)$	Function representing the effect due to axisymmetric flow, [-], page 60
$\text{Fr}$	Froude number, [-], page 5
$\text{Fr}_\tau$	Friction Froude number, [-], page 5
$g$	Acceleration due to gravity, [m/s <sup>2</sup> ], page 5
$H$	Non-dimensional height of the free surface, [-], page 5
$h$	Height of the free surface, [m], page 4
$h_1, h_2, h_3$	Ordered roots of the polynomial $p(H_1; R, S)$ defined in (2.24), [-], page 10

$K(m)$	Complete elliptic integral of the first kind with the parameter $m$ , [-], page 10
$m$	Ch. 2: Parameter of the elliptic integrals and functions, [-], page 10; Ch. 3: Control parameter of the limiting process of a vanishing bottom slope, [-], page 22
$n$	Parameter defining the order of magnitude of the non-dimensional reference radius, [-], page 49
$P$	Non-dimensional pressure, [-], page 5
$p$	Pressure, [Pa], page 5
$Q$	Volume flow rate per unit azimuth angle, [m <sup>3</sup> /s], page 40
$q$	Volume flow rate per unit width, [m <sup>2</sup> /s], page 4
$R$	Non-dimensional radial coordinate, [-], page 48
$r$	Radial coordinate, [m], page 39
$\hat{R}$	Non-dimensional radius referring to the singular point, [-], page 41
$Re$	Reynolds number in terms of the volumetric mean velocity, [-], page 2
$Re_D$	Reynolds number in terms of the hydraulic diameter, [-], page 17
$Re_\tau$	Reynolds number in terms of the friction velocity, [-], page 6
$U$	Non-dimensional velocity component in $X$ - or $R$ -direction, [-], page 5
$u$	Velocity component in $x$ - or $r$ -direction, [m/s], page 4
$\overline{U'^2}$	Non-dimensional Reynolds normal stress in $X$ - or $R$ -direction, [-], page 5
$\overline{u'^2}$	Reynolds normal stress in $x$ - or $r$ -direction, [m <sup>2</sup> /s <sup>2</sup> ], page 5
$\overline{U'V'}$	Non-dimensional Reynolds shear stress, [-], page 5
$\overline{u'v'}$	Reynolds shear stress, [m <sup>2</sup> /s <sup>2</sup> ], page 5
$\Delta\overline{U'V'}$	Deviation of the non-dimensional Reynolds shear stress from fully developed flow in the reference state, [-], page 8
$\overline{U'W'}$	Non-dimensional Reynolds shear stress, [-], page 57
$\overline{u'w'}$	Reynolds shear stress, [m <sup>2</sup> /s <sup>2</sup> ], page 57
$\Delta\overline{U'W'}$	Deviation of the non-dimensional Reynolds shear stress from fully developed flow in the reference state, [-], page 59

$\Delta U$	Non-dimensional velocity defect in the reference state, [-], page 8
$u_m$	Volumetric mean velocity, [m/s], page 17
$U_\tau$	Non-dimensional friction velocity, [-], page 5
$u_\tau$	Friction velocity, [m/s], page 5
$V$	Non-dimensional velocity component in $Y$ -direction, [-], page 5
$v$	Velocity component in $y$ -direction, [m/s], page 4
$\overline{V'^2}$	Non-dimensional Reynolds normal stress in $Y$ -direction, [-], page 5
$\overline{v'^2}$	Reynolds normal stress in $y$ -direction, [m <sup>2</sup> /s <sup>2</sup> ], page 5
$W$	Non-dimensional velocity component in $Z$ -direction, [-], page 48
$w$	Velocity component in $z$ -direction, [m/s], page 47
$\overline{W'^2}$	Non-dimensional Reynolds normal stress in $Z$ -direction, [-], page 57
$\overline{w'^2}$	Reynolds normal stress in $z$ -direction, [m <sup>2</sup> /s <sup>2</sup> ], page 57
$We$	Weber number, [-], page 54
$X$	Non-dimensional longitudinal coordinate, [-], page 5
$x$	Longitudinal coordinate, [m], page 4
$Y$	Non-dimensional lateral coordinate, [-], page 5
$y$	Lateral coordinate, [m], page 4
$Z$	Non-dimensional vertical coordinate, [-], page 48
$z$	Vertical coordinate, [m], page 39

### Greek letters

$\alpha$	Bottom slope, [-], page 15
$\beta$	Dissipation parameter, [-], page 15
$\Gamma$	$\gamma/\beta$ , [-], page 23
$\gamma$	Parameter describing the deviation from a fully developed reference state, [-], page 12
$\delta$	Contraction parameter, [-], page 5
$\varepsilon$	Perturbation parameter, [-], page 7

$\eta$	Non-dimensional distance from the reference state, [-], page 49
$\kappa$	v. Kàrmàn constant, [-], page 6
$\nu$	Kinematic viscosity, [m <sup>2</sup> /s], page 6
$\xi$	Fast non-dimensional longitudinal coordinate, [-], page 7
$\rho$	Density, [kg/m <sup>3</sup> ], page 5
$\sigma$	Surface tension, [N/m], page 54
$\tau_w$	Wall shear stress, [N/m <sup>2</sup> ], page 5
$\Omega$	Slow non-dimensional longitudinal coordinate, [-], page 7
$\omega$	Non-dimensional wave number, [-], page 7

### Subscripts and superscripts

0	Leading-order quantity
1, 2, ...	Indicating a higher-order quantity
*	Critical state, where Fr = 1
i	Initial state
<i>m</i>	Point of maximum
r	Reference state
s	Singular point

# Part I

## Undular hydraulic jumps in open-channel flow

# Chapter 1

## Introduction

In hydraulics, the transition from slightly supercritical to subcritical free-surface flow followed by a wave train with slowly decaying amplitude (see Fig. 1.1) is known as the undular hydraulic jump, cf. [9], p. 439, [14], p. 45, or [23], p. 215. A two-dimensional transition is typically observed in rectangular channels if the upstream Froude number is between unity and about 1.2, [35, 43]. However, undular hydraulic jumps associated with so-called lateral shock waves may occur for upstream Froude numbers as large as 1.7, cf. [13, 35, 40].

The characteristics of undular hydraulic jumps were extensively studied experimentally in both horizontal and inclined channels. In particular, the experiments focused on the effect of developed and developing flow [38], the comparison of wide and narrow channels [39], as well as the effect of the channel slope [21].

Numerical solutions of the full equations of motion were established by Schneider *et al.* [50], using a finite volume method together with an asymptotic iteration procedure to determine the undular shape of the free surface. Rostami *et al.* [44] applied the volume of fluid method in a numerical analysis of the undular jump. Both numerical studies showed good agreement with experimental data and little influence of the employed turbulence models.

In an asymptotic analysis of the undular hydraulic jump in steady turbulent open-channel flow, Grillhofer and Schneider [22] considered a fully developed<sup>1</sup> near-critical

---

<sup>1</sup>In the present study, the term ‘fully developed flow’ is defined as common in the literature of fluid mechanics, i.e. a flow in the state of mechanical equilibrium where the shear stress balances the streamwise component of the gravity force. In hydraulics, however, a flow is often called ‘fully

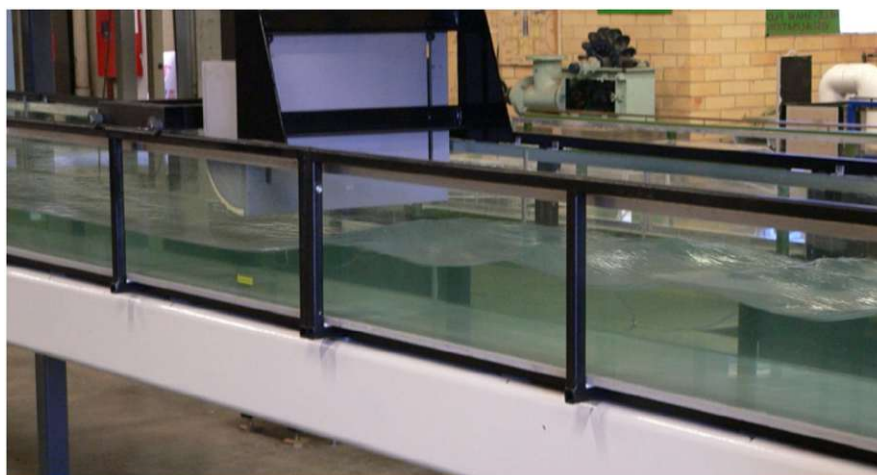


Figure 1.1: The undular hydraulic jump in a laboratory experiment [10], flow from left to right; upstream: Froude number  $Fr_r = 1.35$  (see (2.4) for the definition), Reynolds number  $Re = q/\nu = 1.1 \cdot 10^5$ .

reference state far upstream. Provided the volume flow rate and the depth of the reference state are known for a given bottom slope, the analysis could be kept free of turbulence modelling. In a subsequent analysis, Jurisits and Schneider [28] allowed for small deviations of the reference state from a fully developed flow and derived an extended version of the Korteweg–de Vries (KdV) equation, describing the free-surface elevation of near-critical flow in inclined channels. Steinrück [52] investigated the undular jump by performing a multiple-scales analysis of the basic equations, proving the uniform validity of the extended KdV equation derived in [28]. Comparing solutions of the extended KdV equation with experimental data and numerical solutions of the Reynolds-averaged Navier–Stokes equations showed good agreement, [21, 22, 28, 29, 52].

All previous theoretical studies considered *inclined* bottoms with the basic assumptions of a small deviation from fully developed flow in the reference state. For the particular case of a *horizontal* bottom, however, these assumptions cannot be satisfied as such a fully developed state does not exist. Thus, the undular hydraulic jump in steady turbulent open-channel flow over a horizontal bottom deserves special consideration, cf. [37].

---

developed’ as soon as the boundary layer, which develops at the bottom, has reached the free surface.

# Chapter 2

## Horizontal bottom

### 2.1 Problem formulation

We consider steady turbulent near-critical open-channel flow over horizontal bottoms with very large Reynolds numbers. Surface tension will be neglected as it is known to play a minor role in rivers or hydraulic structures with turbulent flow, see [5, 6], or [11], p. 265. The Cartesian coordinate system is chosen such that the  $x$ -axis is in the bottom plane, while the  $y$ -axis points upwards, see Fig. 2.1. The corresponding velocity components are  $u$  and  $v$ , respectively. The time-averaged flow is assumed to be two-dimensional with given volume flow rate per unit width,  $q$ . Time-averaged quantities are denoted by an overbar and fluctuations around the average by a prime. The time-averaged height of the free surface above the bottom plane is  $\bar{h}(x)$ . The coordinate

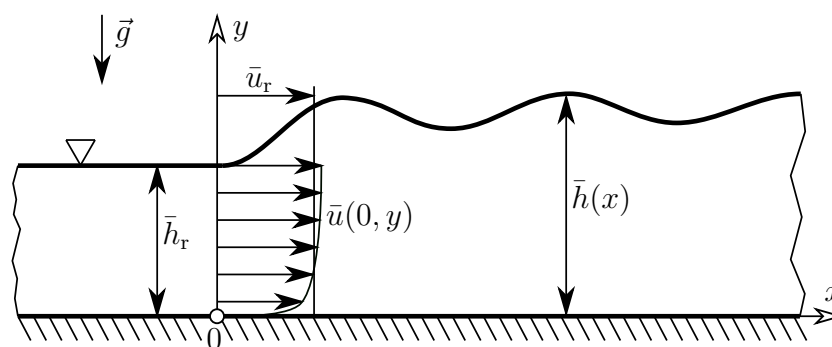


Figure 2.1: The stationary undular hydraulic jump in turbulent open-channel flow over horizontal surfaces.

system's origin is located at the position where the first wave of the undular jump originates from the slightly supercritical inflow. This upstream state is chosen as reference state (subscript  $r$ ), with the free-surface height  $\bar{h}_r = \bar{h}(0)$  and the volumetric mean velocity  $\bar{u}_r = q/\bar{h}_r$  serving as a reference length and a reference velocity, respectively. The pressure  $p$  is referred to the hydrostatic pressure at the bottom of the channel in the reference state,  $\rho g \bar{h}_r$ , where  $\rho$  is the constant fluid density and  $g$  is the acceleration due to gravity. The Reynolds stresses  $\overline{u'^2}$ ,  $\overline{v'^2}$  and  $\overline{u'v'}$  are referred to the square of the reference friction velocity,  $u_{\tau,r}^2$ , where  $u_\tau = \sqrt{\bar{\tau}_w/\rho}$  with the averaged wall shear stress  $\bar{\tau}_w$  at the channel bottom.

Analogue to the analysis by Steinrück [52], non-dimensional variables are introduced as follows:

$$\begin{aligned} X &= \delta \frac{x}{\bar{h}_r}, & Y &= \frac{y}{\bar{h}_r}, & \bar{H} &= \frac{\bar{h}}{\bar{h}_r}, & \bar{U} &= \frac{\bar{u}}{\bar{u}_r}, & \bar{V} &= \delta^{-1} \frac{\bar{v}}{\bar{u}_r}, \\ \bar{P} &= \frac{\bar{p}}{\rho g \bar{h}_r}, & U_\tau &= \frac{u_\tau}{u_{\tau,r}}, & \overline{U'^2} &= \frac{\overline{u'^2}}{u_{\tau,r}^2}, & \overline{V'^2} &= \frac{\overline{v'^2}}{u_{\tau,r}^2}, & \overline{U'V'} &= \frac{\overline{u'v'}}{u_{\tau,r}^2}. \end{aligned} \quad (2.1)$$

with the small parameter  $\delta$  introduced to contract the longitudinal coordinate in the asymptotic expansion, see below.

The continuity equation of incompressible flow in non-dimensional form reads

$$\bar{U}_X + \bar{V}_Y = 0, \quad (2.2)$$

where the subscripts  $X$  and  $Y$  denote partial derivatives with respect to  $X$  and  $Y$ , respectively.

For very large Reynolds numbers, the flow field may be divided into a viscous wall layer adjacent to the channel bottom and a non-viscous defect layer that forms the bulk of the flow field [47], p. 522. As the viscous wall layer is known to have universal properties, cf. [47], p. 524, it suffices to consider only the defect layer in what follows. Then, the equations of motion are

$$\delta \text{Fr}_r^2 (\bar{U}\bar{U}_X + \bar{V}\bar{U}_Y) = -\delta \bar{P}_X - \text{Fr}_{\tau,r}^2 (\delta \overline{U'^2}_X + \overline{U'V'}_Y), \quad (2.3a)$$

$$\delta^2 \text{Fr}_r^2 (\bar{U}\bar{V}_X + \bar{V}\bar{V}_Y) = -\bar{P}_Y - 1 - \text{Fr}_{\tau,r}^2 (\delta \overline{U'V'}_X + \overline{V'^2}_Y), \quad (2.3b)$$

where the reference Froude numbers are defined as

$$\text{Fr}_r := \frac{\bar{u}_r}{\sqrt{g\bar{h}_r}}, \quad \text{Fr}_{\tau,r} := \frac{u_{\tau,r}}{\sqrt{g\bar{h}_r}}. \quad (2.4)$$

For large Reynolds numbers, the effects of friction are known to be small. Hence, it will be assumed that the friction Froude number is very small, while  $\text{Fr}_r$  is slightly above the critical value 1, cf. (2.13) and (2.11), respectively.

The system of basic equations (2.2), (2.3a) and (2.3b) is to be solved subject to appropriate boundary conditions. At the bottom, the conventional boundary condition for the lateral velocity, i.e.

$$\bar{V}(X, 0) = 0, \quad (2.5)$$

is prescribed. Matching with the viscous wall layer yields the boundary condition for  $\overline{U'V'}$  at the bottom, i.e.

$$-\overline{U'V'} = U_\tau^2 \quad \text{as } Y \rightarrow 0. \quad (2.6)$$

A coupling condition for  $U_\tau$  and  $\bar{H}$  is obtained by making use of the logarithmic expression for the velocity in the defect layer [47], p. 544, which reads in the present non-dimensional variables, cf. [28]:

$$\bar{U}(X, \bar{H}) = \frac{\text{Fr}_{\tau,r}}{\text{Fr}_r} U_\tau \left[ \frac{1}{\kappa} \ln(\text{Re}_{\tau,r} U_\tau \bar{H}) + C^+ + \bar{C}(X) \right], \quad (2.7a)$$

$$\bar{C}(X) = \int_0^{\bar{H}} \left[ \frac{\text{Fr}_r}{\text{Fr}_{\tau,r} U_\tau} \bar{U}_Y - \frac{1}{\kappa Y} \right] dY. \quad (2.7b)$$

The Reynolds number is defined in terms of the reference friction velocity,

$$\text{Re}_{\tau,r} := \frac{u_{\tau,r} \bar{h}_r}{\nu}, \quad (2.8)$$

with  $\nu$  denoting the constant kinematic viscosity. In (2.7a),  $\kappa$  is the v. Kàrmàn constant and  $C^+$  is another empirical constant. It will turn out that neither one of these constants will appear in the final result. At the free surface, conventional kinematic and dynamic boundary conditions are imposed. Thus, a streamline defines the averaged interface in the averaged velocity field, i.e.

$$\bar{V}(X, \bar{H}) = \bar{U}(X, \bar{H}) \bar{H}_X, \quad (2.9)$$

and continuity of stresses is expressed by the relations

$$\left[ \bar{P}(X, \bar{H}) + \text{Fr}_{\tau,r}^2 \overline{U'^2}(X, \bar{H}) \right] \delta \bar{H}_X - \text{Fr}_{\tau,r}^2 \overline{U'V'}(X, \bar{H}) = 0, \quad (2.10a)$$

$$\left[ \bar{P}(X, \bar{H}) + \text{Fr}_{\tau,r}^2 \overline{V'^2}(X, \bar{H}) \right] - \text{Fr}_{\tau,r}^2 \overline{U'V'}(X, \bar{H}) \delta \bar{H}_X = 0. \quad (2.10b)$$

## 2.2 Multiple-scales analysis

A multiple-scales analysis represents a suitable means to treat the slowly changing amplitude and wavelength together with the fast oscillations of an undular hydraulic jump [52, 53], [48], p. 228. Following [52], a small perturbation parameter  $\varepsilon$  is introduced according to the relation

$$\text{Fr}_r = 1 + \frac{3}{2}\varepsilon, \quad \varepsilon \ll 1, \quad (2.11)$$

and the contraction parameter is defined as

$$\delta = 3\varepsilon^{1/2}, \quad (2.12)$$

where the coefficients  $3/2$  and  $3$  serve for later convenience. As mentioned above, the reference state's deviation from a fully developed flow cannot be assumed to be small as such a state does not exist for a horizontal bottom. Incorporating this fact and aiming at an analysis free of turbulence modelling but still includes friction effects requires the coupling between the two small parameters  $\varepsilon$  and  $\text{Fr}_{\tau,r}$  according to

$$\text{Fr}_{\tau,r}^2 = B\varepsilon^3, \quad B = \text{const} = O(1), \quad (2.13)$$

such that the velocity defect appears in the equations of  $O(\varepsilon^{3/2})$ , see (2.20). Note that the particular coupling (2.13) represents an essential modification of the analysis in [52], where  $\text{Fr}_{\tau,r}^2 = O(\varepsilon^2)$  was assumed, and thus the velocity defect appeared in the equations of  $O(\varepsilon)$ .

The multiple-scales analysis is performed by substituting the original contracted coordinate  $X$  by a fast and a slow variable  $\xi$  and  $\Omega$ , respectively, and introducing the spatially slowly changing wave number

$$\omega(\Omega) = \frac{d\xi}{dX} = \frac{1}{\varepsilon^{1/2}} \frac{d\Omega}{dX}. \quad (2.14)$$

Thus, all unknowns depend on both length scales, e.g.  $\bar{H} = \bar{H}(\xi, \Omega)$ , and are defined to have period 1 with respect to the fast variable  $\xi$ . Derivatives with respect to  $X$  become a sum of two partial derivatives, i.e.

$$\frac{d}{dX} = \omega \left( \frac{\partial}{\partial \xi} + \varepsilon^{1/2} \frac{\partial}{\partial \Omega} \right). \quad (2.15)$$

The dependent variables are now expanded in terms of powers of  $\varepsilon$ , e.g.

$$\begin{aligned}\bar{U}(\xi, \Omega, Y) &= U_0 + \varepsilon U_1(\xi, \Omega, Y) + \varepsilon^{3/2} U_{3/2}(\xi, \Omega, Y) + \varepsilon^2 U_2(\xi, \Omega, Y) + \varepsilon^{5/2} U_{5/2}(\xi, \Omega, Y) + \dots, \\ \bar{H}(\xi, \Omega) &= H_0 + \varepsilon H_1(\xi, \Omega) + \varepsilon^{3/2} H_{3/2}(\xi, \Omega) + \varepsilon^2 H_2(\xi, \Omega) + \varepsilon^{5/2} H_{5/2}(\xi, \Omega) + \dots,\end{aligned}\quad (2.16)$$

for the non-dimensional velocity in X-direction, and height of the free surface, respectively, neglecting terms of order  $\varepsilon^3$  and smaller.

Expanding the governing equations and boundary conditions accordingly, the leading-order terms represent the basic state:

$$U_0 = 1, \quad V_0 = 0, \quad P_0 = 1 - Y, \quad H_0 = 1. \quad (2.17)$$

The leading order of the Reynolds shear stress is assumed to be of the form

$$(\overline{U'V'})_0 = Y - 1 + \Delta \overline{U'V'}(Y), \quad (2.18)$$

where the term  $\Delta \overline{U'V'}(Y) = O(1)$  allows for a deviation of the reference state from the linear profile of a fully developed flow. Of course, the term  $\Delta \overline{U'V'}(Y)$  has to comply with the boundary conditions at the bottom and the free surface, i.e.  $\Delta \overline{U'V'}(0) = \Delta \overline{U'V'}(1) = 0$ . To avoid turbulence modelling in Ch. 3, a condition for the derivative of the deviation at the free surface will be given in (3.9). Note that  $(\overline{U'V'})_0$  does not appear in the leading order of the equation of motion, (2.3a), since the term is multiplied with  $\text{Fr}_{\tau,r}^2$ , and thus shifted to a higher order.

Performing the analysis as described in [52, 53]<sup>1</sup> yields

$$U_1 = -H_1, \quad V_1 = \omega H_{1,\xi} Y, \quad P_1 = H_1, \quad (2.19)$$

as  $O(\varepsilon)$  results, and from the equations of  $O(\varepsilon^{3/2})$  follows

$$U_{3/2} = -H_{3/2} + \sqrt{B} \Delta U(Y), \quad V_{3/2} = \omega (H_{1,\Omega} + H_{3/2,\xi}) Y, \quad P_{3/2} = H_{3/2}. \quad (2.20)$$

The subscripts  $\xi$  and  $\Omega$  denote partial derivatives with respect to  $\xi$  and  $\Omega$ , respectively. The term  $\Delta U(Y)$  in (2.20) represents the velocity defect in the reference state. With

<sup>1</sup>Formally the results of  $O(\varepsilon)$  and of  $O(\varepsilon^{3/2})$  are the same as in [52, 53], except that in the present analysis the velocity defect term appears in  $U_{3/2}$  instead of  $U_1$ . However, in [52, 53] the results of  $O(\varepsilon^{3/2})$  are not given explicitly. Instead, it is stated that the subscript ‘1’ of the  $O(\varepsilon)$  results is to be replaced by ‘3/2’, without mentioning the term containing  $H_{1,\Omega}$  in the result of  $V_{3/2}$ .

flows close to separation being excluded, the velocity defect is of the order of the friction velocity [47], p. 536, i.e.  $\bar{U}_r(Y) = 1 + \text{Fr}_{\tau,r} \Delta U(Y)$  with  $\Delta U(Y) = O(1)$ , in accordance with the first equation of (2.20). Since a volumetric mean value has been chosen as reference velocity, the integral of  $\Delta U(Y)$  over the whole channel cross section vanishes per definitionem. As a consequence,  $\Delta U(Y)$  will not appear in the final result of the analysis.

$H_1(\xi, \Omega)$ ,  $H_{3/2}(\xi, \Omega)$  and  $\omega(\Omega)$  remain undetermined in the framework of equations of  $O(\varepsilon)$  and  $O(\varepsilon^{3/2})$ . Investigation of the following orders  $O(\varepsilon^2)$  and  $O(\varepsilon^{5/2})$  leads to the solvability conditions

$$\omega^2 H_{1,\xi\xi\xi} + H_{1,\xi}(H_1 - 1) = 0, \quad (2.21)$$

and

$$\omega^2 H_{3/2,\xi\xi} + H_{3/2}H_1 - H_{3/2} = r, \quad (2.22a)$$

$$\omega r_\xi = -3\omega^2(\omega H_{1,\xi\xi})_\Omega - \omega H_{1,\Omega}(H_1 - 1) - B/9, \quad (2.22b)$$

for  $H_1$  and  $H_{3/2}$ , respectively.

Integrating (2.21) with respect to  $\xi$ , multiplying the result with  $H_{1,\xi}$  and integrating with respect to  $\xi$  once again yields

$$3\omega^2 \left( \frac{\partial H_1}{\partial \xi} \right)^2 = p(H_1; R, S), \quad (2.23)$$

with the polynomial

$$p(H_1; R, S) := -H_1^3 + 3H_1^2 + 6R(\Omega)H_1 + S(\Omega), \quad (2.24)$$

where  $R(\Omega)$  and  $S(\Omega)$  are slowly changing functions of integration. In order to derive equations for  $R(\Omega)$  and  $S(\Omega)$ , the solvability conditions (2.21) and (2.22) are manipulated and combined as described in [52], leading to

$$\omega \frac{dR}{d\Omega} = -\frac{B}{9}, \quad (2.25a)$$

$$\omega \frac{dS}{d\Omega} = \frac{B}{9} \int_0^1 H_1 d\xi. \quad (2.25b)$$

Aiming at an analytical solution of  $H_1(\xi, \Omega)$ , it will be convenient to represent the third-order polynomial defined in (2.24) in terms of its three ordered roots  $h_1 \leq h_2 \leq h_3$ ,

i.e.  $p(H_1; R, S) = [H_1 - h_1(R, S)][H_1 - h_2(R, S)][h_3(R, S) - H_1]$ . Differential equations for the three roots can be deduced from (2.25) by applying the algebraic relations between  $R(\Omega)$ ,  $S(\Omega)$  and  $h_1(\Omega)$ ,  $h_2(\Omega)$ ,  $h_3(\Omega)$ , summarised in Appendix A. Moreover, we have to use the fact that the integral from 0 to 1 with respect to  $\xi$  corresponds to twice the integral from  $h_2$  to  $h_3$  (i.e. a half period) with respect to  $H_1$ . Thus, with the definition

$$I_j = \int_{h_2}^{h_3} \frac{H_1^j dH_1}{\sqrt{(H_1 - h_1)(H_1 - h_2)(h_3 - H_1)}}, \quad j = 0, 1, \quad (2.26)$$

the ODEs for the roots are

$$\frac{dh_1}{d\Omega} = \frac{4B}{\sqrt{3}} \frac{I_1 - I_0 h_1}{(h_1 - h_2)(h_1 - h_3)}, \quad (2.27a)$$

$$\frac{dh_2}{d\Omega} = \frac{4B}{\sqrt{3}} \frac{I_1 - I_0 h_2}{(h_2 - h_3)(h_2 - h_1)}, \quad (2.27b)$$

$$\frac{dh_3}{d\Omega} = \frac{4B}{\sqrt{3}} \frac{I_1 - I_0 h_3}{(h_3 - h_1)(h_3 - h_2)}. \quad (2.27c)$$

Note that one of the three ODEs is redundant since the relation  $h_1 + h_2 + h_3 = 3$  holds. The integrals (2.26) can be expressed analytically [51], i.e.

$$I_0 = \frac{2K(m)}{\sqrt{h_3 - h_1}}, \quad (2.28a)$$

$$I_1 = \frac{2}{\sqrt{h_3 - h_1}} [h_1 K(m) + (h_3 - h_1) E(m)], \quad (2.28b)$$

with  $K(m)$  and  $E(m)$  denoting the complete elliptic integral of the first and second kind, respectively, and the parameter  $m$  being defined as  $m = (h_3 - h_2)/(h_3 - h_1)$ ; cf. [1], p. 569. In Ch. 3 the letter  $m$  will denote the control parameter for the analysis of the limiting process of a vanishing bottom slope.

In the course of deriving an analytical expression for  $H_1(\xi, \Omega)$ , (2.23) is used twice. First, by means of a definite integral to obtain an analytical expression for  $\omega(\Omega)$ , and second, by means of an indefinite integral to obtain the final result for  $H_1(\xi, \Omega)$ . Therefore, integration of (2.23) over one period by making use of the above mentioned relation between the integrals with respect to  $\xi$  and  $H_1$ , together with (2.28a), gives for the wave number

$$\omega(\Omega) = \frac{\sqrt{h_3 - h_1}}{4\sqrt{3}K(m)}. \quad (2.29)$$

Furthermore, following, e.g., Drazin and Johnson [17], pp. 26–29, the indefinite integration of (2.23) yields the classical cnoidal wave solution for the free-surface elevation,

$$H_1(\xi, \Omega) = h_2 + (h_3 - h_2)\text{cn}^2 [2K(m)(\xi - \xi_r)|m], \quad (2.30)$$

where  $\text{cn}$  is the cnoidal Jacobian elliptic function, see [1], Ch. 16. The constant of integration,  $\xi_r$ , is chosen such that  $H_1(\xi = 0, \Omega = 0) = H_1(X = 0) = 0$ , i.e.

$$\xi_r = \frac{\text{sgn}[H_{1,X}(0)]}{2K(m)} \text{cn}^{-1} \left[ \sqrt{\frac{h_2}{h_2 - h_3}} \Big| m \right] \Big|_{\Omega=0}, \quad (2.31)$$

with  $\text{sgn}[x] := 1$  if  $x \geq 0$ , and  $\text{sgn}[x] := -1$  if  $x < 0$ ; cf. [27], p. 53.  $H_{1,X}(0)$  is the initial slope of the free-surface elevation in terms of the original coordinate  $X$ .

The free-surface elevation in terms of the original coordinate,  $H_1(X)$ , is found by the following solution procedure. First, the roots  $h_1, h_2, h_3$  are determined by solving (2.27). Therefore, initial conditions are derived from the algebraic relations between the roots, and  $R, S$ , given in Appendix A, (A.10–A.12), by substituting  $R(0) = H_{1,XX}(0)$  and  $S(0) = (1/2)H_{1,X}^2(0)$ .  $H_{1,XX}(0)$  is the initial curvature of the free-surface elevation. With the solution for the three roots, both  $\omega(\Omega)$  and  $H_1(\xi, \Omega)$  are determined according to (2.29) and (2.30), respectively. According to (2.14), the fast and slow variables are not independent of each other. Thus,  $H_1(\xi, \Omega)$  may be rewritten as  $H_1(\Omega)$  using  $\xi = \Omega/\varepsilon^{1/2}$ . Eventually, the original coordinate  $X$  follows from

$$X = \frac{1}{\varepsilon^{1/2}} \int_0^\Omega \frac{d\Omega}{\omega(\Omega)}, \quad (2.32)$$

which relates  $H_1(X)$  to  $H_1(\Omega)$ .

## 2.3 Uniformly valid differential equation

A different approach than a multiple-scales analysis was chosen by Grillhofer and Schneider [22] and Jurisits and Schneider [28], by deriving a uniformly valid differential equation. Performing an asymptotic analysis of the governing equations given in Sec. 2.1 in

the same manner as described in [22, 28] means to introduce the relations (2.11–2.13) and expand all dependent variables in terms of small values of  $\varepsilon$ , e.g.

$$\begin{aligned}\bar{H}(X) &= 1 + \varepsilon H_1(X) + \varepsilon^2 H_2(X) + \dots, \\ \bar{U}(X, Y) &= 1 + \varepsilon U_1(X, Y) + \varepsilon^2 U_2(X, Y) + \dots, \\ \bar{P}(X, Y) &= 1 - Y + \varepsilon P_1(X, Y) + \varepsilon^2 P_2(X, Y) + \dots,\end{aligned}\tag{2.33}$$

neglecting terms of order  $\varepsilon^3$  and smaller. Note that here (2.17) and (2.18), i.e. the basic state, are used as leading-order terms. The following relationships are the results of the first-order equations:

$$U_1 = -H_1 + \varepsilon^{1/2} \sqrt{B} \Delta U(Y), \quad V_1 = H_{1,X} Y, \quad P_1 = H_1.\tag{2.34}$$

The second term of  $U_1$  containing the velocity defect is half an order of magnitude smaller than the rest of the  $O(\varepsilon)$  results. This is permitted in the course of deriving a uniformly valid differential equation.

The free-surface elevation  $H_1(X)$  remains free in the framework of the first-order equations and is to be determined from a solvability condition of the second-order equations. Performing the analysis as described in [22, 28], the second-order equations resulting from the momentum equation in  $X$ -direction, (2.3a), and from the kinematic boundary condition, (2.9), are compatible if

$$H_{1,XXX} + H_{1,X}(H_1 - 1) = -\gamma,\tag{2.35}$$

with

$$\gamma = \frac{B}{9} \varepsilon^{1/2} = \frac{\text{Fr}_{\tau,r}^2}{9\varepsilon^{5/2}}.\tag{2.36}$$

The non-linear third-order ODE (2.35) is known [28] as a steady-state version of an extended Korteweg–de Vries (KdV) equation describing the free-surface elevation as a function of the contracted longitudinal coordinate  $X$ . The constant extension  $\gamma$  on the right-hand side represents the deviation of the reference state from a fully developed flow.

Integrating (2.35) twice yields the system of first-order ODEs

$$3H_{1,X}^2 = -H_1^3 + 3H_1^2 + 6RH_1 + S,\tag{2.37a}$$

$$R_X = -\gamma,\tag{2.37b}$$

$$S_X = \gamma H_1,\tag{2.37c}$$

where  $R$  and  $S$  are functions of integration, cf. [51].

Following [52], the system of ODEs (2.37) may serve as starting point of a multiple-scales analysis as discussed in the preceding section. Thus, the fast and slow variable  $\xi$  and  $\Omega$ , respectively, together with the wave number  $\omega(\Omega)$  according to (2.14) are introduced. Then,  $H_1(\xi, \Omega)$ ,  $R(\xi, \Omega)$  and  $S(\xi, \Omega)$  are assumed to be periodic functions with period 1 with respect to  $\xi$ . Applying the relation (2.15) to the system of ODEs (2.37) and strictly separating the orders  $O(1)$  and  $O(\varepsilon^{1/2})$  gives  $R = R(\Omega)$  and  $S = S(\Omega)$  as leading-order results from (2.37b) and (2.37c), respectively. Moreover, the leading order of (2.37a) turns into (2.23). The  $O(\varepsilon^{1/2})$  terms of (2.37b) and (2.37c) give (2.25a) and (2.25b), respectively.

Thus, the multiple-scales analysis of (2.37) results in the same set of differential equations (2.23–2.29) as the multiple-scales analysis of the basic equations. This proves that (2.37) and consequently the extended KdV equation (2.35) are uniformly valid, i.e. valid on both fast and slow scales.

## 2.4 Results and discussion

The system of ODEs (2.27) as well as the extended KdV equation (2.35) may be solved numerically using the standard function `ode45` of the commercial software package Matlab R2018b. The solution of (2.27) is obtained prescribing a maximum step size of  $2 \cdot 10^{-6}$ , and the default values for the relative and absolute error tolerances of  $10^{-3}$  and  $10^{-6}$ , respectively. Equation (2.35) is solved with a maximum step size of  $10^{-3}$ , a relative error tolerance of  $10^{-4}$ , and an absolute error tolerance of  $10^{-8}$ .

### 2.4.1 Comparison between solutions of the multiple-scales analysis and the extended KdV equation

In Fig. 2.2 the multiple-scales solution according to (2.30) is compared with the numerical solution of the extended KdV equation (2.35), subject to equal initial conditions and parameter values. Both solutions are in excellent agreement for quite a large distance. At  $X \approx 27.6$ , the real roots  $h_1$  and  $h_2$  coalesce. This point confines the region of possible multiple-scales solutions [29]. A little bit downstream, the numerical solution of (2.35) experiences a breakdown, approaching the singular point  $X_s$  as  $H_1 \sim -12/(X_s - X)^2$ .

However, the two solutions start to deviate from each other already before the last wave crest, raising the question of what happens in this particular region. The answer may be found in the behaviour of the roots  $h_1$  and  $h_2$ . As the green curve comes closer to the end of the region of possible multiple-scales solutions,  $h_1$  and  $h_2$  approach each other, i.e.  $h_2 - h_1 \rightarrow 0$ . This leads to a singularity in (2.27a) and (2.27b), violating the request that both sides of the equation are of the same order of magnitude. Moreover, a singularity implies that the roots are no longer slowly changing. Thus, the multiple-scales solution is not valid in this region, and the validity condition reads

$$\frac{1}{h_2 - h_1} = O(1). \quad (2.38)$$

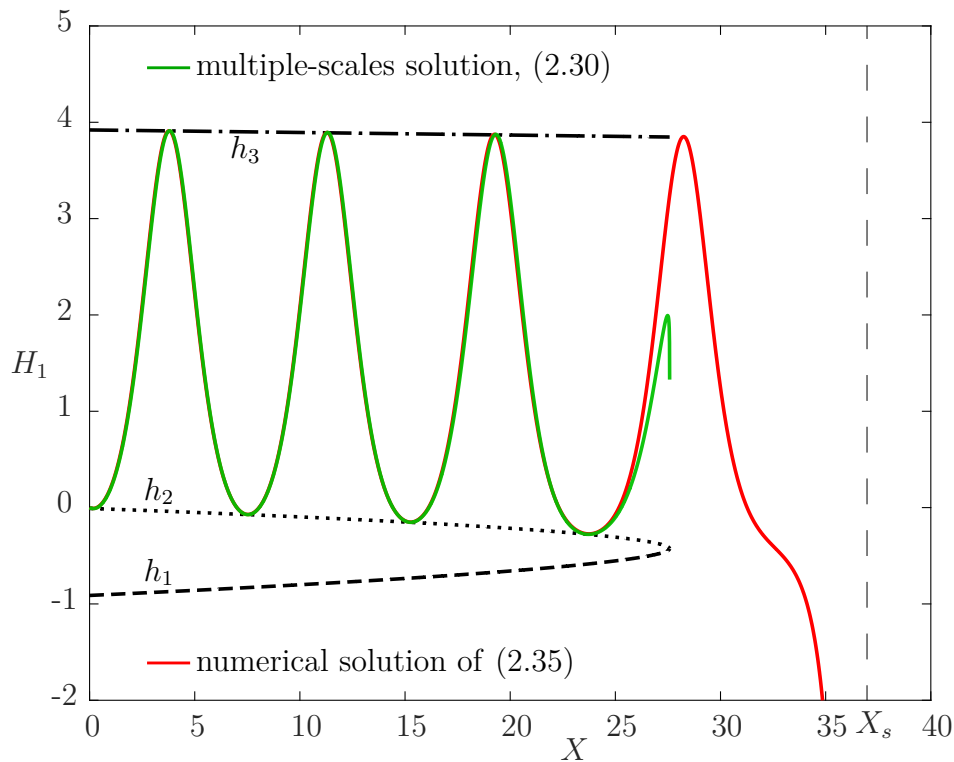


Figure 2.2: Comparison of a numerical solution of the extended KdV equation, (2.35), with the corresponding multiple-scales solution, (2.30), for  $Fr_r = 1.0044$  and  $Fr_{\tau,r} = 1.1 \cdot 10^{-4}$ , i.e.  $\varepsilon = 2.9 \cdot 10^{-3}$ ,  $\gamma = 3 \cdot 10^{-3}$ . Initial conditions:  $H_1(0) = 0$ ,  $H_{1,X}(0) = -0.1$ ,  $H_{1,XX}(0) = 0.6$ .

### 2.4.2 Comparison with the theory of inclined bottoms

Jurisits and Schneider [28] investigated undular hydraulic jumps arising in non-developed turbulent free-surface flows over slightly inclined surfaces, i.e. bottom slope  $\alpha = O(\varepsilon^2)$ . Based on the assumptions  $\text{Fr}_{\tau,r}^2 = O(\varepsilon^2)$  and a small deviation of the reference state from a fully developed flow, they derived the extended KdV equation

$$H_{1,XXX} + H_{1,X}(H_1 - 1) = \beta H_1 - \gamma, \quad (2.39)$$

with

$$\beta = \frac{\text{Fr}_{\tau,r}^2}{3\varepsilon^{3/2}}, \quad \gamma = \frac{\text{Fr}_{\tau,r}^2 - \alpha}{9\varepsilon^{5/2}}. \quad (2.40)$$

Equation (2.39) is a uniformly valid differential equation, [52], with  $\beta$  and  $\gamma$  representing the effect of dissipation and the deviation from a fully developed reference state, respectively.

As mentioned above, the case of a horizontal bottom is not included in the theory of undular hydraulic jumps over inclined bottoms. However, for the sake of comparison we shall now consider (2.39) with  $\alpha = 0$  and  $\text{Fr}_{\tau,r}$  according to (2.13), i.e. (2.39) represents (2.35) extended by the linear dissipation term  $\beta H_1 = O(\varepsilon^{3/2})$ .

Both (2.35) and (2.39) are solved numerically, using the function `ode45` of Matlab R2018b with a maximum step size of  $10^{-3}$ , a relative error tolerance of  $10^{-4}$  and an absolute error tolerance of  $10^{-8}$ . In Fig. 2.3 the numerical solutions of (2.35) and (2.39) are compared using three different values for the initial curvature  $H_{1,XX}(0)$ . The initial value and initial slope of the free surface as well as  $\text{Fr}_r$  and  $\text{Fr}_{\tau,r}$  remain fixed. The smallest initial curvature of  $H_{1,XX}(0) = 0.1$  (dashed lines) leads to small differences between the solutions of (2.35) and (2.39). With a larger value  $H_{1,XX}(0) = 0.8$  (dash-dotted lines) the solution of (2.39) develops three wave crests before a breakdown, while the solution of (2.35) breaks down immediately after the first wave crest. With an initial curvature as large as  $H_{1,XX}(0) = 1$  (solid lines), the solution of (2.35) develops a second wave crest. However, for the same case the solution of (2.39) leads to double the amount of crests.

This comparison shows that even if  $\beta H_1$  in (2.39) is of  $O(\varepsilon^{3/2})$  and should drop out of the equation, i.e. leading to (2.35), the term seems to be essential for the development of undulations when moderate initial curvature values are prescribed. Thus, for undular jumps originating from a flow with a mild free-surface curvature, in a first approach,

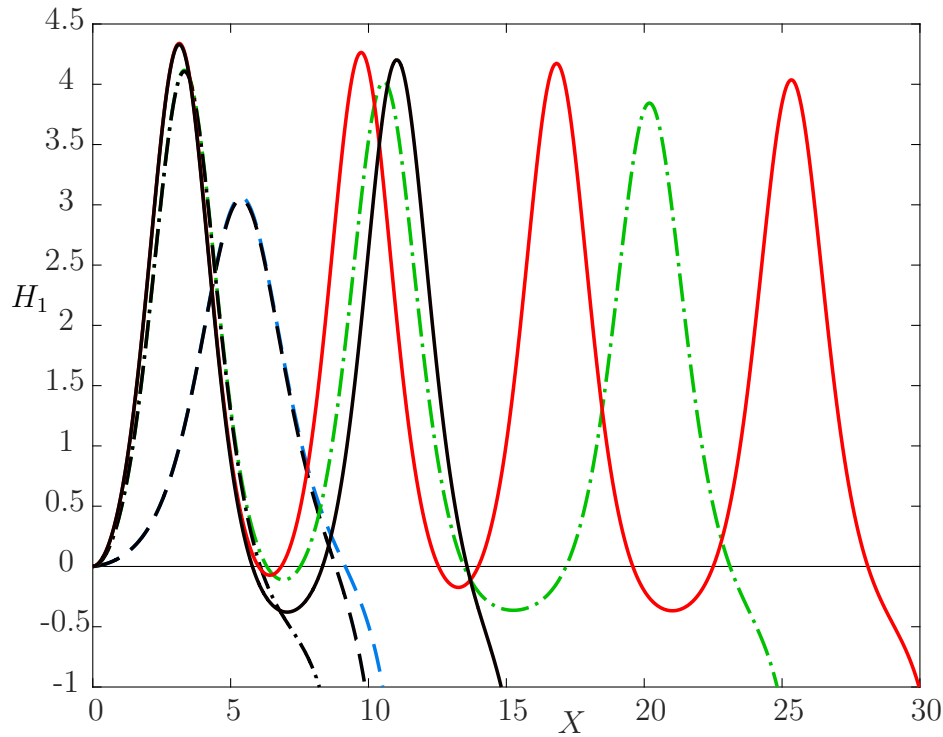


Figure 2.3: Numerical solutions of the extended KdV equation for horizontal bottoms, (2.35), and for inclined bottoms, (2.39), shown as black and coloured lines, respectively, for  $\text{Fr}_r = 1.12$ ,  $\text{Fr}_{\tau,r} = 1.89 \cdot 10^{-2}$ ,  $\alpha = 0$ . Initial conditions:  $H_1(0) = 0$ ,  $H_{1,X}(0) = 2.2 \cdot 10^{-2}$ ; dashed:  $H_{1,XX}(0) = 0.1$ , dash-dotted:  $H_{1,XX}(0) = 0.8$ , solid:  $H_{1,XX}(0) = 1$ .

the theory of [28] may be applied even to horizontal bottoms by using the modified order of magnitude of  $\text{Fr}_{\tau,r}^2 = O(\varepsilon^3)$ .

### 2.4.3 Comparison with experimental data

A comparison between the theory and experimental measurements requires the knowledge of both Froude numbers at the toe of the undular jump experiment, that is,  $\text{Fr}_r$  and  $\text{Fr}_{\tau,r}$ . With the measured discharge per unit width  $q$  and the averaged height of the free surface in the reference state  $\bar{h}_r$ , the Froude number is  $\text{Fr}_r = q/\sqrt{g\bar{h}_r^3}$ . The friction Froude number is determined via the definition of the local friction coefficient

$$c_f := 2 \frac{u_\tau^2}{u_m^2} = 2 \frac{\text{Fr}_\tau^2}{\text{Fr}^2}, \quad (2.41)$$

with  $\bar{u}_m = q/\bar{h}$  being the local time-averaged volumetric mean velocity. Further,  $c_f$  may be computed from the friction law of plane channel flow according to [20], p. 594,

$$\sqrt{\frac{2}{c_f}} = \frac{1}{\kappa} \ln \left[ \sqrt{\frac{c_f}{2}} \text{Re}_D \right] + D, \quad (2.42)$$

with the v. Kàrmàn constant  $\kappa = 0.41$  and the empirical constant  $D = -0.08$  (for smooth walls). The Reynolds number

$$\text{Re}_D := \frac{\bar{u}_m D_h}{\nu}, \quad (2.43)$$

is defined in terms of the hydraulic diameter  $D_h$ , see e.g. [47], p. 103. For open-channel flows with channel width  $b$ , the hydraulic diameter is  $D_h = 4\bar{h}b/(2\bar{h} + b)$ .

Generally, applying the concept of the hydraulic diameter would require the use of the friction law of circular pipe flow, i.e. (2.42) with  $D = 0.27$ , cf. [20], p. 527. In the experiments used for comparison, however, the ratio  $\bar{h}/b$  is relatively small, and thus the friction law (2.42) with the empirical constant for plane channel flow,  $D = -0.08$ , will be used to compute  $c_f$ .

Only very few experiments of the undular hydraulic jump over a *horizontal* bottom with detailed measurement of the surface elevation are available in the literature. Reinauer and Hager [43] conducted their experiment at  $\text{Fr}_r = 1.36$ , which reportedly represents the limiting case to wave breaking. Gotoh *et al.* [21] presented a horizontal experiment with  $\text{Fr}_r = 1.5$ . Both experiments will not be used here since the Froude numbers are relatively large and the similarity parameter  $B$ , representing a measure for the validity of the present theory, is smaller than the corresponding perturbation parameter  $\varepsilon$ . The experiment by Chanson [12], CD1, with  $b = 0.5$  m and the measured values  $q = 9.14 \cdot 10^{-2}$  m<sup>2</sup>/s and  $\bar{h}_r = 81$  mm leads to  $\text{Fr}_r = 1.266$  and  $\text{Fr}_{\tau,r} = 5.54 \cdot 10^{-2}$  (i.e.  $\varepsilon = 0.177$ ,  $B = 0.23$ ), and seems to be the most suitable for comparison with the present theory. However, note that the experimental configuration leads to a value of  $B$  which is rather of order  $\varepsilon$  than of order 1, and, furthermore, a recirculation bubble below the first wave crest was observed, whereas flow reversal is excluded in the present analysis. Thus, only modest agreement between measurements and theoretical predictions should be expected.

In Fig. 2.4 numerical solutions of the extended KdV equation (2.35) are compared with surface elevation measurements of [12]. The numerical solutions of (2.35) are obtained by keeping the initial values of the surface elevation, and surface slope fixed

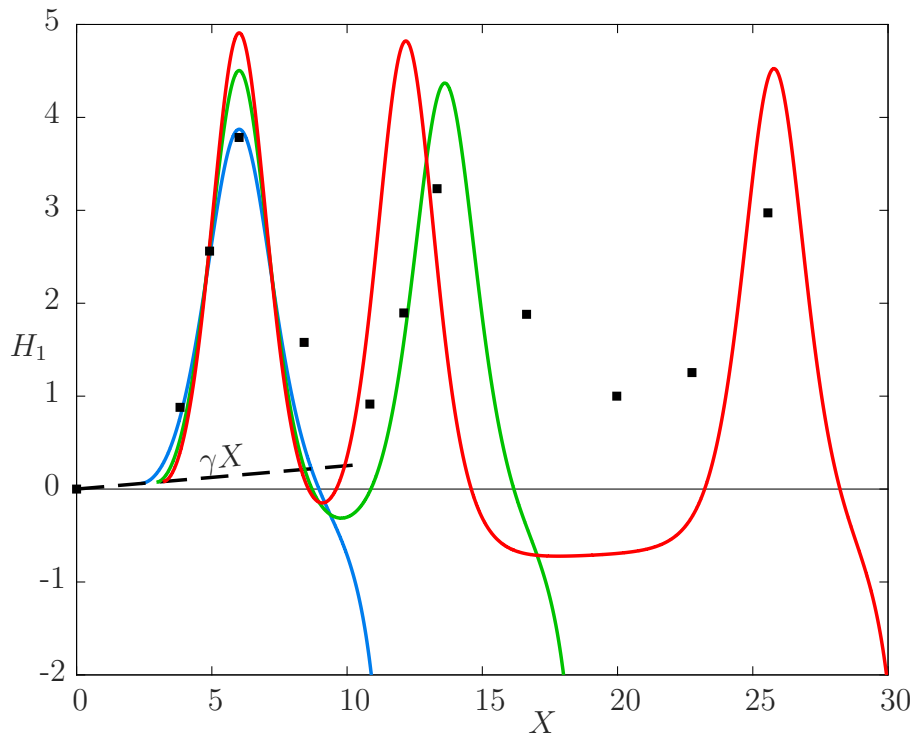


Figure 2.4: Comparison of experimental data [12] (black squares) for  $Fr_r = 1.266$  and  $Fr_{\tau,r} = 5.54 \cdot 10^{-2}$  (i.e.  $\varepsilon = 0.177$ ,  $\gamma = 0.025$ ) with numerical solutions of the extended KdV equation (2.35). Initial conditions:  $H_1(0) = 0$ ,  $H_{1,X}(0) = \gamma$ ; blue:  $H_{1,XX}(0) = 0.57$ , green:  $H_{1,XX}(0) = 1.1$ , red:  $H_{1,XX}(0) = 1.51$ .

while altering the initial curvature  $H_{1,XX}(0)$ . The resulting curves are shifted along the straight line  $H_1 = \gamma X$  such that the first wave crest corresponds to the experimental data. The solution due to the lowest initial curvature, i.e. the blue curve, shows good agreement in terms of the first wave amplitude but breaks down immediately afterwards. Increasing  $H_{1,XX}(0)$  leads to the development of a second crest (green curve). A solution with three crests, reasonably approximating the wavelengths between first and second, as well as second and third measured crests, is found with  $H_{1,XX}(0) = 1.513$ , i.e. the red curve. However, for the latter case, the predicted amplitudes are too large.

The comparisons of Figs. 2.3 and 2.4 lead to the conclusion that the solution of (2.35) strongly depends on the initial curvature, and undular solutions are only possible with relatively large values. Moreover, the theories of inclined bottom [27, 28, 52] show better agreement with experiments, even if they were conducted with a horizontal bottom, cf.

[27], pp. 97–98, and [28], Fig.10.<sup>2</sup> Thus, an investigation of the limiting case of the bottom slope tending to zero, while  $Fr_r$  and  $Fr_{\tau,r}$  remain fixed, seems necessary to gain a better understanding of the undular hydraulic jump over horizontal surfaces.

---

<sup>2</sup>In [27], Fig. 6.6, and [28], Fig. 10, some measurement points are inaccurate, and the measured maximum of the first wave is cut off. Nevertheless, comparing the theory with the corrected measurement points shows satisfactory agreement.

# Chapter 3

## The limiting process of vanishing bottom slope

### 3.1 Problem formulation

The theory of undular hydraulic jumps over *horizontal* bottoms, i.e. solutions of the extended KdV equation (2.35), performed poorly in the comparison with experimental data, cf. Sec. 2.4.3. The predicted amplitudes were too large, and extraordinarily large initial curvature values were needed to obtain undular solutions. Moreover, a comparison with the theory of inclined bottoms, Sec. 2.4.2, showed that the term  $\beta H_1$  in the extended KdV equation appears favourable for the development of undulations. Thus, the investigation of the limiting case of the bottom slope tending to zero, [36], appears promising to gain a better understanding of the undular hydraulic jump over horizontal bottoms and obtain satisfactory agreement between analysis and experiments.

The assumptions and considerations regarding the flow do not change with respect to Sec. 2.1, except for a bottom slope  $\alpha \rightarrow 0$  instead of a horizontal bottom, see Fig. 3.1. The coordinate system's origin is located in the region of the undular jump's origin. Depending on the position where the boundary conditions are prescribed, the origin of the undular jump may be slightly downstream or upstream of the reference state at  $X = 0$ , see Sec. 3.4.1 and 3.4.2, respectively. Non-dimensional variables are introduced according to (2.1). While the continuity equation (2.2) remains unchanged,

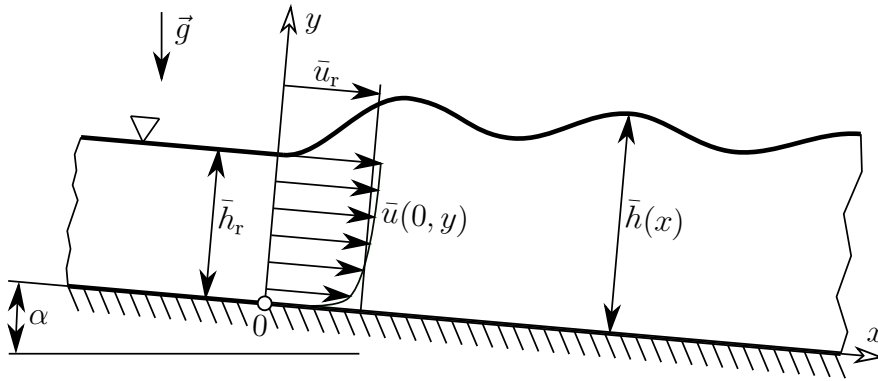


Figure 3.1: The stationary undular hydraulic jump in turbulent open-channel flow over inclined surfaces.

the equations of motion for the defect layer become

$$\delta \text{Fr}_r^2 (\bar{U} \bar{U}_X + \bar{V} \bar{U}_Y) = -\delta \bar{P}_X + \alpha - \text{Fr}_{\tau,r}^2 (\delta \bar{U}'^2_X + \bar{U}' \bar{V}'_Y), \quad (3.1a)$$

$$\delta^2 \text{Fr}_r^2 (\bar{U} \bar{V}_X + \bar{V} \bar{V}_Y) = -\bar{P}_Y - 1 - \text{Fr}_{\tau,r}^2 (\delta \bar{U}' \bar{V}'_X + \bar{V}'^2_Y), \quad (3.1b)$$

with the Froude numbers defined in (2.4). All boundary and matching conditions (2.5–2.10) remain unaffected by the introduction of  $\alpha \rightarrow 0$ , see Sec. 2.1 for details.

## 3.2 Asymptotic analysis

Following [28], the asymptotic analysis of the governing equations is based on a slightly supercritical reference Froude number and the definition of the contraction parameter according to (2.11) and (2.12), respectively.

Guided by relationships that apply to fully developed flow, it was assumed in previous studies [22, 28, 52] that the bottom slope, as well as the friction Froude number, vanish with vanishing  $\varepsilon$ . Obviously, that approach is not suitable for studying undular hydraulic jumps in the limit of vanishing bottom slopes. Thus, the basic idea of the present analysis is to introduce a coupling between the non-dimensional parameters  $\alpha$ ,  $\text{Fr}_{\tau,r}$ ,  $\varepsilon$  that satisfies the following three requirements:

1. The limiting process  $\alpha \rightarrow 0$  ought to be studied with  $\varepsilon$  fixed.
2. Both terms  $\beta H_1$  and  $\gamma$  are retained on the right-hand side of the extended KdV equation, cf. (2.39) and (2.40).

3. Allowing to perform the analysis without the use of any turbulence modelling or empirical parameters.

These requirements are satisfied by coupling the small parameters  $\alpha$ ,  $\text{Fr}_{\tau,r}$ ,  $\varepsilon$  as follows:

$$\alpha = \text{Fr}_{\tau,r}^2(1 - \varepsilon^{3m}) = 3\text{Fr}_{\tau,r}^2 m \ln(1/\varepsilon) + \dots \quad \text{with} \quad m \rightarrow 0, \quad \varepsilon \text{ fixed}, \quad (3.2)$$

$$\text{Fr}_{\tau,r}^2 = B\varepsilon^{5/2-m}, \quad (3.3)$$

where  $B$  is a constant of the order 1. Thus, the limiting process of a vanishing bottom slope is controlled by the coupling parameter  $m$ , which is not to be mistaken with the parameter of elliptic integrals in Sec. 2.2.

The dependent variables are now expanded in terms of small values of  $\varepsilon$ , cf. (2.33). The basic state does not change with respect to the case of a horizontal bottom, i.e. (2.17) and (2.18). The following relationships are obtained for the first-order quantities:

$$U_1 = -H_1 + \varepsilon^{(1-2m)/4}\sqrt{B}\Delta U(Y), \quad V_1 = H_{1,X}Y, \quad P_1 = H_1. \quad (3.4)$$

Without turbulence modelling, the first-order perturbation of the Reynolds shear stresses can be determined only at the boundaries, i.e.

$$(\overline{U'V'})_1(X, 0) = 2H_1, \quad (\overline{U'V'})_1(X, 1) = -H_1[1 + (\Delta\overline{U'V'})_Y(1)]. \quad (3.5)$$

The first equation in (3.5) is obtained by expanding the logarithmic law up to first-order terms, using the relation (2.6). The second equation follows from the dynamic boundary condition at the free surface, (2.10a), neglecting terms of order  $\varepsilon^{1+m}$  and smaller.

Analogue to Sec. 2.3,  $H_1(X)$  is to be determined from a solvability condition of the second-order equations. Performing the analysis as described in [22, 28], the second-order perturbation equations resulting from the momentum equation in  $X$ -direction, (3.1a), and from the kinematic boundary condition, (2.9), are compatible if

$$H_{1,XXX} + H_{1,X}(H_1 - 1) = \beta H_1 \left[ 1 + \frac{1}{3}(\Delta\overline{U'V'})_Y(1) \right] - \gamma, \quad (3.6)$$

with

$$\beta = \frac{\text{Fr}_{\tau,r}^2}{3\varepsilon^{3/2}} = \frac{B}{3}\varepsilon^{1-m}, \quad \gamma = \frac{\text{Fr}_{\tau,r}^2 - \alpha}{9\varepsilon^{5/2}} = \frac{B}{9}\varepsilon^{2m}. \quad (3.7)$$

To obtain an extended KdV equation of the form of (2.39), i.e.

$$H_{1,XXX} + H_{1,X}(H_1 - 1) = \beta H_1 - \gamma, \quad (3.8)$$

it is assumed that

$$(\Delta \overline{U'V'})_Y(1) \ll 1. \quad (3.9)$$

This assumption corresponds to an upstream flow according to the hydraulic approximation, as discussed in the next section.

### 3.3 Hydraulic approximation

A one-dimensional flow approximation together with a hydrostatic pressure distribution is often called the ‘hydraulic approximation’. Dropping the term  $H_{1,XXX}$  in (3.8) leads to the hydraulic approximation in the limit  $\varepsilon \ll 1$  [27]<sup>1</sup>:

$$\frac{dH_1}{dX} = \frac{\beta H_1 - \gamma}{H_1 - 1}. \quad (3.10)$$

Obviously, (3.10) becomes singular as the surface elevation approaches the critical value  $H_1 = 1$ , where the local Froude number  $\text{Fr} = q/\sqrt{gh^3} = 1$ . This shows the inability of the one-dimensional flow approximation of classical hydraulics, cf. [23], Sec. 3.3, to describe undular hydraulic jumps. However, it may serve as an approximate solution for the flow upstream of the jump. An example will be given below. For that purpose (3.10) is integrated, choosing  $H_1(0) = 0$  as boundary condition, to obtain the following implicit solution for  $H_1(X)$  in one-dimensional (‘hydraulic’) approximation:

$$X(H_1) = [H_1 + (\Gamma - 1) \ln(1 - H_1/\Gamma)]/\beta, \quad (3.11)$$

with  $\Gamma = \gamma/\beta$ . We shall see that (3.11) may also be used to determine appropriate initial conditions for (3.8), i.e. initial value  $H_1(X_i)$ , slope  $H_{1,X}(X_i)$  and curvature  $H_{1,XX}(X_i)$ , for any value  $X = X_i$  chosen sufficiently far away from the critical value  $X = X^*$ , where  $H_1 = 1$ .

If the term  $H_{1,XXX}$  were dropped in (3.6) rather than in (3.8), the result would not be in accord with the hydraulic approximation. Thus, the assumption (3.9) is consistent with describing the flow upstream of the hydraulic jump with the equations of the hydraulic approximation.

<sup>1</sup>The equation given in [27], p. 36, differs from the present one by a coefficient 5/3 in the  $\beta$ -term, due to an unusual definition of the local friction coefficient, using the reference velocity instead of the local velocity.

## 3.4 Results and discussion

Equation (3.8) may be solved numerically with standard methods, using the commercial software Matlab R2018b. Solutions of the initial value problem are obtained with the function `ode45`, and a relative error tolerance of  $10^{-4}$ , an absolute error tolerance of  $10^{-6}$ , and a maximum step size of  $10^{-4}$ . The two-point boundary-value problem is solved by means of the function `bvp4c`, with a relative and absolute error of  $10^{-5}$  and  $10^{-10}$ , respectively, and a maximum of  $10^5$  mesh points.

### 3.4.1 Numerical solutions of the extended KdV equation in the limit of vanishing bottom slope

As mentioned above, the purpose of this study is to analyse the behaviour of the undular hydraulic jump as the bottom slope  $\alpha \rightarrow 0$ , independently from  $\varepsilon$  and  $\text{Fr}_{\tau,r}$ . In Fig. 3.2 solutions of the extended KdV equation (3.8) with  $\beta$  and  $\gamma$  according to (3.7) are shown for the fixed values  $\text{Fr}_r = 1.06$  and  $\text{Fr}_{\tau,r} = 1.5 \cdot 10^{-2}$ . The bottom slope at which the reference state would be fully developed is  $\alpha_{\text{dev}} = \text{Fr}_{\tau,r}^2 = 2.25 \cdot 10^{-4}$ . Choosing the slope smaller than  $\alpha_{\text{dev}}$ , e.g.  $\alpha = 1.84 \cdot 10^{-4}$  (black curve), yields a solution that leads to a pool of liquid with horizontal surface far downstream (‘deep water’), cf. [28]. Slightly reducing the  $\alpha$  value (orange and green curves) leads to solutions with a breakdown at some distance downstream. With decreasing slope, the number of wave crests decreases until a single crest with breakdown immediately afterwards remains for  $\alpha = 1.74 \cdot 10^{-4}$  (red curve). In the case of a horizontal bottom, a breakdown of the solution is not surprising since a fully developed state, meaning mechanical equilibrium between friction force and weight force, does not exist. However, it is remarkable that by reducing the slope by  $10^{-5}$ , which is far beyond the usual measurement uncertainty in experiments, the solution of (3.8) undergoes a transition from approaching ‘deep water’ far downstream to only one wave crest with still almost the same amplitude. Note that by varying  $\alpha$ , according to (3.7) only the parameter  $\gamma$  changes, i.e.  $\gamma \rightarrow \text{O}(1)$  as  $\alpha \rightarrow 0$ . Thus, the damping effect of  $\gamma$  becomes dominant, and undulations are suppressed.

The black and red dashed curves in Fig. 3.2 represent solutions of (3.11) for  $\alpha = 1.84 \cdot 10^{-4}$  and  $\alpha = 1.74 \cdot 10^{-4}$ , respectively. This shows that the position of the critical state according to the hydraulic approximation at  $X = X^*$  moves upstream as the

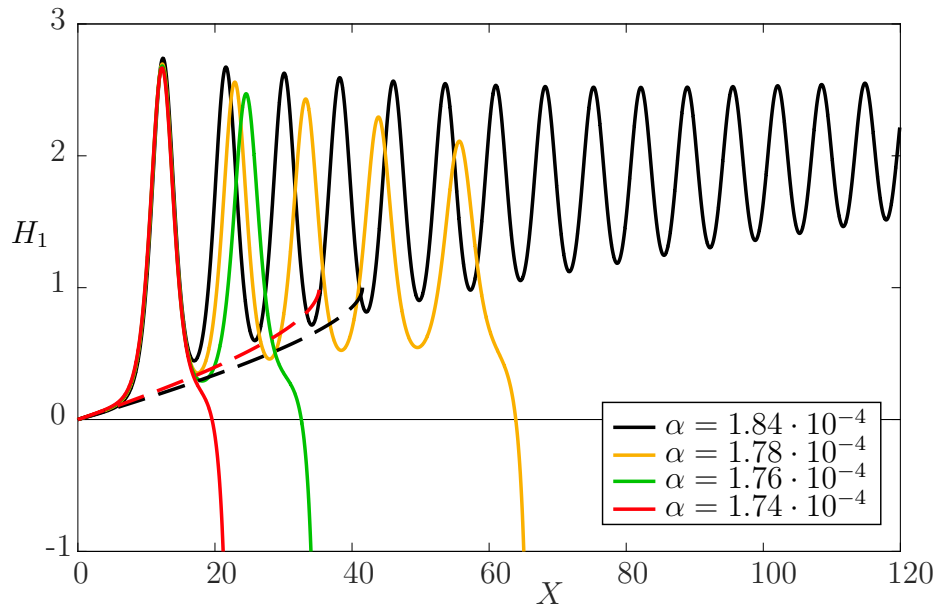


Figure 3.2: Numerical solutions of the extended KdV equation (3.8) for fixed Froude numbers  $Fr_r = 1.06$  ( $\varepsilon = 0.04$ ),  $Fr_{\tau,r} = 1.5 \cdot 10^{-2}$  and very small bottom slopes. Parameters:  $\beta = 9.38 \cdot 10^{-3}$ ,  $\gamma$  according to (3.7) ranging from  $\gamma = 1.42 \cdot 10^{-2}$  ( $\alpha = 1.84 \cdot 10^{-4}$ ) to  $\gamma = 1.77 \cdot 10^{-2}$  ( $\alpha = 1.74 \cdot 10^{-4}$ ). Initial conditions:  $H_1(0) = 0$ ,  $H_{1,X}(0) = \gamma$ ,  $H_{1,XX}(0) = \gamma^2$ . Dashed lines represent solutions of the hydraulic approximation (3.11) for  $\alpha = 1.84 \cdot 10^{-4}$  (black) and  $\alpha = 1.74 \cdot 10^{-4}$  (red).

slope decreases. More precisely,  $X^* \rightarrow [1 - (1 - 1/3\varepsilon) \ln(1 - 3\varepsilon)]/\beta$  as  $\alpha \rightarrow 0$ , that is,  $X^* \rightarrow 6.67$  for the chosen values of  $\varepsilon$  and  $Fr_{\tau,r}$  in Fig. 3.2. As will be discussed in the next section, it is reasonable to choose an initial point  $X_i$  for the solution of (3.8) in accord with the corresponding solution of (3.11). For the sake of comparison, in Fig. 3.2 the common initial point for all solid curves is  $X_i = 0$ , which is the only point where all curves according to (3.11) intersect.

### 3.4.2 Transition to fully developed flow far downstream

However small but different from 0 the bottom slope might be, a fully developed state far downstream exists provided that  $\Gamma > 1$ . Thus, the current analysis of the limiting process of vanishing bottom slope includes this special case, which is characterised by the downstream boundary condition  $H_1 = \Gamma$  as  $X \rightarrow \infty$ , cf. [28], or [27], p. 20.

In Fig. 3.3 the numerical solution of (3.8) as a two-point boundary-value problem with  $\beta = 0.12$  and  $\Gamma = 1.8$  is shown as a red curve. The boundary conditions at the upstream boundary are obtained by determining the position  $X_i$  and the corresponding slope  $H_{1,X}(X_i)$  from (3.11) and (3.10), respectively, for the chosen value  $H_1(X_i) = -3$ . The asymptotic downstream boundary condition has to be prescribed sufficiently far downstream, where the undulations are decayed, and uniform flow is reached. The position of this state strongly depends on the numerical values of both  $\beta$  and  $\Gamma$ . For  $\beta = 0.12$  and  $\Gamma = 1.8$ ,  $X = 100$  is sufficiently far downstream to prescribe  $H_1(100) = \Gamma = 1.8$ . However, for different combinations of  $\beta$  and  $\Gamma$ ,  $X = 100$  may not be far downstream enough, see e.g. Fig. 3.4. In general, small  $\beta$  values together with relatively large  $\Gamma$

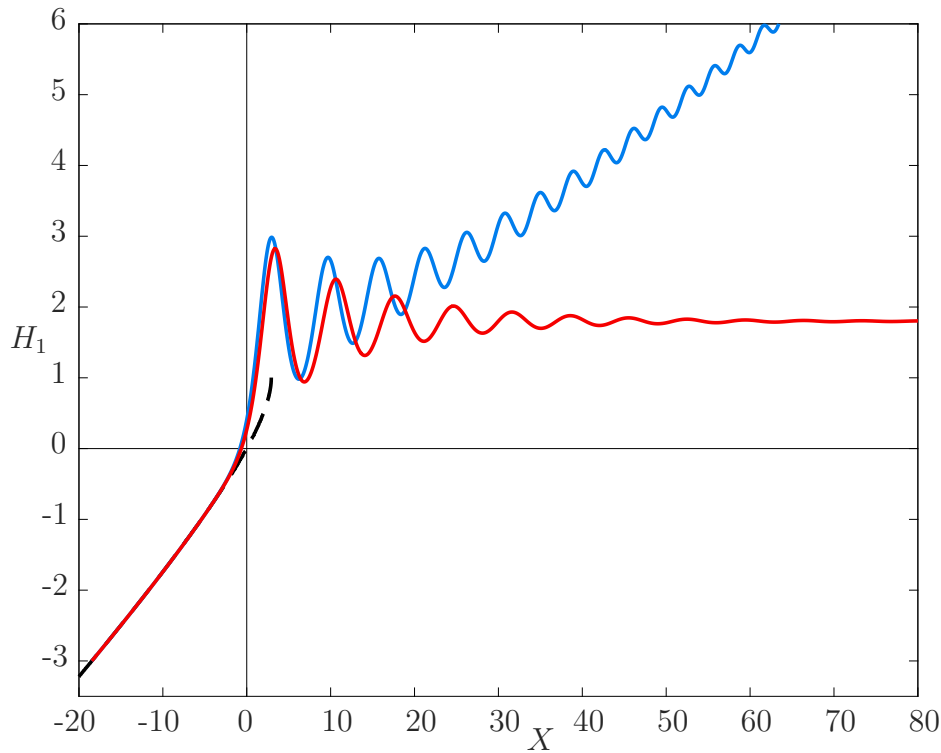


Figure 3.3: Comparison of numerical solutions of the extended KdV equation (3.8) with  $\beta = 0.12$ ,  $\Gamma = 1.8$ , solved as an initial value problem (blue) and as a two-point boundary-value problem approaching fully developed flow far downstream (red). Boundary and initial conditions: Two-point boundary-value problem:  $H_1(-18.46) = -3$ ,  $H_{1,X}(-18.46) = 0.144$ ,  $H_1(100) = 1.8$ ; Initial value problem:  $H_1(-18.46) = -3$ ,  $H_{1,X}(-18.46) = 0.144$ ,  $H_{1,XX}(-18.46) = 9.01 \cdot 10^{-2}$ . Dashed line: solution of the hydraulic approximation (3.11).

values cause more undulations, and thus the downstream boundary condition is to be prescribed further downstream. Interestingly, the red curve in Fig. 3.3 closely follows the hydraulic approximation (dashed line) for quite a long distance. Nevertheless, shortly before the coordinate system's origin, the solution of (3.8) develops into an undular hydraulic jump with strongly decaying amplitude. This behaviour indicates that the extended KdV equation (3.8) is not only uniformly valid downstream of the jump, [52], but also accurately represents the inflow.

The curvature of the red curve at the initial point  $X_i = -18.46$  is 4.24% larger than the curvature of the corresponding solution of the hydraulic approximation, (3.11), at this position. Using the enlarged curvature, together with the initial value and initial slope prescribed for the two-point boundary-value problem, to solve (3.8) as an initial value problem yields the blue curve in Fig. 3.3. As discussed in [27], p. 45, the numerical error always gives rise to a solution of the initial value problem, approaching the asymptote  $H_1 = \beta X$  rather than  $H_1 = \Gamma$  as  $X \rightarrow \infty$ . However, the blue curve initially also closely follows the hydraulic theory's solution (dashed curve). It appears that choosing  $X_i = 0$  as the upstream boundary for the two-point boundary-value problem as well as for the initial value problem, as it was done in previous studies, [27, 28], has to be taken with reservations. As shown in see Fig. 3.3, the solutions of (3.8) may bifurcate from the one-dimensional hydraulic theory already before  $X = 0$ .

In Fig. 3.4 solutions of (3.8) as a two-point boundary-value problem are compared, prescribing decreasing bottom slope values. Keeping the Froude numbers  $Fr_r = 1.15$  and  $Fr_{\tau,r} = 8.65 \cdot 10^{-2}$  (i.e.  $\beta = 7.89 \cdot 10^{-2}$ ) fixed, solutions of (3.8) are obtained by altering the slope from  $\alpha = 4 \cdot 10^{-3}$  to  $\alpha = 2 \cdot 10^{-3}$ . The decreasing slope results in increasing values of  $\Gamma$ . For all curves the upstream boundary conditions are obtained by determining  $X_i$  and the corresponding slope  $H_{1,X}(X_i)$  from (3.11) for the chosen value  $H_1(X_i) = -3$ . The asymptotic downstream boundary condition  $H_1 = \Gamma$  is prescribed at  $X = 450$ , where a uniform flow is reached even for the largest used  $\Gamma$  value. The comparison shows that in contrast to solutions of the initial value problem (cf. Fig. 3.2), a decreasing bottom slope leads to a rising number of undulations and rising amplitudes. Two reasons are responsible for this behaviour: First, with decreasing slope, the fully developed state is reached further downstream. In Fig. 3.4 the blue curve ( $\alpha = 4 \cdot 10^{-3}$ ) reaches the fully developed state, i.e. the position where the undulations decay, at  $X \approx 100$ , while the green curve ( $\alpha = 2 \cdot 10^{-3}$ ) only at  $X \approx 270$ . Second, an increasing value of  $\Gamma$

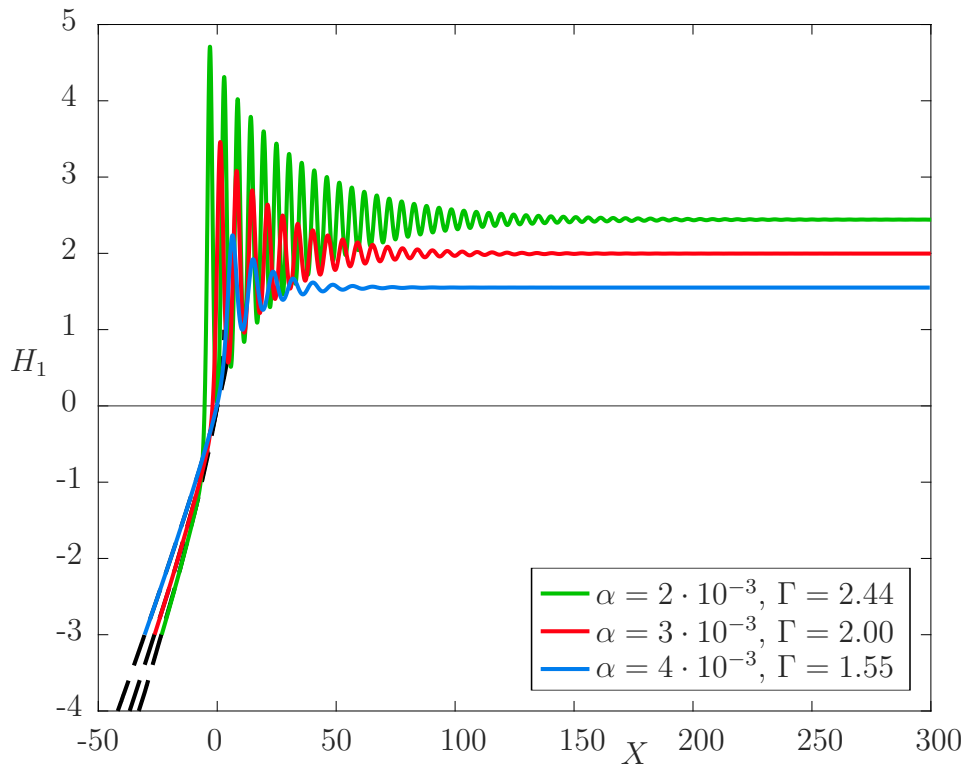


Figure 3.4: Numerical solutions of the extended KdV equation (3.8) as a two-point boundary-value problem for decreasing bottom slope.  $Fr_r = 1.15$ ,  $Fr_{\tau,r} = 8.65 \cdot 10^{-2}$ , i.e.  $\beta = 7.88 \cdot 10^{-2}$ . Upstream boundary conditions:  $H_1(X_i) = -3$ ,  $X_i$  and  $H_{1,X}(X_i)$  according to (3.11) and (3.10), respectively. Downstream boundary condition  $H_1(450) = \Gamma$ . Dashed lines are the corresponding solutions of the hydraulic approximation (3.11).

corresponds to stronger wave damping, cf. Sec. 3.4.1. Thus, higher amplitudes at the beginning of the jump are required to reach the fully developed state far downstream together with this stronger damping.

To obtain a numerical solution of the extended KdV equation as a two-point boundary-value problem is not straightforward. Whether Matlab finds a solution or not strongly depends on the initial guess. Especially, to find solutions for small values of  $\alpha$ , e.g. the red curve in Fig. 3.4, can be rather cumbersome. Thus, the solution procedure will be described in what follows. First, the parameters  $\beta$  and  $\Gamma = \gamma/\beta$  are computed from the desired values of  $Fr_r$ ,  $Fr_{\tau,r}$  and  $\alpha$  according to (3.7). In the next step a first approximate solution of (3.8) has to be computed starting from a uniform initialization, i.e.  $H_1 \equiv \Gamma$ .

For that purpose, it might be necessary to choose  $\beta$  larger than the desired value while keeping  $\Gamma$  unchanged. For the red curve in Fig. 3.4 one may choose  $\beta = 0.35$  and  $\Gamma = 2$ . The resulting curve will have few undulations, similar to the blue curve in Fig. 3.4, and will serve as an initial guess for the next computation. In the following steps, the value of  $\beta$  is successively decreased until the target value ( $\beta = 7.88 \cdot 10^{-2}$  for the red curve) is reached, always using the solution of the previous step as the initial guess for the next step. The number of undulations will continuously increase. At some point, the computational domain may have to be extended to guarantee that the boundary condition  $H_1 = \Gamma$  is prescribed sufficiently far downstream of the decaying undulations.

### 3.4.3 Comparison with experimental data

The experiment by Chanson [12], CD1, with  $Fr_r = 1.266$  and  $Fr_{\tau,r} = 5.54 \cdot 10^{-2}$ , and the experiment by Reinauer and Hager [43], Fig. 11a, with  $Fr_r = 1.447$  and  $Fr_{\tau,r} = 6.07 \cdot 10^{-2}$  are chosen for comparison with the present theory. The friction Froude numbers are determined from the relations (2.41–2.43). Both experiments were performed in horizontal channels. Since the present analysis is based on vanishing but non-zero bottom slope, a small but finite value  $\alpha = 10^{-8}$  is used for the comparisons.

In Fig. 3.5 the measured surface elevation [12] is represented by squares. Chanson [12] indicates an uncertainty in the measurement of the volume flow rate  $q$  of about 2%. Therefore, solutions of (3.8) were first obtained for a parameter set corresponding to  $q = 9.14 \cdot 10^{-2} \text{ m}^2/\text{s}$  as reported by Chanson [12] (blue solid curve), and then for parameters corresponding to a 2% smaller volume flow rate (red solid curve). Both the blue and red solid curves are shifted along the corresponding solution of (3.11), i.e. the blue and red dashed line, respectively, such that the first wave crest is in accord with the experimental data. Whereas the first wave crests of both solid curves are almost identical, the successive crests show significant differences, especially concerning the wavelength. Reasonable agreement between experimental data and the solution of the extended KdV equation (3.8) is obtained only by incorporating the measurement uncertainty. This indicates the sensitivity of the surface elevation with respect to small changes in the volume flow rate, as already observed in [22, 28].

In Fig. 3.6 the black squares represent the experimental data obtained by Reinauer and Hager [43], presented as white squares in their Fig. 11a. While the authors referred to the third measurement point and reported  $Fr_r = 1.36$ , we refer to the second

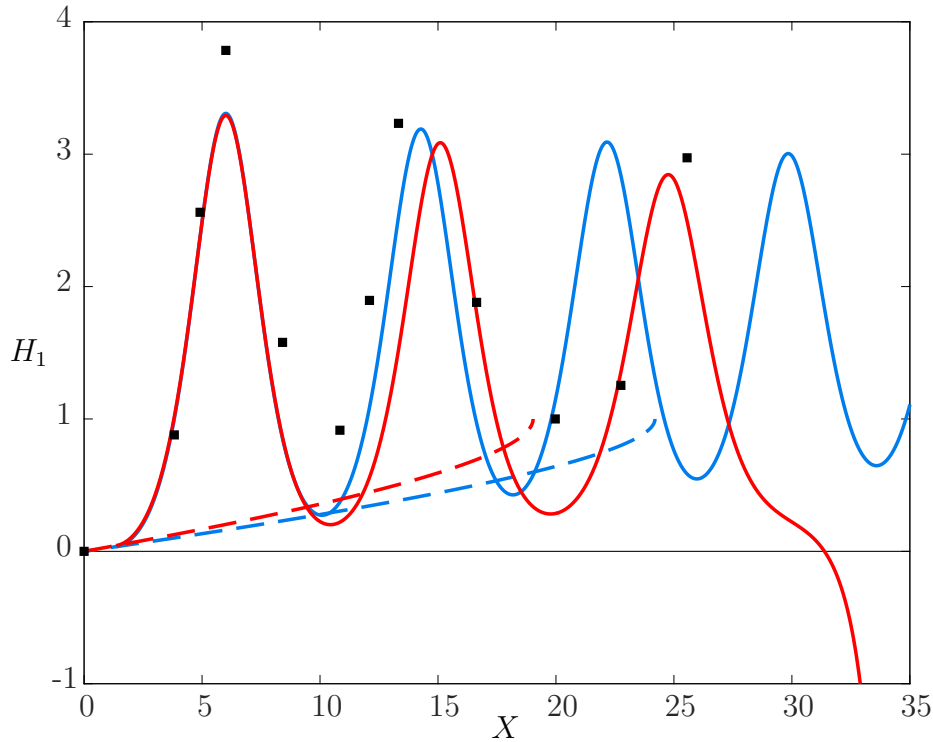


Figure 3.5: Comparison of solutions of the extended KdV equation (3.8) with experimental data considering measurement uncertainties. Squares: Measured surface elevation [12] in a horizontal channel of width  $b = 0.5$  m,  $\bar{h}_r = 81$  mm,  $q = 9.14 \cdot 10^{-2}$  m<sup>2</sup>/s  $\pm 2\%$   $\Rightarrow Fr_r = 1.266 \pm 2\%$ ,  $Fr_{\tau,r} = 5.54 \cdot 10^{-2} \pm 1.8\%$ . Dashed lines: solutions of the hydraulic approximation (3.11). Solid lines: Numerical solutions of (3.8) for the initial conditions  $H_1(0) = 0$ ,  $H_{1,X}(0) = \gamma$ ,  $H_{1,XX}(0) = 0.2$ . Blue curves:  $Fr_r = 1.266$ ,  $Fr_{\tau,r} = 5.54 \cdot 10^{-2}$ , i.e.  $\varepsilon = 0.177$ ,  $\beta = 1.37 \cdot 10^{-2}$ ,  $\gamma = 2.58 \cdot 10^{-2}$ . Red curves:  $Fr_r = 1.266 - 2\%$ ,  $Fr_{\tau,r} = 5.54 \cdot 10^{-2} - 1.8\%$ , i.e.  $\varepsilon = 0.160$ ,  $\beta = 1.53 \cdot 10^{-2}$ ,  $\gamma = 3.19 \cdot 10^{-2}$ .

measurement point in order to compare also the inflow behaviour, and thus obtain  $Fr_r = 1.447$ , cf. [28], Fig. 10. The solid line shows the numerical solution of (3.8), prescribing the initial value and initial slope in accord with the hydraulic approximation (3.11) and the initial curvature 20% larger than the corresponding value according to (3.11). Both experimental data and numerical solution of (3.8) initially follow the hydraulic approximation, indicated by the dashed line. After some distance, the undular jump develops, and the shape of the first wave crest is well approximated by the

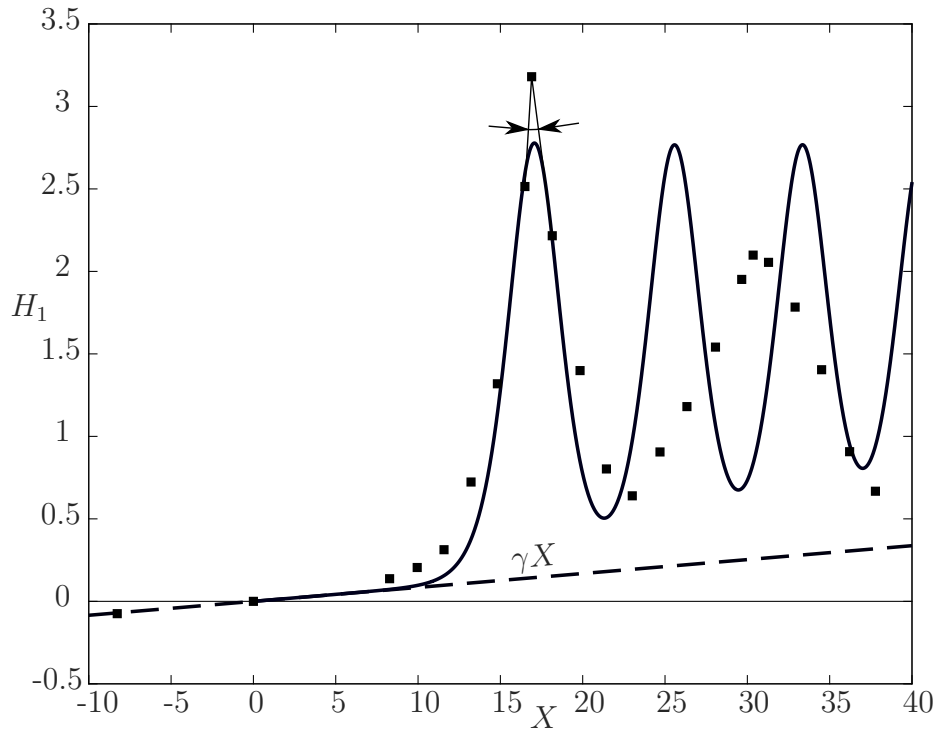


Figure 3.6: Comparison of the surface observed by [43] (squares) with a numerical solution of the extended KdV equation (3.8) (solid line). The experimental data  $b = 0.5$  m,  $\bar{h}_r = 105$  mm,  $q = 0.154$  m<sup>2</sup>/s correspond to  $Fr_r = 1.447$  ( $\varepsilon = 0.298$ ),  $Fr_{r,r} = 6.07 \cdot 10^{-2}$  and the parameters  $\beta = 7.55 \cdot 10^{-3}$ ,  $\gamma = 8.44 \cdot 10^{-3}$  used for solving (3.8) with the initial conditions  $H_1(0) = 0$ ,  $H_{1,X}(0) = \gamma$ ,  $H_{1,XX}(0) = 1.2\gamma(\gamma - \beta) = 9.01 \cdot 10^{-6}$ .

solid line, except for the sharp peak. However, Reinauer and Hager stated that this experiment represented the limiting case to the first wave crest's incipient breaking, a phenomenon that is excluded in the current theory. Computation of the angle between the three measurement points at the first crest from the original data, i.e. height  $\bar{h}$  at a position  $x$ , both in metres, yields an angle of  $120.88^\circ$ . This value is in excellent agreement with the theoretical angle of  $120^\circ$  enclosed between the two tangents at the crest of a breaking wave, see [34], Sec. 14.50.

# Chapter 4

## Conclusions of Part I

In this part of the thesis, we investigated the undular hydraulic jump in steady turbulent open-channel flow in the limit of very large Reynolds numbers and Froude numbers close to the critical value 1. Both a horizontal bottom and a bottom in the limit of vanishing slope were considered. The first-order results remain free of turbulence modelling by restricting the investigation to a specific parameter regime characterised by an order 1 coupling parameter  $B$ . In the case of a vanishing bottom slope, the inflow is prescribed according to the hydraulic approximation, i.e. (3.11).

To investigate the flow over a horizontal bottom, a multiple-scales analysis was performed analogous to [52]. The results show that the extended KdV equation, (2.35), where the constant extension represents the deviation of the reference state from a fully developed flow, is uniformly valid. However, the comparison of numerical solutions of (2.35) with the theory of undular hydraulic jumps over inclined bottoms [28] demonstrates that undular solutions of (2.35) are only possible by prescribing extraordinarily large initial curvatures. A linear second extension term representing dissipation seems essential in the extended KdV equation to obtain undular jump solutions with moderate initial curvature values, cf. (2.39). In comparison with experimental data [12] the numerical solutions of (2.35) predicted too large amplitudes.

To gain more insight into the undular hydraulic jump, the limiting process of a vanishing bottom slope  $\alpha$  was analysed. Introducing the control parameter  $m \rightarrow 0$  according to (3.2) and (3.3), allowed to perform the limiting process  $\alpha \rightarrow 0$  by keeping the Froude and Reynolds numbers fixed. The main result of the asymptotic analysis of near-critical flow is the extended KdV equation (3.8) with the two extension parameters

according to (3.7). Numerical solutions of (3.8) as an initial value problem were analysed by solely altering the bottom slope. As  $\alpha$  decreases, wave damping becomes stronger, and the number of undulations decreases until, eventually, one single wave crest with immediate breakdown afterwards remains. Interestingly, solving (3.8) as a two-point boundary-value problem with the asymptotic boundary condition of fully developed flow far downstream shows entirely different behaviour. With decreasing  $\alpha$ , the number of undulations and their amplitudes rise due to the combination of stronger damping and a fully developed state, which is reached further downstream. The analysis shows further that upstream of the jump, the solution of (3.8) is in accord with the one-dimensional hydraulic approximation (3.11). This suggests to choose an initial point for the solution of (3.8) sufficiently far upstream of the jump, and with initial conditions according to (3.11), in order to minimise the error introduced by unrealistic upstream conditions. Using extremely small slope values, e.g.  $\alpha = 10^{-8}$ , models very well the case of a horizontal bottom and yields undular jump solutions by prescribing moderate initial curvatures. The comparison of numerical solutions of (3.8) with experimental data, [12], turned out to be rather sensitive to relatively small uncertainties in the measurements. The comparison with an experiment conducted with marginal wave breaking, [43], showed that the inflow, as well as the first wave, were well represented by the solution of (3.8), except for the measured sharp peak. Given the remarkable fact that the analytical results are free of empirical constants, the agreement between theory and experiments can be considered satisfactory.

## Part II

# Undular hydraulic jumps in axisymmetric flow

# Chapter 5

## Introduction

The classical circular hydraulic jump (without undulations) is a phenomenon occurring in everyday life, e.g. when a jet of liquid impinges on a horizontal plate and spreads radially. Therefore, it is often referred to as the ‘kitchen sink problem’ and first found attention by Lord Rayleigh [42] as early as in 1914, who observed the jump in his experiments. In the past century, various aspects of the circular hydraulic jump have been examined both experimentally and theoretically, and in recent times also numerically.

Viscosity has been shown to be essential for the development of the classical circular jump, and thus considering inviscid flow is a rather strong oversimplification [2, 16]. Most theoretical studies are dedicated to the prediction of the jump radius. Therefore, applying the hydraulic approximation seems to be a suitable approach, cf. [2, 16, 30, 54]. Assuming the jump to be a discontinuity between the supercritical and the subcritical flow regimes, Bohr *et al.* [2] defined jump conditions and determined the jump radius by taking into account the radius of the edge of the bottom plate. The jump conditions were extended by Kasimov [30] considering the effect of surface tension. In a comprehensive analysis, Watson [58] studied the thin film upstream of the jump by the boundary layer equations and derived a similarity solution. Jump conditions were defined by distinguishing between hydraulic jumps occurring before and after the boundary layer reaches the free surface. Moreover, while most studies consider laminar hydraulic jumps, Watson analysed both laminar and turbulent flow by introducing an eddy viscosity. However, compared with experiments, the laminar flow solution showed better agreement than the solution for turbulent flow.

Laminar circular hydraulic jumps are generally divided into type I and type II jumps

[3]. Type I jumps are characterised by a recirculation bubble attached to the wall just below the jump. The separation occurs due to the abrupt increase of the hydrostatic pressure at the jump, [32]. In type II jumps, additionally to the recirculation bubble at the wall, a second eddy appears on the free surface, commonly called surface roller. The surface roller is essentially associated with surface tension and may be observed if the downstream flow depth is relatively large, and thus the transition from super- to sub-critical flow causes a strong curvature of the free surface [59]. If the downstream depth is further increased, it will become higher than the surface roller, and the transition will appear as a double jump, [8, 32].

In a surface tension dominated flow, oscillating capillary waves develop upstream of the circular jump [4, 15, 24]. Bush and Aristoff [7] extended Watson's theory, [58], by a correction term taking into account surface tension. Their comparison with experiments showed that surface tension effects are generally weak in laboratory settings and become more important in jumps of small radius and height.

In highly viscous liquids, symmetry-breaking hydraulic jumps may occur as steady as well as time-dependent, i.e. rotating, structures. In their experimental analysis of increasing downstream flow depth, Bohr *et al.* [3] observed hexagonal rotating jumps as the final stage before the jumps disappeared. Stationary polygonal jumps such as a pentagon were reported by Ellegaard *et al.* [18]. In both studies, the symmetry-breaking jumps are characterised by sharp corners that carry large radial flow rates, while the structures' sides generate resistance to the flow. A new class of even more irregular structures restricted to a very narrow parameter regime was presented by Bush *et al.* [8]. This class includes jumps of the shape of cat-eyes, three- and four-leaf clovers, and butterflies, the latter exhibiting only a single symmetry plane. All symmetry-breaking structures emerge exclusively from circular type II jumps and show a clear dependence on surface tension as they relax to circular jumps if a surfactant is added, [8]. Also, Kasimov [30] observed that increasing surface tension acts destabilizing on the laminar circular jump, possibly causing the transition to symmetry-breaking instabilities.

Surface tension dominated circular jumps have been experimentally observed by Mathur *et al.* [33] when molten iron droplets impinged on a solid substrate and solidified into cup-shaped containers of femtoliter capacity.

The present part of the thesis addresses *undular* hydraulic jumps in steady axisymmetric flow, which are hardly discussed in the literature. Ishigai *et al.* [26] showed

sketches of the different types of observed circular hydraulic jumps (Fig. 7 in [26]) depending on the upstream Froude number  $Fr$ , indicating an undular transition if  $1 < Fr < 2$ . However, Craik *et al.* [15] reported that in their transient experiments where a tank slowly got filled by a jet of liquid impinging on the bottom plate, the undular jump was never observed while the following types shown in [26] did occur. The laminar internal circular jump was investigated by Thorpe and Kavčič [55] introducing a saline solution at a constant flow rate through a tube into a tank filled with fresh water. They observed an undular transition during the initial stage, such as reported in [26]. Due to the stratified flow, surface tension plays a minor role, and undulations can develop, in contrast to experiments with a free surface as e.g. in [15]. This conclusion is supported by the analysis of Fernandez-Feria *et al.* [19] who compared numerical solutions of the Navier–Stokes equations by considering and neglecting surface tension. Their results show undular circular jumps by neglecting surface tension even for upstream Froude numbers  $7.6 < Fr < 9.4$ . However, the undulations were suppressed by taking surface tension effects into account.

Undular hydraulic jumps with curved front can also be observed in natural environments. Figure 5.1 shows the photograph of an undular hydraulic jump with a concave front, formed when rainwater was flowing over the pavement across the street towards the manhole. A photograph of an undular jump with a convex front is shown in Fig. 5.2, where artistic obstacles in a flume triggered the curved undular hydraulic jump. Throughout the thesis’s development, these photographs served as motivation for the investigation, as concave and convex undular jumps are expected to occur in near-critical axisymmetric source and sink flow, see Ch. 8 and 9, respectively. However, both phenomena were observed outside of laboratory settings with an irregular curvature radius and inclined bottoms. In contrast, the analysis in this thesis will be restricted to axisymmetric flow over horizontal surfaces.

To the author’s knowledge, the *circular* undular hydraulic jump in *turbulent* free-surface flow has neither been observed in laboratory experiments nor has it ever been analysed theoretically or numerically. The present part of the thesis is dedicated to answering under which conditions such a flow phenomenon may occur.

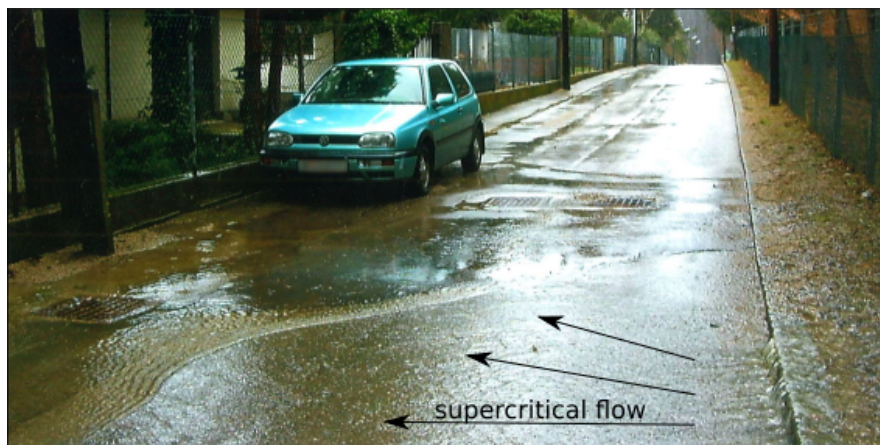


Figure 5.1: Observation of an undular hydraulic jump with concave front. Photograph taken by R. Kolda in Vienna, Austria on 7 March 2009.



Figure 5.2: Observation of an undular hydraulic jump with convex front. Photograph taken by H. Steinrück in Karlsruhe, Germany on 24 March 2010.

# Chapter 6

## Hydraulic approximation

We consider steady turbulent axisymmetric free-surface flow over a horizontal bottom, see Fig. 6.1. Cylindrical coordinates are introduced, with  $r$  and  $z$  in radial and vertical direction, respectively. An overbar denotes a time-averaged quantity. In the following, surface tension will be neglected as it plays a minor role in hydraulic structures with turbulent flow, see [11], p. 265.

The hydraulic approximation is a one-dimensional flow approximation considering a hydrostatic pressure distribution, cf. [2, 16, 54, 56]. We know from previous studies, [22, 27, 36], that the hydraulic approximation is incapable of representing an undular jump, cf. also Sec. 3.3. Nevertheless, it may give valuable insight into the upstream flow behaviour and the differences between plane and axisymmetric flow. Thus, the continuity equation reads

$$r\bar{h}\bar{u}_m = Q = \text{const}, \quad (6.1)$$

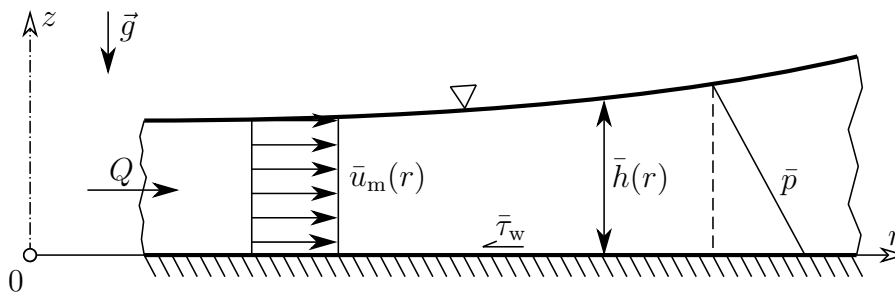


Figure 6.1: The hydraulic approximation of axisymmetric free-surface flow over a horizontal bottom.

where  $\bar{u}_m(r)$  is the local volumetric mean velocity and  $Q$  denotes the volume flow rate per unit azimuth angle. The equation of motion in radial direction is

$$\bar{u}_m \frac{d\bar{u}_m}{dr} + g \frac{d\bar{h}}{dr} = -\frac{c_f}{2} \frac{\bar{u}_m^2}{\bar{h}}, \quad (6.2)$$

using a hydrostatic pressure distribution  $\bar{p} = \rho g(\bar{h} - z)$ , and the effect of friction represented by the friction coefficient  $c_f = 2\bar{\tau}_w/\rho\bar{u}_m^2$ . The local Froude number is defined as

$$\text{Fr}(r) := \frac{Q}{r\sqrt{g\bar{h}^3}}. \quad (6.3)$$

Combination of (6.1–6.3) leads to the differential equation for the local Froude number,

$$\frac{d\text{Fr}}{dr} = \frac{\text{Fr}^3}{2(\text{Fr}^2 - 1)} \left[ \frac{1}{r} \frac{\text{Fr}^2 + 2}{\text{Fr}^2} - 3 \frac{c_f}{2} \left( \frac{g}{Q^2} \right)^{1/3} (r\text{Fr})^{2/3} \right], \quad (6.4)$$

which has a singularity at  $\text{Fr} = 1$ .

## 6.1 Inviscid flow

With a sufficiently large Reynolds number, corresponding to a very small friction coefficient, the flow can be assumed as inviscid. In the framework of the hydraulic approximation the inviscid flow condition,  $c_f \ll \bar{h}/r$ , follows from (6.4) by substituting  $Q^2/g = \text{Fr}^2 r^2 \bar{h}^3$  according to (6.3). With that condition satisfied, the last term in (6.4) drops out, and the equation reduces to

$$\frac{d\text{Fr}}{dr} = \frac{1}{r} \frac{\text{Fr}(\text{Fr}^2 + 2)}{2(\text{Fr}^2 - 1)}. \quad (6.5)$$

Integration yields an implicit relation for the local Froude number, i.e.

$$\frac{r}{r^*} = \frac{(2 + \text{Fr}^2)^{3/2}}{3\sqrt{3}\text{Fr}}. \quad (6.6)$$

The asterisk refers to the critical state, where  $\text{Fr} = 1$ . Note that (6.6) is ‘universal’ as it is free of parameters describing the upstream state. A near-critical version of the hydraulic approximation is obtained by expanding (6.6) for  $|\text{Fr} - 1| \ll 1$ . The result is

$$\text{Fr} = 1 \pm \sqrt{\frac{3}{2} \left( \frac{r}{r^*} - 1 \right)}, \quad (6.7)$$

with the positive and negative signs corresponding to the supercritical and subcritical branches, respectively. In Ch. 7 solutions of both (6.6) and (6.7) will be used for comparison with a theory for undular hydraulic jumps in near-critical inviscid axisymmetric source flow, see Figs. 7.2 and 7.3.

## 6.2 Constant friction coefficient

In a first approximation the friction coefficient in (6.4) is assumed to be constant. Equation (6.4) describes spiral curves, cf. [2, 16], with the focal point at the critical state  $\text{Fr} = 1$  and the radius

$$r_s = \left( \frac{8Q^2}{c_f^3 g} \right)^{1/5}. \quad (6.8)$$

Thus, the singularity position only depends on the constant values of the discharge  $Q$  and the friction coefficient  $c_f$ .

Referring to the focal point, (6.4) can be rewritten in terms of the non-dimensional radius  $\hat{R} = r/r_s$ :

$$\frac{d\text{Fr}}{d\hat{R}} = \frac{\text{Fr}^3}{2(\text{Fr}^2 - 1)} \left[ \frac{1}{\hat{R}} \frac{\text{Fr}^2 + 2}{\text{Fr}^2} - 3(\text{Fr}\hat{R})^{2/3} \right]. \quad (6.9)$$

Equation (6.9) is again free of parameters describing the upstream state, and thus its solutions are a universal family of curves of the local Froude number  $\text{Fr}(\hat{R})$ , see Fig. 6.2. The curves shown in Fig. 6.2 were determined by transforming  $\text{Fr}$  and  $\hat{R}$  in (6.9) into the polar coordinates  $\xi$  and  $\phi$  according to

$$\hat{R} = 1 + \xi \cos\phi, \quad \text{Fr} = 1 + \xi \sin\phi, \quad (6.10)$$

and integrating in both clockwise and counter-clockwise direction starting from the critical point, where  $\text{Fr}(r^*) = 1$  and  $\hat{R}^* = r^*/r_s$  ranges from 0.35 to 0.95.

The enumerator on the right-hand side of (6.9) is zero if

$$\hat{R} = \left( \frac{(2 + \text{Fr}^2)^3}{27\text{Fr}^8} \right)^{1/5}, \quad (6.11)$$

which is a relation for the position where the sub- and supercritical branches of the integral curves reach their minima and maxima, respectively. The dash-dotted curve in Fig. 6.2 is plotted according to (6.11). The close-up illustrates the continuous spiralling towards the focal point at  $\text{Fr} = 1$ ,  $\hat{R} = 1$ . Due to the lack of asymptotic states as

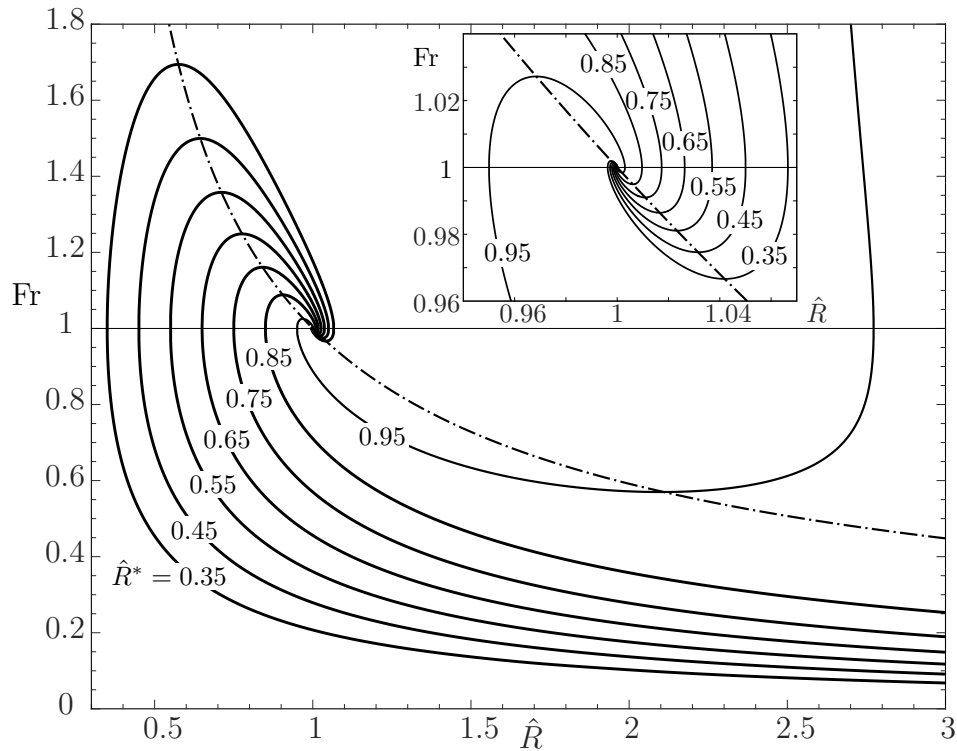


Figure 6.2: Universal family of curves (solid lines) of the hydraulic approximation of axisymmetric flow with constant friction coefficient, (6.9). Along the dash-dotted line, i.e. the solution of (6.11), the sub- and supercritical branches of the solid curves reach their minimum and maximum values, respectively.

$\hat{R} \rightarrow \infty$ , the spiralling also continues away from the focal point, cf. [2]. Following the subcritical branches of the integral curves, with increasing  $\hat{R}$  each of them will eventually turn around, as shown for the innermost curve ( $\hat{R}^* = 0.95$ ). These turnarounds confine the regions of possible subcritical flow solutions along each particular integral curve. Following the integral curves in a counter-clockwise direction past these turnarounds leads to a rapidly changing Froude number. This violates the hydraulic approximation's basic assumption of a slowly varying flow, similar to the invalidity at the critical state, where  $dFr/d\hat{R}$  diverges. Thus, a branch with such large gradients must be considered as beyond the theory's validity limits.

Instead of referring to the singular point  $r_s$ , one may refer to the critical radius  $r^*$ , i.e. the leftmost radius  $\hat{R}^*$  of each curve in Fig. 6.2. Figure 6.3 shows the solid curves of Fig. 6.2 by referring to  $r^*$ . This means that a curve with a certain value of  $\hat{R}^*$  in Fig. 6.2 corresponds to the curve with  $r_s/r^* = 1/\hat{R}^*$  in Fig. 6.3. In the representation of

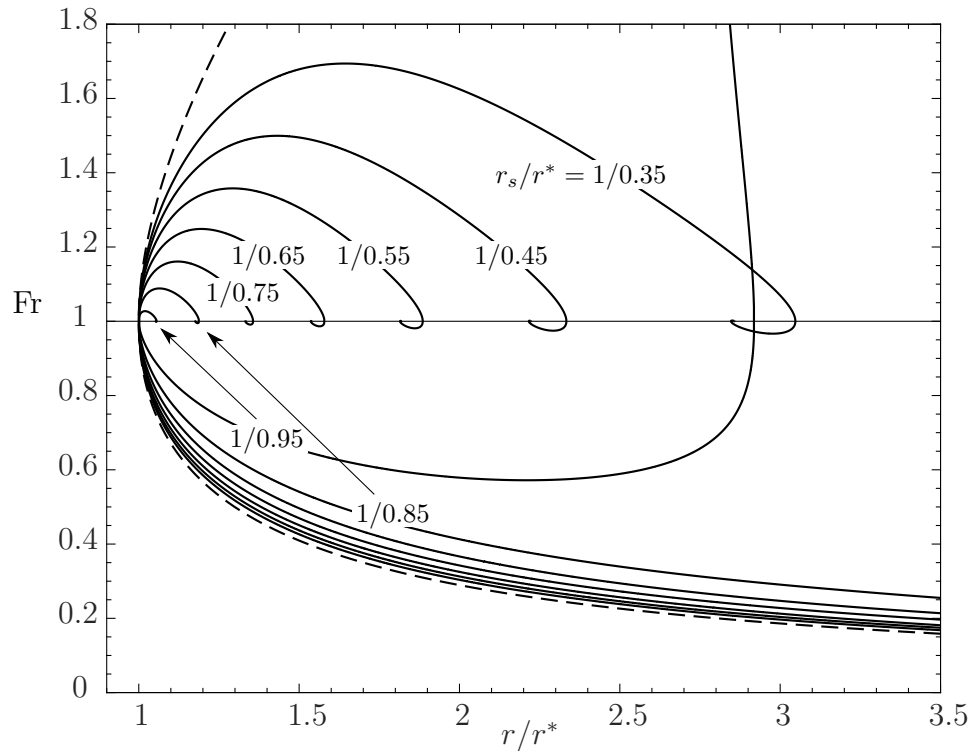


Figure 6.3: Diagram of the hydraulic approximation of axisymmetric flow with constant friction coefficient referring to the critical radius  $r^*$ . Solid lines: Solutions of the hydraulic approximation (6.9) for various values of  $r_s/r^*$ . Dashed line: Inviscid flow solution (6.6), cf. [56], Fig. 2b.

Fig. 6.3, for a fixed discharge, each solid curve corresponds to a different value of  $c_f$ , with  $c_f$  decreasing as  $r_s/r^*$  increases, cf. (6.8). The dashed line represents the inviscid flow solution, (6.6), and encloses all possible solid curves as  $r_s/r^*$  increases. The smaller the value of  $c_f$ , the closer the corresponding sub- and supercritical branches of the solid curve approach the dashed curve. However, due to the cumulative effect of friction also in this diagram, the subcritical branches approach a critical state, as shown for the innermost curve ( $r_s/r^* = 1/0.95$ ) at  $r/r^* \approx 2.9$ . The comparison between the inviscid flow solution and curves considering friction in Fig. 6.3 shows that the cumulative friction effect acts stronger on the supercritical branches than on the subcritical branches.

## 6.3 Variable friction coefficient

Considering a variable friction coefficient  $c_f(r)$  requires the use of a friction law. Due to the lack of a friction law for turbulent axisymmetric free-surface flow, it is state of the art to use the concept of the hydraulic diameter  $D_h$ , which is in this case  $D_h = 4\bar{h}$ , see e.g. [47], p. 103. Therefore, the friction law of turbulent pipe flow is applied, i.e. (2.42) with the empirical constant  $D = 0.27$ , [20], p. 527.

Although the concept of hydraulic diameter is widely used, it should be applied with caution. For Couette–Poiseuille flows, Gersten and Herwig [20], p. 575, introduced the equivalent diameter  $D_{ae}$  to be used as characteristic length for the Reynolds number, in order to apply the friction law of pipe flow. However,  $D_{ae}$  differs from  $D_h$  by a factor depending on the flow, e.g. for plane channel flow  $D_{ae} = 0.87D_h$ . For tubes with non-circular cross section Idelchik [25], p. 97, suggested to multiply the friction coefficient according to (2.42) with  $D = 0.27$  by a correction factor based on empirical investigations. Schneider [49] derived a friction law for fully developed turbulent open-channel flow, which is of the same form as (2.42) but with a different value of the constant  $D$ .

None of the above-mentioned approaches seems to be more suitable for the present axisymmetric free-surface flow than the classical concept of hydraulic diameter. Thus, we shall continue by applying (2.42) and (2.43). Introducing  $c_f(r_s)$  according to (6.8), and evaluating  $\text{Re}_D$  at  $r_s$ , (2.42) becomes

$$\left(\frac{r_s^5 g}{Q^2}\right)^{1/6} = \frac{1}{\kappa} \ln \left[ \frac{4}{\nu} \left(\frac{Q^8}{r_s^{11} g}\right)^{1/6} \right] + D, \quad (6.12)$$

i.e. an implicit relation to determine the radius of the singular point  $r_s$  for chosen values of  $Q$  and  $\nu$ . Combining (6.1–6.3) and introducing the non-dimensional radius  $\hat{R} = r/r_s$  leads to

$$\frac{d\text{Fr}}{d\hat{R}} = \frac{\text{Fr}^3}{2(\text{Fr}^2 - 1)} \left[ \frac{1}{\hat{R}} \frac{\text{Fr}^2 + 2}{\text{Fr}^2} - 3 \frac{c_f(\hat{R})}{c_f(1)} (\text{Fr}\hat{R})^{2/3} \right], \quad (6.13)$$

with  $c_f(1)$  being the friction coefficient at the singular point  $\hat{R} = 1$ . Note that the ratio  $c_f(\hat{R})/c_f(1)$  is the only difference with respect to the equation for  $c_f = \text{const}$ , (6.9). This means that the error between considering a variable and a constant friction coefficient decreases as the singular point is approached and vanishes at  $\hat{R} = 1$ .

Due to the dependence of  $r_s$  and thus  $c_f(1)$  on  $Q$  and  $\nu$ , the universality of the equation for  $\text{Fr}(\hat{R})$  is lost. A family of solutions of (6.13) may be determined for a specific combination of  $Q$  and  $\nu$ . A discharge of  $Q = 0.2 \text{ m}^3/\text{s}$  appears meaningful for technical applications and will be used in Figs. 6.4 and 6.5, together with the viscosity  $\nu = 10^{-6} \text{ m}^2/\text{s}$  of water at a temperature of  $20^\circ$  [57], p. 154. In Fig. 6.4 the family of solutions of (6.13) shown as solid lines, is compared with the universal family of solutions of (6.9), shown as dashed lines. In this comparison the dashed lines correspond to a constant friction coefficient  $c_f(1) = 5 \cdot 10^{-3}$ . The deviations between the solid and dashed lines with the same value of  $\hat{R}^*$  in the vicinity of the singular point are relatively small as shown in Fig. 6.4. This is due to  $c_f(\hat{R})/c_f(1)$  being close to unity in this region. However, with increasing radius, the ratio  $c_f(\hat{R})/c_f(1)$  rises as shown by the red line in Fig. 6.5. The solid and dashed black curves with  $\hat{R}^* = 0.95$  remain close to each other even at the position of their turnaround since the variable friction coefficient at

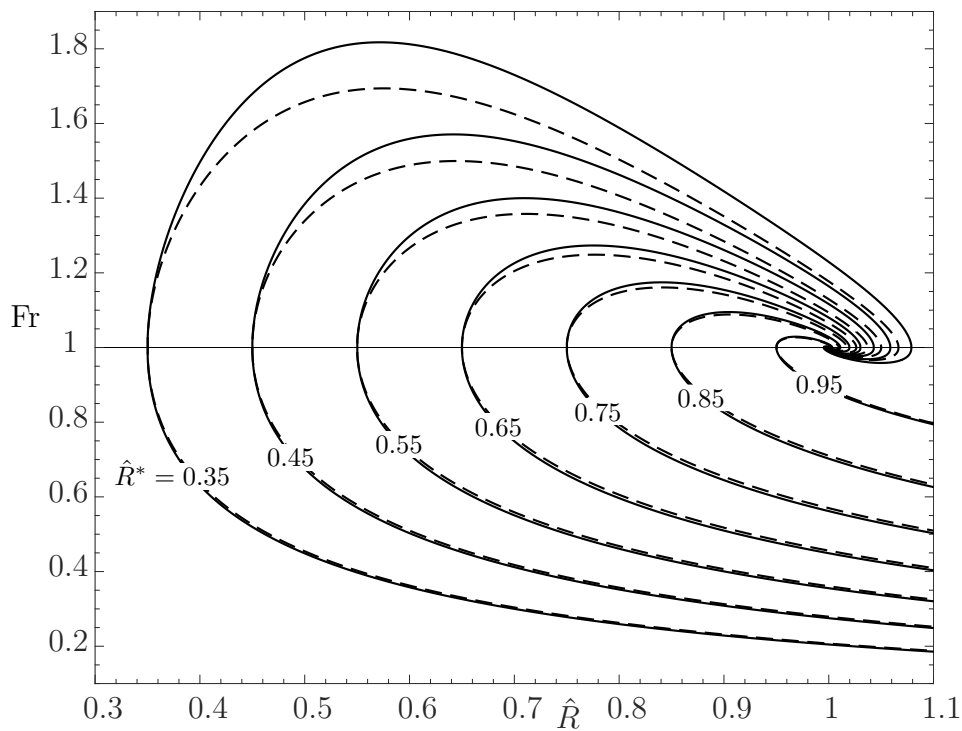


Figure 6.4: Comparison of the universal family of solutions of the hydraulic approximation with constant  $c_f$  (dashed), (6.9), and the family of solutions of the hydraulic approximation with variable  $c_f$  (solid), (6.13), for  $Q = 0.2 \text{ m}^3/\text{s}$  and  $\nu = 10^{-6} \text{ m}^2/\text{s}$ , i.e.  $r_s = 12.13 \text{ m}$ .

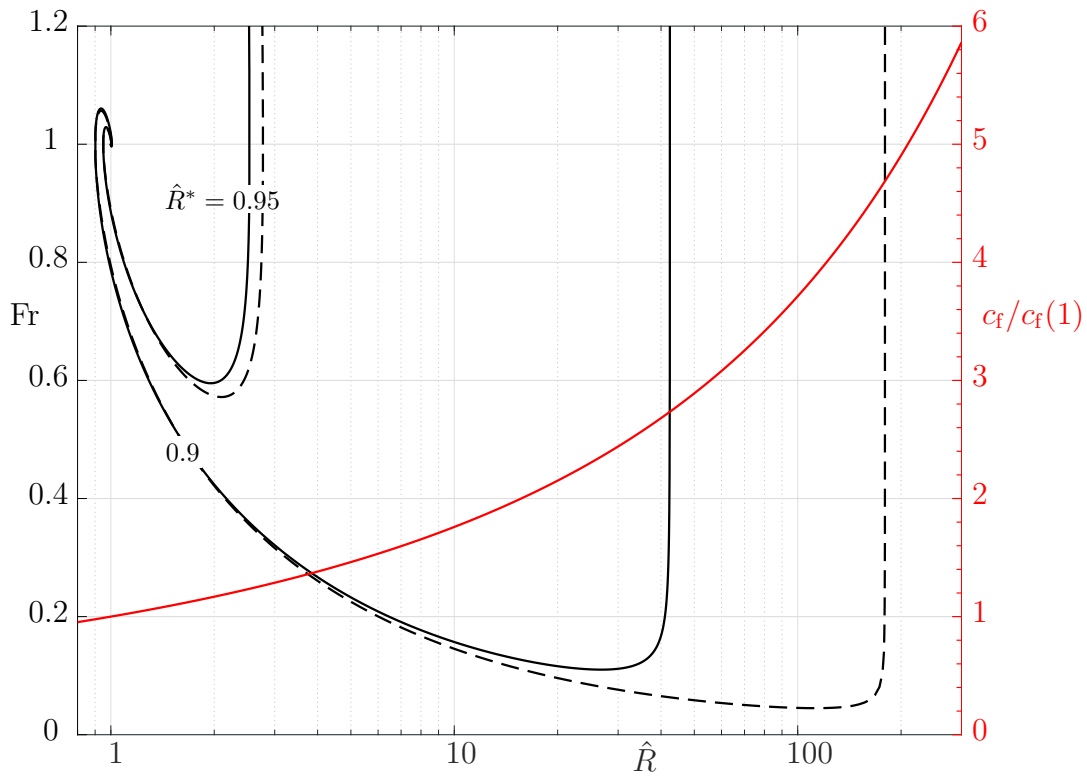


Figure 6.5: Comparison of solutions of the hydraulic approximation with constant  $c_f$  (dashed), (6.9), and variable  $c_f$  (solid), (6.13), at large radii, for  $Q = 0.2 \text{ m}^3/\text{s}$  and  $\nu = 10^{-6} \text{ m}^2/\text{s}$ ; black curves, scale on the left. Friction coefficient ratio  $c_f(\hat{R})/c_f(1)$  with  $c_f(1) = 5 \cdot 10^{-3}$ ; red curve, scale on the right.

this position ( $\hat{R} \approx 23$ ) differs only slightly from  $c_f(1)$ , i.e.  $c_f/c_f(1) \approx 1.2$ . For  $\hat{R}^* = 0.9$ , the turnaround positions of the solid and the dashed curves differ considerably because at the radius  $\hat{R} \approx 40$  the ratio  $c_f/c_f(1) \approx 2.7$  is not close unity anymore, shifting the turnaround to a larger radius.

The present comparison leads to the conclusion that a constant friction coefficient, and thus the universal family of solutions of (6.9) are a good approximation as long as  $\hat{R} = O(1)$ . Moreover, Fig. 6.4 shows that near-critical flow, as it will be considered in the following chapters, is very well approximated by  $c_f = \text{const}$ .

# Chapter 7

## Near-critical inviscid axisymmetric source flow

### 7.1 Problem formulation

In *plane* flow, e.g. in open channels, the undular hydraulic jump is inherently associated with dissipation and cannot exist in inviscid flow [22]. In the present chapter, we shall see that in the case of *axisymmetric* flow, the situation changes, and the governing equations of inviscid flow permit an undular hydraulic jump under certain conditions. A condition how small the friction Froude number, corresponding to a large Reynolds number, has to be such that the flow can be considered as inviscid will be given in Sec. 8.3.3. Consequently, steady near-critical inviscid source flow with a free surface over a horizontal bottom is considered, see Fig. 7.1. The assumption of negligible surface tension will be justified by a large Weber number in Sec. 7.3.1. The cylindrical coordinates  $r$  and  $z$  are introduced with the corresponding velocity components  $u$  and  $w$ , respectively. It is assumed that a circular undular hydraulic jump may arise at a relatively large jump radius such that, in leading order, the flow behaves like plane free-surface flow, cf. [22, 28]. Therefore, the reference radius  $r_r$ , being the position of the toe of the jump, is assumed to be sufficiently large. A more detailed description of what ‘sufficiently large’ means will be given below.

Non-dimensional variables are introduced analogue to Sec. 2.1 by referring to the

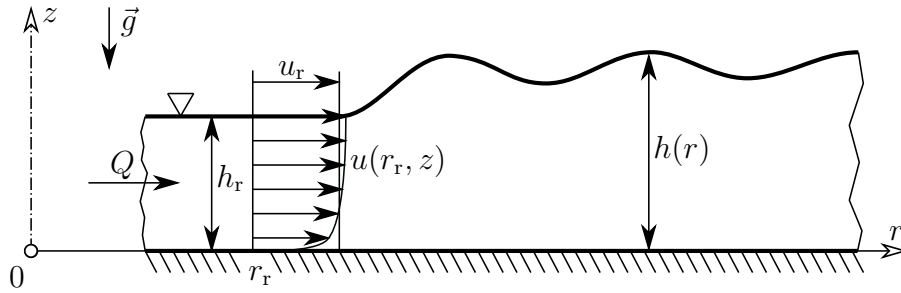


Figure 7.1: The stationary undular hydraulic jump in inviscid axisymmetric free-surface flow over a horizontal bottom.

reference state and using the small contraction parameter  $\delta \ll 1$ :

$$R = \delta \frac{r}{h_r}, \quad Z = \frac{z}{h_r}, \quad H = \frac{h}{h_r}, \quad U = \frac{u}{u_r}, \quad W = \delta^{-1} \frac{w}{u_r}, \quad P = \frac{p}{\rho g h_r}. \quad (7.1)$$

The reference velocity is defined as  $u_r := Q/r_r h_r$ . The continuity equation of incompressible flow in non-dimensional form reads

$$U/R + U_R + W_Z = 0, \quad (7.2)$$

with the subscripts  $R$  and  $Z$  denoting partial derivatives with respect to  $R$  and  $Z$ , respectively. The Euler equations in non-dimensional form are

$$\text{Fr}_r^2 (UU_R + WU_Z) = -P_R, \quad (7.3a)$$

$$\delta^2 \text{Fr}_r^2 (UW_R + WW_Z) = -P_Z - 1, \quad (7.3b)$$

with the reference Froude number

$$\text{Fr}_r = \frac{Q}{r_r \sqrt{g h_r^3}}. \quad (7.4)$$

The system of equations (7.2), (7.3a) and (7.3b) is to be solved subject to appropriate boundary conditions. At the bottom, a vanishing vertical velocity is prescribed,

$$W(R, 0) = 0. \quad (7.5)$$

At the free surface, the interface is defined by a streamline,

$$W(R, H) = U(R, H)H_R, \quad (7.6)$$

and the pressure is set to zero,

$$P(R, H) = 0. \quad (7.7)$$

## 7.2 Asymptotic analysis

The asymptotic analysis of the governing equations is performed inspired by previous studies of the undular jump, [22, 28]. Thus, the slightly supercritical reference Froude number and the contraction parameter are defined according to (2.11) and (2.12), respectively. As mentioned above, the reference radius is assumed to be large, i.e.

$$R_r = \tilde{R}\varepsilon^{-n}, \quad \tilde{R} = \text{const} = O(1), \quad (7.8)$$

with  $2 \leq n \leq 5/2$ . The order of magnitude of  $R_r$  is carefully chosen such that the terms due to axisymmetric flow will affect the final result only weakly or, at most, as an order 1 effect. Further, the non-dimensional radius is decomposed in

$$R = R_r + \eta \quad \text{with} \quad dR = d\eta. \quad (7.9)$$

All dependent variables are expanded in terms of powers of  $\varepsilon$ :

$$\begin{aligned} H(\eta) &= 1 + \varepsilon H_1(\eta) + \varepsilon^2 H_2(\eta) + \dots, \\ U(\eta, Z) &= 1 + \varepsilon U_1(\eta, Z) + \varepsilon^2 U_2(\eta, Z) + \dots, \\ W(\eta, Z) &= \varepsilon W_1(\eta, Z) + \varepsilon^2 W_2(\eta, Z) + \dots, \\ P(\eta, Z) &= 1 - Z + \varepsilon P_1(\eta, Z) + \varepsilon^2 P_2(\eta, Z) + \dots, \end{aligned} \quad (7.10)$$

neglecting terms of order  $\varepsilon^3$  and smaller. Note that here the basic state, (2.17), is used as leading-order terms with  $Y$  and  $V$  replaced by the present vertical coordinate  $Z$  and velocity component  $W$ , respectively. The following relationships are the results of the first-order equations:

$$U_1 = c_1(Z) - H_1, \quad W_1 = H_{1,\eta}Z, \quad P_1 = H_1. \quad (7.11)$$

The subscript  $\eta$  denotes the derivative with respect to  $\eta$ . The free-surface elevation  $H_1(\eta)$  remains undetermined in the framework of first-order equations. The function of integration  $c_1(Z)$  defines the velocity profile and can be chosen freely as it will not affect the final result for  $H_1$ . Since the reference velocity  $u_r$  is defined as the volumetric mean velocity, the integral of  $c_1(Z)$  has to vanish:

$$\int_0^1 c_1(Z) dZ = 0. \quad (7.12)$$

In the case of potential flow, the additional condition of an irrotational velocity field has to be satisfied. In the present non-dimensional variables this means  $\partial U_1/\partial Z = 0$ . Together with the integral condition (7.12), the function of integration becomes  $c_1(Z) \equiv 0$ . However, the potential flow solution is not the only possible velocity distribution, and thus another type of flow may lead to a different result for  $c_1$ .

Due to the choice of  $2 \leq n \leq 5/2$  in (7.8), the term  $U/R$  in the continuity equation (7.2) does neither affect the leading-order nor the first-order results. Following [28], a solvability condition for  $H_1(\eta)$  may be derived from the second-order equations by considering terms that are of  $O(\varepsilon^2)$  or half an order of magnitude smaller, i.e.  $O(\varepsilon^{5/2})$ . Thus, depending on the particular choice of  $R_r$ 's order of magnitude, the term  $U/R$  appears differently in the second-order continuity equation, i.e.

$$U/R = \varepsilon^n/\tilde{R} + \dots, \quad (7.13)$$

neglecting terms of order  $\varepsilon^3$  and smaller.

Performing the analysis of the second-order equations as described in [28], the Euler equation in radial direction, (7.3a), and the kinematic boundary condition, (8.4), are compatible if

$$H_{1,\eta\eta\eta} + H_{1,\eta}(H_1 - 1) = \varepsilon^{n-2}/3\tilde{R}. \quad (7.14)$$

Equation (7.14) is an extended steady-state version of the KdV equation. The constant right-hand side stems from the term  $U/R$  in the continuity equation, cf. (7.13), and represents the effect due to axisymmetric flow. If  $n = 5/2$ , i.e.  $R_r = O(\varepsilon^{-5/2})$ , the right-hand side is of the order  $\varepsilon^{1/2}$ . If  $n = 2$ , the smaller reference radius enhances the effect due to axisymmetric flow, and the right-hand side of (7.14) is of the order 1.

The extended KdV equation is to be solved for appropriate initial conditions. At the reference state  $\eta = 0$  the initial value is  $H_1(0) = 0$ . The initial slope and curvature may be chosen according to the hydraulic approximation, cf. Sec. 6.1. Therefore, we will use the relation between the local Froude number and  $H_1(\eta)$ , i.e.

$$\text{Fr}(\eta) = 1 + 3\varepsilon(1 - H_1)/2, \quad (7.15)$$

which follows from introducing the expanded variables according to (7.10) into the definition of Fr according to (6.3). Further, the near-critical hydraulic approximation

of inviscid axisymmetric flow, (6.7), is transformed by referring to  $r_r$  instead of  $r^*$ , using the relation (7.15), and expanding for  $\varepsilon \ll 1$ , resulting in

$$H_1 = 1 \mp \sqrt{1 + 2\varepsilon^{n-2}\eta/3\tilde{R}}, \quad (7.16a)$$

$$H_{1,\eta} = \frac{\varepsilon^{n-2}}{3\tilde{R}(H_1 - 1)}, \quad (7.16b)$$

$$H_{1,\eta\eta} = -\frac{\varepsilon^{2n-4}}{(3\tilde{R})^2(H_1 - 1)^3}. \quad (7.16c)$$

The upper and lower sign in (7.16a) corresponds to the super- and subcritical branch, respectively. Both (6.7) and (7.16a) are near-critical hydraulic approximations. They differ from each other due to the different reference states, i.e.  $\text{Fr} = 1$  at  $r = r^*$  for (6.7) and  $H_1 = 0$  at  $\eta = 0$  ( $r = r_r$ ) for (7.16a). Note that (7.16b) is equal to (7.14) without the term  $H_{1,\eta\eta\eta}$ , meaning that the extended KdV equation without the third-order term is equivalent to the near-critical hydraulic approximation.

It follows from (7.16a) that the condition  $H_1 = O(1)$  for the validity of the asymptotic expansion is only satisfied if

$$\varepsilon^{n-2}\eta = O(1). \quad (7.17)$$

Thus, the range of validity for  $n = 5/2$  is  $\eta = O(\varepsilon^{-1/2})$ , while it reduces to  $\eta = O(1)$  for  $n = 2$ .

It may be worth mentioning that if  $R_r$  were chosen to be of  $O(\varepsilon^{-3/2})$ , the resulting solvability condition and the results of the hydraulic approximation are of a different form than (7.14) and (7.16), respectively. Nevertheless, the validity condition (7.17) is still applicable. Consequently, an area of validity of  $\eta = O(\varepsilon^{1/2})$  is too small to be of practical interest.

## 7.3 Results and discussion

The extended KdV equation (7.14) is solved numerically as an initial value problem with standard methods, using the commercial software Matlab R2018b. For both  $n = 5/2$  and  $n = 2$ , solutions are obtained with the function `ode45`, a relative and absolute error tolerance of  $10^{-4}$  and  $10^{-8}$ , respectively, and a maximum step size of  $10^{-4}$ .

### 7.3.1 Undular jumps at a reference radius of $O(\varepsilon^{-5/2})$

Solving (7.14) with  $n = 5/2$  and the initial value, slope and curvature being in accord with the supercritical branch of the near-critical hydraulic approximation (7.16) in the reference state ( $\eta = 0$ ) yields an undular jump solution. In Fig. 7.2a) the black curve representing the solution of (7.14) shows a distinct transition from supercritical to subcritical ( $H_1 > 1$ ) flow within the first two undulations. Initially following the blue supercritical branch of the near-critical hydraulic approximation, (7.16a), downstream of the transition, the black curve oscillates around the blue subcritical branch of (7.16a) as it is typical for undular hydraulic jumps. Note that the form of the extended KdV equation for both inviscid axisymmetric flow (7.14) with  $n = 5/2$  and for open-channel flow over a horizontal bottom (2.35) is conspicuously similar. In both cases, the right-hand side is a constant of order  $\varepsilon^{1/2}$ , yet with a different sign. As we have seen in Fig. 2.4, for a negative right-hand side in (2.35) extremely large initial curvatures are required to obtain undular solutions. It is therefore remarkable to observe in Fig. 7.2a) that a positive right-hand side in (7.14) permits undular solutions without perturbing the reference state according to (7.16). Considering the origin of the extension terms in (2.35) and (7.14), we may conclude that in (2.35) the effect of friction is counter-productive, while the effect due to axisymmetric flow in (7.14) acts enhancing for the development of undular jumps. Both effects will be combined in Sec. 8.3.1.

The red curve in Fig. 7.2a) depicts the solution of the full hydraulic approximation (6.6) in terms of  $H_1(\eta)$ , i.e. referring to  $r_r$  instead of  $r^*$ , and using the definition of the local Froude number in terms of the non-dimensional variables with  $H = 1 + \varepsilon H_1$ :

$$\text{Fr}(\eta) = \frac{\text{Fr}_r}{(1 + \varepsilon^n \eta / \tilde{R})(1 + \varepsilon H_1)^{3/2}}. \quad (7.18)$$

The denominator is not expanded since the full hydraulic approximation is valid for any Froude number and radius, and hence  $\varepsilon H_1 \gg 1$  as well as  $\varepsilon^n \eta \gg 1$  are allowed. Equation (7.18) is applicable for  $2 \leq n \leq 5/2$  and will also be used for  $n = 2$  in the next section.

In Fig. 7.2b) the curves of Fig. 7.2a) are illustrated in the same colors but in terms of the local Froude number  $\text{Fr}$ . The radial coordinate is referred to the critical radius; see the bottom scale. The radial limits of the diagram correspond to the limits in terms of  $\eta$ ; see the top scale. The green curve represents the solution of the near-critical hydraulic approximation according to (6.7). The different reference states of the two

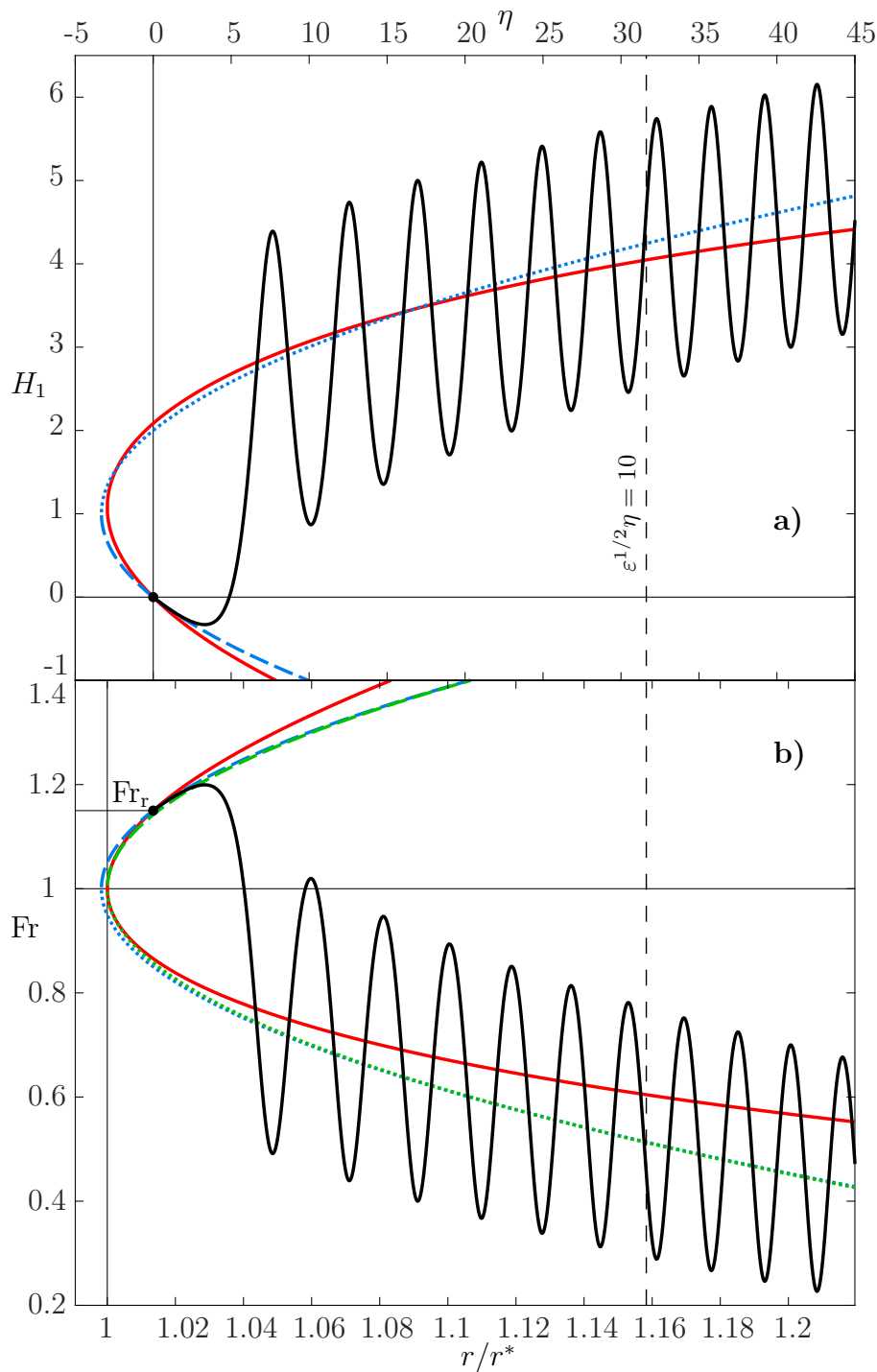


Figure 7.2: Results of an undular hydraulic jump in inviscid axisymmetric flow with  $R_r = O(\varepsilon^{-5/2})$ ;  $\varepsilon = 0.1$  ( $Fr_r = 1.15$ ),  $\tilde{R} = 0.7$ . a) Non-dimensional surface elevation,  $H_1$ , b) Local Froude number,  $Fr$ . Black: Numerical solution of the extended KdV equation (7.14) for initial conditions according to the hydraulic approximation (7.16) with  $n = 5/2$ , i.e.  $H_1(0) = 0$ ,  $H_{1,\eta}(0) = -0.15$ ,  $H_{1,\eta\eta}(0) = 2.27 \cdot 10^{-2}$ . Red: Full hydraulic approximation according to (6.6). Super- (dashed) and subcritical (dotted) branch of the near-critical hydraulic approximation according to (7.16a) in blue, and according to (6.7) in green.

near-critical hydraulic approximations, i.e.  $Fr = 1$  at  $r = r^*$  for the green curve and  $Fr = Fr_r$  at  $\eta = 0$  ( $r = r_r$ ) for the blue curve, are clearly distinguishable. In order to plot the solution of (7.14), the critical radius is required. Due to  $r/r^* = R/R^*$  the non-dimensional critical radius  $R^* = 218.4$  is determined from (6.6) using the parameter values of the reference state  $Fr_r = 1.15$  and  $R_r = 221.4$ , corresponding to  $\varepsilon = 0.1$  and  $\tilde{R} = 0.7$ . The dashed vertical line indicates the validity condition  $\varepsilon^{1/2}\eta = O(1)$  and restricts the validity of the results to the region of the first six to seven undulations.

To give an idea of which dimensional relations can be expected from the parameters of Fig. 7.2, i.e.  $Fr_r = 1.15$  and  $R_r = 221.4$ , the reference values will be computed. A discharge per unit azimuth angle  $Q = 10 \text{ l/s} = 10^{-2} \text{ m}^3/\text{s}$  is chosen to obtain reference values that are reasonable for applications. Therefore, from (7.1) and (7.4) follows  $h_r = 11 \text{ mm}$ ,  $r_r = 2.501 \text{ m}$ , and consequently  $u_r = 0.37 \text{ m/s}$ . From  $R^* = 218.4$  follows a critical radius of  $r^* = 2.468 \text{ m}$  that is located only a few centimetres upstream of the reference state. The small distance between  $r^*$  and  $r_r$  is not surprising since according to the universal hydraulic approximation of inviscid flow, (6.6), any near-critical state can only be located in the vicinity of the unique critical state, see the dashed line in Fig. 6.3. Using the density  $\rho = 998.2 \text{ kg/m}^3$  and surface tension  $\sigma = 72.7 \cdot 10^{-3} \text{ N/m}$  of water at a temperature of  $20 \text{ }^\circ\text{C}$  [57], pp. 154–156, yields a Weber number  $We_r := \rho u_r^2 h_r / \sigma = 21$  in the reference state. Such a large Weber number points out the weak effect of surface tension and justifies its negligence. For comparison, the same discharge of  $Q = 10 \text{ l/s}$  with a slightly larger Froude number  $Fr_r = 1.3$  and  $R_r = 54.9$  (i.e.  $\tilde{R} = 0.98$ ) yields  $h_r = 18 \text{ mm}$ ,  $r_r = 1 \text{ m}$ ,  $u_r = 0.55 \text{ m/s}$ ,  $r^* = 0.953 \text{ m}$ , and  $We_r = 76$ .

### 7.3.2 Undular jumps at a reference radius of $O(\varepsilon^{-2})$

Choosing the reference radius of  $O(\varepsilon^{-2})$  means moving closer towards the axis of the cylindrical coordinate system. For the same parameters as used in Fig. 7.2,  $\varepsilon = 0.1$  ( $Fr_r = 1.15$ ) and  $\tilde{R} = 0.7$ , the non-dimensional reference radius is  $R_r = 70$ . Choosing again  $Q = 10 \text{ l/s}$  to obtain realistic reference values leads to  $h_r = 17 \text{ mm}$ ,  $r_r = 1.254 \text{ m}$  and  $u_r = 0.47 \text{ m/s}$ . Thus, the reference state is shifted to half the radius with respect to the case of the same Froude number and  $R_r = O(\varepsilon^{-5/2})$ . The critical radius is  $R^* = 69.1$  and consequently  $r^* = 1.237 \text{ m}$ .

Solving the extended KdV equation (7.14) with  $n = 2$ , with initial conditions according to the supercritical branch of the near-critical hydraulic approximation (7.16)

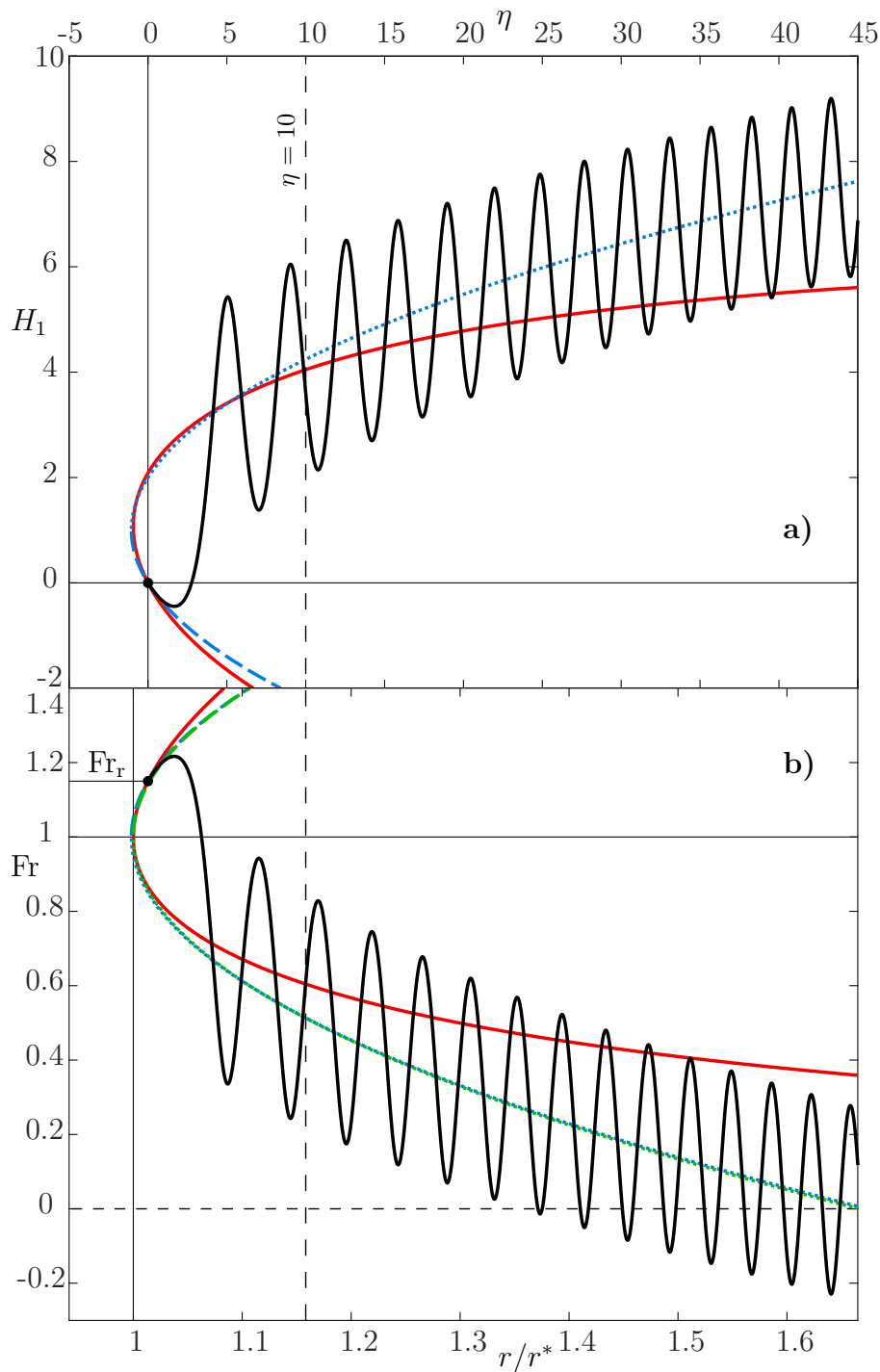


Figure 7.3: Results of an undular hydraulic jump in inviscid axisymmetric flow with  $R_r = O(\varepsilon^{-2})$ ;  $\varepsilon = 0.1$  ( $Fr_r = 1.15$ ),  $\tilde{R} = 0.7$ . a) Non-dimensional surface elevation,  $H_1$ , b) Local Froude number,  $Fr$ . Black: Numerical solution of the extended KdV equation (7.14) for initial conditions according to the hydraulic approximation (7.16) with  $n = 2$ , i.e.  $H_1(0) = 0$ ,  $H_{1,\eta}(0) = -0.48$ ,  $H_{1,\eta\eta}(0) = 0.23$ . Red: Full hydraulic approximation according to (6.6). Super- (dashed) and subcritical (dotted) branch of the near-critical hydraulic approximation according to (7.16a) in blue, and according to (6.7) in green.

yields again an undular jump, shown as black curve in Fig. 7.3a). However, the condition  $\eta = O(1)$ , indicated by the vertical dashed line, restricts the solution's validity to the first few undulations. For larger values of  $\eta$  also the blue near-critical hydraulic approximation deviates strongly from the full hydraulic approximation in red.

The validity limit becomes even more visible in the diagram of the local Froude number, Fig. 7.3b). With each successive wave crest,  $Fr$  decreases rapidly and even becomes negative at  $r/r^* \approx 1.37$ . This state is, of course, unphysical. Already before, the flow is far from near-critical, which violates the basic assumption of the asymptotic theory. With the present choice of  $R_r = O(\varepsilon^{-2})$  the distance between the reference radius and the critical radius,  $r_r - r^*$ , is strongly decreased with respect to  $R_r = O(\varepsilon^{-5/2})$ , cf. the distance between the vertical lines  $\eta = 0$  and  $r/r^* = 1$  in Figs. 7.2 and 7.3. Thus, in Fig. 7.3b) the blue and the green curve almost coincide.

# Chapter 8

## Near-critical turbulent axisymmetric source flow

### 8.1 Problem formulation

In this chapter, we will investigate undular hydraulic jumps in steady near-critical turbulent axisymmetric source flow over a horizontal bottom, see Fig. 8.1. The considerations of Ch. 7 regarding surface tension, the cylindrical coordinate system, and the reference state are adopted. By applying a Reynolds decomposition [41], p. 83, to the turbulent flow quantities, time-averaged quantities are denoted by an overbar and fluctuations around the average by a prime. Analogue to (2.1), the non-dimensional variables are introduced by referring to the reference state:

$$\begin{aligned}
 R &= \delta \frac{r}{\bar{h}_r}, & Z &= \frac{z}{\bar{h}_r}, & \bar{H} &= \frac{\bar{h}}{\bar{h}_r}, & \bar{U} &= \frac{\bar{u}}{\bar{u}_r}, & \bar{W} &= \delta^{-1} \frac{\bar{w}}{\bar{u}_r}, \\
 \bar{P} &= \frac{\bar{p}}{\rho g \bar{h}_r}, & U_\tau &= \frac{u_\tau}{u_{\tau,r}}, & \overline{U'^2} &= \frac{\overline{u'^2}}{u_{\tau,r}^2}, & \overline{W'^2} &= \frac{\overline{w'^2}}{u_{\tau,r}^2}, & \overline{U'W'} &= \frac{\overline{u'w'}}{u_{\tau,r}^2}.
 \end{aligned} \tag{8.1}$$

The continuity equation of incompressible flow in non-dimensional form reads

$$\bar{U}/R + \bar{U}_R + \bar{W}_Z = 0. \tag{8.2}$$

In the defect layer, the equations of motion in non-dimensional form are

$$\delta \text{Fr}_r^2 (\bar{U}\bar{U}_R + \bar{W}\bar{U}_Z) = -\delta \bar{P}_R - \text{Fr}_{\tau,r}^2 \left[ \delta (\overline{U'^2}_R + \overline{U'^2}/R) + \overline{U'W'}_Z \right], \tag{8.3a}$$

$$\delta^2 \text{Fr}_r^2 (\bar{U}\bar{W}_R + \bar{W}\bar{W}_Z) = -\bar{P}_Z - 1 - \text{Fr}_{\tau,r}^2 \left[ \delta (\overline{U'W'}_R + \overline{U'W'}/R) + \overline{W'^2}_Z \right], \tag{8.3b}$$

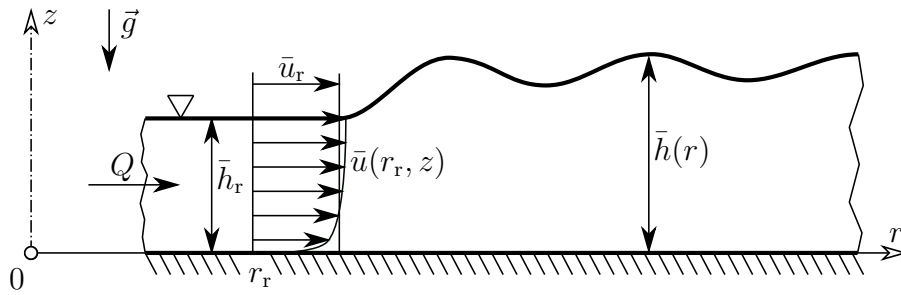


Figure 8.1: The stationary undular hydraulic jump in turbulent axisymmetric free-surface flow over a horizontal bottom.

with the reference Froude numbers defined as in (2.4) and accordingly (7.4).

The governing equations (8.2), (8.3a) and (8.3b) are to be solved subject to appropriate boundary and matching conditions. At the bottom, the defect layer is matched with the viscous wall layer. According to Schlichting and Gersten [47], Sec. 20.1.2, the logarithmic velocity law for plane flow also holds for the present turbulent axisymmetric flow. Therefore, the conditions given in Sec. 2.1, i.e. (2.5–2.8), are prescribed by substituting  $X$  with  $R$ ,  $Y$  with  $Z$ , and  $V$  with  $W$ . The same substitution is applied to the boundary conditions at the free surface, (2.9–2.10). The kinematic boundary condition then becomes

$$\bar{W}(R, \bar{H}) = \bar{U}(R, \bar{H}) \bar{H}_R, \quad (8.4)$$

and the dynamic boundary conditions read

$$\left[ \bar{P}(R, \bar{H}) + \text{Fr}_{\tau,r}^2 \bar{U}^2(R, \bar{H}) \right] \delta \bar{H}_R - \text{Fr}_{\tau,r}^2 \bar{U}' \bar{W}'(R, \bar{H}) = 0, \quad (8.5a)$$

$$\left[ \bar{P}(R, \bar{H}) + \text{Fr}_{\tau,r}^2 \bar{W}^2(R, \bar{H}) \right] - \text{Fr}_{\tau,r}^2 \bar{U}' \bar{W}'(R, \bar{H}) \delta \bar{H}_R = 0. \quad (8.5b)$$

## 8.2 Asymptotic analysis

The asymptotic analysis of the governing equations of near-critical axisymmetric turbulent flow represents a combination of the analysis of plane turbulent flow in Sec. 2.2 and the analysis of axisymmetric inviscid flow in Sec. 7.2. Thus, the near-critical reference Froude number, the contraction parameter, and the reference friction Froude number are defined according to (2.11–2.13), respectively. The non-dimensional radius is decomposed as in (7.9) with the large non-dimensional reference radius according to

(7.8) and  $2 \leq n \leq 5/2$ . All dependent variables are expanded in terms of powers of  $\varepsilon$ , e.g.

$$\bar{H}(\eta) = 1 + \varepsilon H_1(\eta) + \varepsilon^2 H_2(\eta) + \dots, \quad (8.6)$$

for the non-dimensional height of the free surface, neglecting terms of order  $\varepsilon^3$  and smaller. The leading-order terms represent the reference state and are identical to the inviscid flow case, see (7.10). As discussed in Ch. 2, due to the horizontal bottom, a fully developed flow neither exists in the reference state nor anywhere else. Thus, the leading-order Reynolds shear stress is assumed to be of the same form as in (2.18), i.e.

$$(\overline{U'W'})_0 = Z - 1 + \Delta\overline{U'W'}(Z), \quad (8.7)$$

with the term  $\Delta\overline{U'W'}(Z) = O(1)$  representing the deviation of the reference state from the linear profile of a fully developed flow. In order to satisfy the boundary conditions at the bottom and at the free surface,  $\Delta\overline{U'W'}(0) = \Delta\overline{U'W'}(1) = 0$  holds. The results of the analysis of the first-order equations are

$$U_1 = -H_1 + \varepsilon^{1/2}\sqrt{B}\Delta U(Z), \quad W_1 = H_{1,\eta}Z, \quad P_1 = H_1, \quad (8.8)$$

with  $\Delta U(Z) = O(1)$  being the velocity defect in the reference state.

From the comparison between the hydraulic approximation of axisymmetric inviscid and viscous flow, Fig. 6.3, we know that even weak friction effects accumulate and eventually lead to a breakdown of the flow, indicated by a turnaround of the spiral curve. To incorporate this effect, the present analysis aims at deriving a uniformly valid differential equation, representing the initial behaviour of the undular jump and the breakdown far downstream. Therefore, the denominator of the term  $\bar{U}/R$  in the continuity equation, which first appears in the second-order equations, will not be expanded as in (7.13), such that the term reads

$$\bar{U}/R = \varepsilon^n \frac{1 + \varepsilon U_1 + \dots}{\tilde{R} + \varepsilon^n \eta}, \quad (8.9)$$

allowing for  $\varepsilon^n \eta \gg 1$ .

The analysis of the second-order equations is again performed as described in [28], and the equation of motion in radial direction, (8.3a), and the adapted kinematic boundary condition, (2.9), i.e. (8.4) by introducing overbars over the dependent variables, are compatible if

$$H_{1,\eta\eta} + H_{1,\eta}(H_1 - 1) = f(\eta; n) - \gamma, \quad (8.10)$$

with

$$f(\eta; n) = \frac{\varepsilon^{n-2}}{3(\tilde{R} + \varepsilon^n \eta)}, \quad (8.11)$$

and the constant  $\gamma$  according to (2.36). The solvability condition (8.10) is a steady-state version of an extended KdV equation with two extension terms on the right-hand side. The first term represents the effect of axisymmetric flow and slowly decays with increasing distance from the reference state. The constant  $\gamma = O(\varepsilon^{1/2})$  represents the effect of friction in terms of the reference state's deviation from a fully developed flow.

In the case of  $n = 5/2$ , i.e.  $R_r = O(\varepsilon^{-5/2})$ , both terms on the right-hand side of (8.10) are of  $O(\varepsilon^{1/2})$  and counteract each other. At  $\eta = 0$ , the right-hand side's sign depends on the particular values of the order 1 constants  $\tilde{R}$  and  $B$ . Initially, the right-hand side is either positive if  $B\tilde{R} < 3$ , or negative if  $B\tilde{R} > 3$ . These two distinctions will play an essential role in the analysis of possible undular solutions of (8.10) in Sec. 8.3.1. For  $B\tilde{R} = 3$ , the right-hand side vanishes at  $\eta = 0$ , and (8.10) turns into the classical KdV equation [17], p. 21. In the case of  $n = 2$ , i.e.  $R_r = O(\varepsilon^{-2})$ , the effect due to axisymmetric flow becomes enhanced and the first extension term in (8.10) is of  $O(1)$  while  $\gamma$  is unchanged. This implies a positive right-hand side at  $\eta = 0$  for any values of  $B$  and  $\tilde{R}$ .

A near-critical hydraulic approximation for  $\varepsilon^n \eta \ll 1$  is derived from the full hydraulic approximation (6.4) using the relations (2.41) and (7.15), and expanding for  $\varepsilon \ll 1$ :

$$H_{1,\eta}(H_1 - 1) = \varepsilon^{n-2}/3\tilde{R} - \gamma. \quad (8.12)$$

Since (8.12) is only valid for  $\varepsilon^n \eta \ll 1$ , the near-critical hydraulic approximation may serve to determine appropriate initial conditions for (8.10) but does not deliver insight into the downstream behaviour of the extended KdV equation's solution.

As we will see in Sec. 8.3, the solution of the extended KdV equation (8.10) oscillates around the subcritical branch of the solution of (8.10) without the third-order term, i.e.

$$H_1 = 1 \mp \sqrt{1 - 2\gamma\eta + \frac{2}{3\varepsilon^2} \ln \left( 1 + \frac{\varepsilon^n \eta}{\tilde{R}} \right)}, \quad (8.13a)$$

$$H_{1,\eta} = \frac{f(\eta; n) - \gamma}{H_1 - 1}, \quad (8.13b)$$

$$H_{1,\eta\eta} = -\frac{(f(\eta; n) - \gamma)^2}{(H_1 - 1)^3}, \quad (8.13c)$$

using the lower sign in (8.13a). We will refer to (8.13) as the hydraulic approximation of the extended KdV equation (8.10). Note that for  $\varepsilon^n \eta \ll 1$ , (8.13a) is very well approximated by the solution of (8.12), see Fig. 8.2.

The oscillations of the extended KdV equation's solution around the subcritical branch of (8.13a) have amplitudes of order 1. Thus, to determine the validity limits for the asymptotic results, it suffices to analyse the behaviour of the subcritical branch of (8.13a). Figure 8.2 shows that this branch (dotted line) first increases up to the position

$$\eta_m = \tilde{R} \varepsilon^{-n} \left( \varepsilon^{n-5/2} \frac{3}{B \tilde{R}} - 1 \right), \quad (8.14)$$

where  $H_1$  reaches its maximum. Downstream of  $\eta_m$ ,  $H_1$  decreases and approaches a

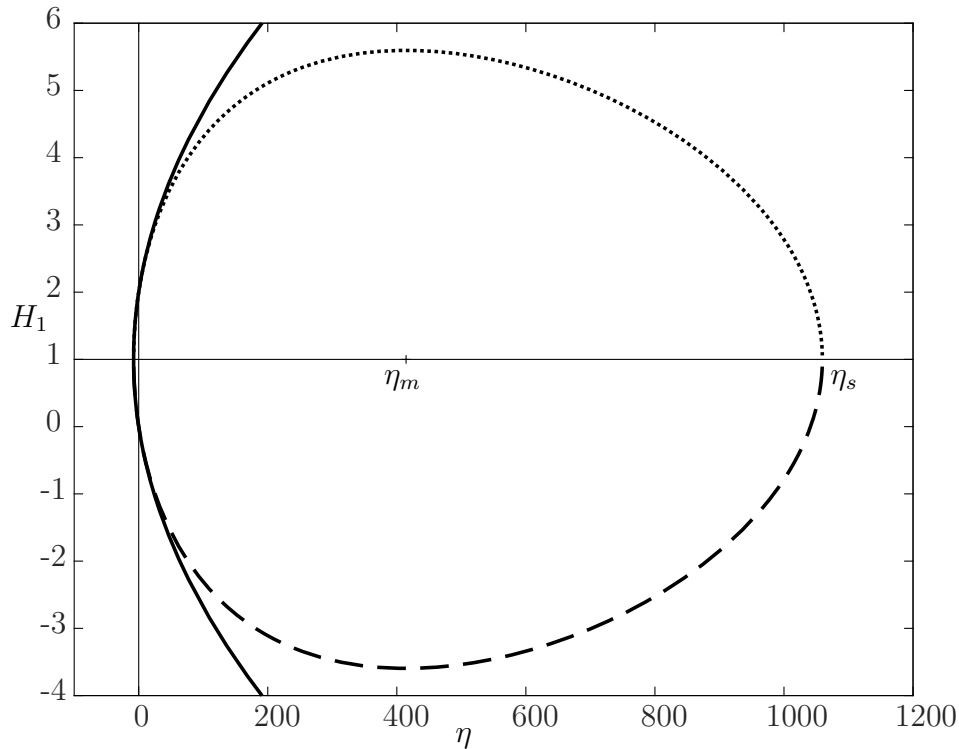


Figure 8.2: The dotted and dashed line shows the subcritical and supercritical branch, respectively, of the hydraulic approximation of the extended KdV equation, (8.13a), with  $n = 5/2$ . The solution of the near-critical hydraulic approximation, (8.12), for  $n = 5/2$  is shown as solid line. The parameter values  $\varepsilon = 0.08$ ,  $\tilde{R} = 0.75$ ,  $B = 2$  correspond to  $C = -1.77$ ,  $\eta_m = 414$ ,  $\eta_s = 1060$ .

singularity at  $\eta_s$  as

$$H_1 = 1 \mp \frac{1}{\varepsilon} \sqrt{\frac{2}{3} \ln \left( \frac{1 + \varepsilon^n \eta / \tilde{R}}{1 + \varepsilon^n \eta_s / \tilde{R}} \right)}, \quad (8.15)$$

with the lower sign corresponding to the subcritical branch. A physical interpretation may be that upstream of  $\eta_m$  the effect due to axisymmetric flow dominates the effect due to friction, and vice versa downstream of  $\eta_m$ . In Fig. 8.2 solutions of (8.12) and (8.13a) are presented for  $n = 5/2$ . For  $n = 2$  the solutions show the same qualitative behaviour, and thus the conclusions may be adopted. The condition for the validity of the asymptotic expansion is  $H_1 = O(1)$ . However, for  $n = 5/2$  it turns out that this leads to the validity condition  $B\tilde{R}/3 = 1$ , which is just the case of vanishing right-hand side of the extended KdV equation (8.10) at  $\eta = 0$ , and does not permit undular solutions. Therefore, the weaker condition  $H_1 = O(\varepsilon^{-1/2})$  is prescribed. Consequently, applying  $H_1(\eta_m) = O(\varepsilon^{-1/2})$  to (8.13a) yields the validity condition

$$\varepsilon^{5/2-n} \frac{B\tilde{R}}{3} = 1 + \varepsilon^{1/2} C, \quad |C| = \text{const} = O(1). \quad (8.16)$$

For  $n = 5/2$ ,  $C \leq 0$  defines whether the right-hand side of (8.10) is positive or negative at  $\eta = 0$ . The combination of (8.14) and (8.16) gives  $\eta_m = -C\tilde{R}\varepsilon^{-2} + \dots$ . Thus,  $C \leq 0$  corresponds to  $\eta_m \geq 0$ , meaning that the reference state ( $\eta = 0$ ) lies either upstream or downstream of the position where the subcritical branch of  $H_1$  according to (8.13a) reaches its maximum.

For  $n = 2$ , the condition (8.16) requires that the product of the order 1 parameters  $B\tilde{R} = O(\varepsilon^{-1/2})$ . Strictly speaking, this violates the basic assumptions of an asymptotic treatment. However, in the present framework of the derivation of a uniformly valid differential equation, deviations of half an order of magnitude are tolerated.

## 8.3 Results and discussion

The extended KdV equation (8.10) may be solved numerically as an initial value problem with standard methods, using the commercial software Matlab R2018b. For both  $n = 5/2$  and  $n = 2$  solutions are obtained with the function `ode45`, a relative error tolerance of  $10^{-4}$ , an absolute error tolerance of  $10^{-8}$ , and a maximum step size of  $10^{-4}$ .

### 8.3.1 Undular jumps at a reference radius of $O(\varepsilon^{-5/2})$

A solution of the extended KdV equation (8.10) with  $n = 5/2$  is shown as black curve in Fig. 8.3a). The solution is obtained without any perturbation of the reference state, meaning initial conditions at  $\eta = 0$  exactly according to the blue dashed supercritical branch of (8.13). Initially the black curve closely follows the supercritical branch of the hydraulic approximation of (8.10), i.e. (8.13a). However, after some distance an undular jump with oscillations around the blue dotted subcritical branch of (8.13a) develops. The red solution of the full hydraulic approximation is determined by integrating (6.9) in terms of polar coordinates, as described in Sec. 6.2. The reference state with  $Fr_r$  and  $\hat{R}_r = (B\tilde{R}/3)^{3/5}(1 - 12\varepsilon/5)$  is used as starting point for the integration in both clockwise and counter-clockwise direction. In order to plot the solution of (6.9) in terms of  $H_1$  in Fig. 8.3a), the relation (7.18) is applied. The deviation between the red and the blue dashed curve in the reference state stems from the expansion of (6.9) for  $\varepsilon \ll 1$  to obtain the near-critical hydraulic approximation (8.13a), and thus vanishes as  $\varepsilon \rightarrow 0$ .

In Fig. 8.3b) the black solution of the extended KdV equation (8.10) in terms of the local Froude number shows that the transition from super- to subcritical flow happens within the first two undulations. The radial coordinate is referred to the critical radius; see the bottom scale. The radial limits of the diagram correspond to the limits in terms of  $\eta$ ; see the top scale. The solutions of (8.10) and (8.13a), both equations were derived for near-critical flow, are plotted in terms of  $Fr$  by applying the relation

$$Fr(\eta) = \frac{1 + 3\varepsilon(1 - H_1)/2}{1 + \varepsilon^n \eta / \tilde{R}}, \quad (8.17)$$

which is (7.18) expanded for  $\varepsilon \ll 1$  but allowing for  $\varepsilon^n \eta = O(1)$ . Due to the  $\eta$ -term in the denominator of (8.17), with increasing distance from the reference state, the oscillations' amplitude decays in terms of  $Fr$  while it remains almost constant in terms of  $H_1$ .

This effect becomes visible by comparing the behaviour of the black solution of the extended KdV equation at large radii in terms of  $H_1$  and  $Fr$  shown in Fig. 8.4a) and b), respectively. Due to the strongly skewed scales of the abscissa and the ordinate, individual oscillations are hardly distinguishable. The solution of (8.10) appears as a thick black bar. Moreover, the relation (8.17) implies that along the allegedly supercritical (blue dashed) branch of (8.13a) the local Froude number is larger than unity only for a small part of the solution, see Fig. 8.4b). The dependence of the local Froude

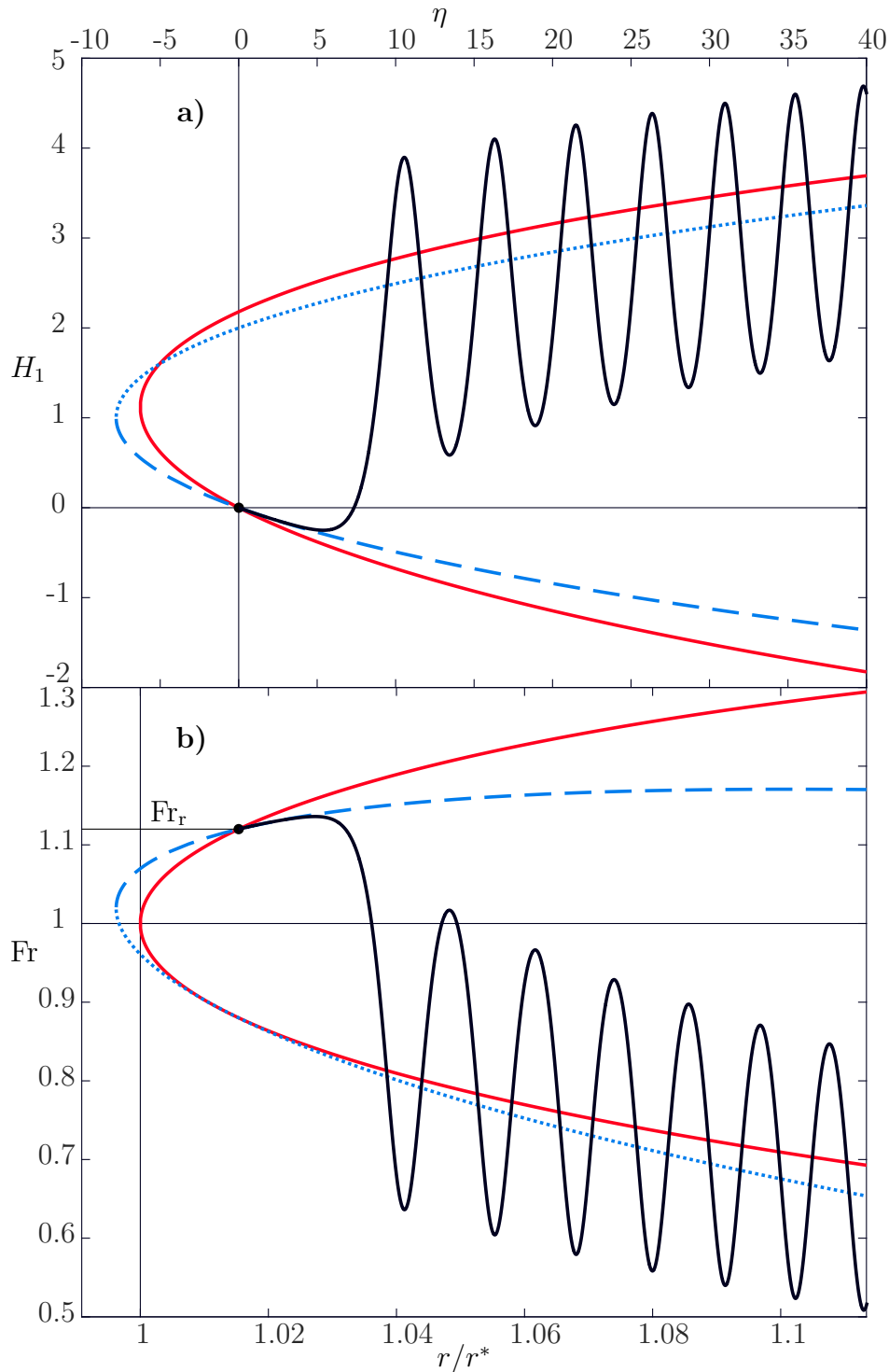


Figure 8.3: Initial behaviour of an undular hydraulic jump in turbulent axisymmetric flow with  $R_r = O(\varepsilon^{-5/2})$ ;  $\varepsilon = 0.08$  ( $\text{Fr}_r = 1.12$ ),  $\tilde{R} = 0.75$ ,  $B = 2$ , i.e.  $C = -1.77$ . a) Non-dimensional surface elevation,  $H_1$ , b) Local Froude number,  $\text{Fr}$ . Black: Numerical solution of the extended KdV equation (8.10) for initial conditions according to (8.13) with  $n = 5/2$ , i.e.  $H_1(0) = 0$ ,  $H_{1,\eta}(0) = -6.29 \cdot 10^{-2}$ ,  $H_{1,\eta\eta}(0) = 3.95 \cdot 10^{-3}$ . Red: Full hydraulic approximation according to (6.9). Blue dashed and dotted: Super- and subcritical branch, respectively, of the hydraulic approximation of the extended KdV equation, (8.13a).

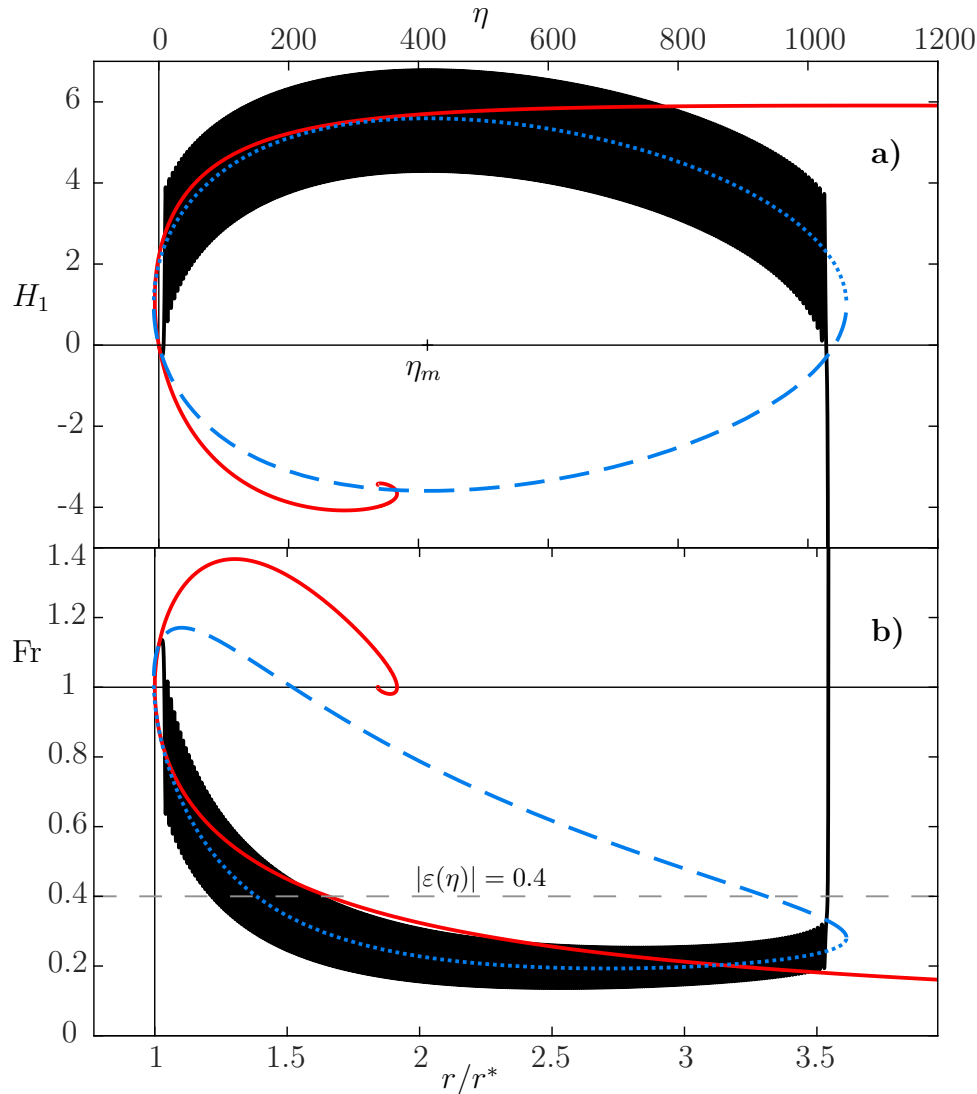


Figure 8.4: Behaviour of an undular hydraulic jump in turbulent axisymmetric flow with  $R_r = O(\varepsilon^{-5/2})$  at large radii;  $\varepsilon = 0.08$  ( $Fr_r = 1.12$ ),  $\tilde{R} = 0.75$ ,  $B = 2$ , i.e.  $C = -1.77$ ,  $\eta_m = 414$ . a) Non-dimensional surface elevation,  $H_1$ , b) Local Froude number,  $Fr$ . Black: Numerical solution of the extended KdV equation (8.10) for initial conditions according to (8.13) with  $n = 5/2$ , i.e.  $H_1(0) = 0$ ,  $H_{1,\eta}(0) = -6.29 \cdot 10^{-2}$ ,  $H_{1,\eta\eta}(0) = 3.95 \cdot 10^{-3}$ . Red: Full hydraulic approximation according to (6.9). Blue dashed and dotted: Super- and subcritical branch, respectively, of the hydraulic approximation of the extended KdV equation, (8.13a).

number on the radial coordinate  $\eta$  also impacts the validity of the present theory for near-critical turbulent axisymmetric flow. While the solution of (8.10) in terms of  $H_1$  remains of order 1, the solution in terms of  $\text{Fr}$  exceeds the limit of near-critical flow, indicated by the horizontal dashed line for the local perturbation parameter that is determined by substituting  $\text{Fr}_r$  with  $\text{Fr}(\eta)$  in (2.11).

However, the extended KdV equation's solution strongly depends on the parameter values  $\varepsilon$ ,  $\tilde{R}$ , and  $B$ . The solution's sensitivity becomes evident in Fig. 8.5, where only slightly changed parameters with respect to Fig. 8.4 yield a solution that is much closer to the validity limit for near-critical flow. Moreover, in Fig. 8.5b) the agreement between the blue dotted subcritical branch of the hydraulic approximation and the red full hydraulic approximation is truly remarkable. The reference values of Figs. 8.4 and 8.5 are listed in Table 8.1 for the discharge  $Q = 2.3 \text{ m}^3/\text{s}$ , which was chosen to obtain appropriately large Reynolds numbers. In both figures the characteristic behaviour of the solutions of the extended KdV equation is comparable. The black curves oscillate around the corresponding subcritical branch of (8.13a) almost up to the position where the dashed and dotted branches of (8.13a) coalesce. Shortly before the coalescence the solutions of the extended KdV equation break down, which is to be interpreted as the plate edge, cf. [46]. The singularity at  $\eta_s$  is approached by the black curve as  $H_1 = -12/(\eta_s - \eta)^2$ , in the same way as in the case of near-critical turbulent open-channel flow over a horizontal bottom, see Sec. 2.4.1. Since the local Reynolds number is inversely proportional to the radius, at the position of the breakdown  $\text{Re} = Q/r\nu$  decays to  $4.1 \cdot 10^4$  and  $2.0 \cdot 10^4$  in Fig. 8.4 and 8.5, respectively.

As discussed at the end of Sec. 8.2, the reference state is located either far upstream or far downstream of the position  $\eta_m$  where the solution of (8.13a) reaches its extremum, depending on  $B\tilde{R} \lesseqgtr 3$ , equivalent to  $C \lesseqgtr 0$ . This strongly affects the solution of (8.10). While in Figs. 8.3, 8.4, 8.5 the parameters correspond to  $C < 0$ , in Fig. 8.6 the parameters are chosen such that  $C = 2.5 > 0$ . Thus, the reference state is just upstream of the position where the blue sub- and supercritical branches of (8.13a) coalesce. Moreover, the reference state is located downstream of the full hydraulic approximation's spiral point, according to (6.9), shown in red. Solving the extended KdV equation (8.10) for initial conditions exactly according to the supercritical branch of (8.13) yields a breakdown shortly after the reference state, shown as a black dashed curve. Increasing the initial curvature by 20% only shifts the breakdown further downstream; see the black

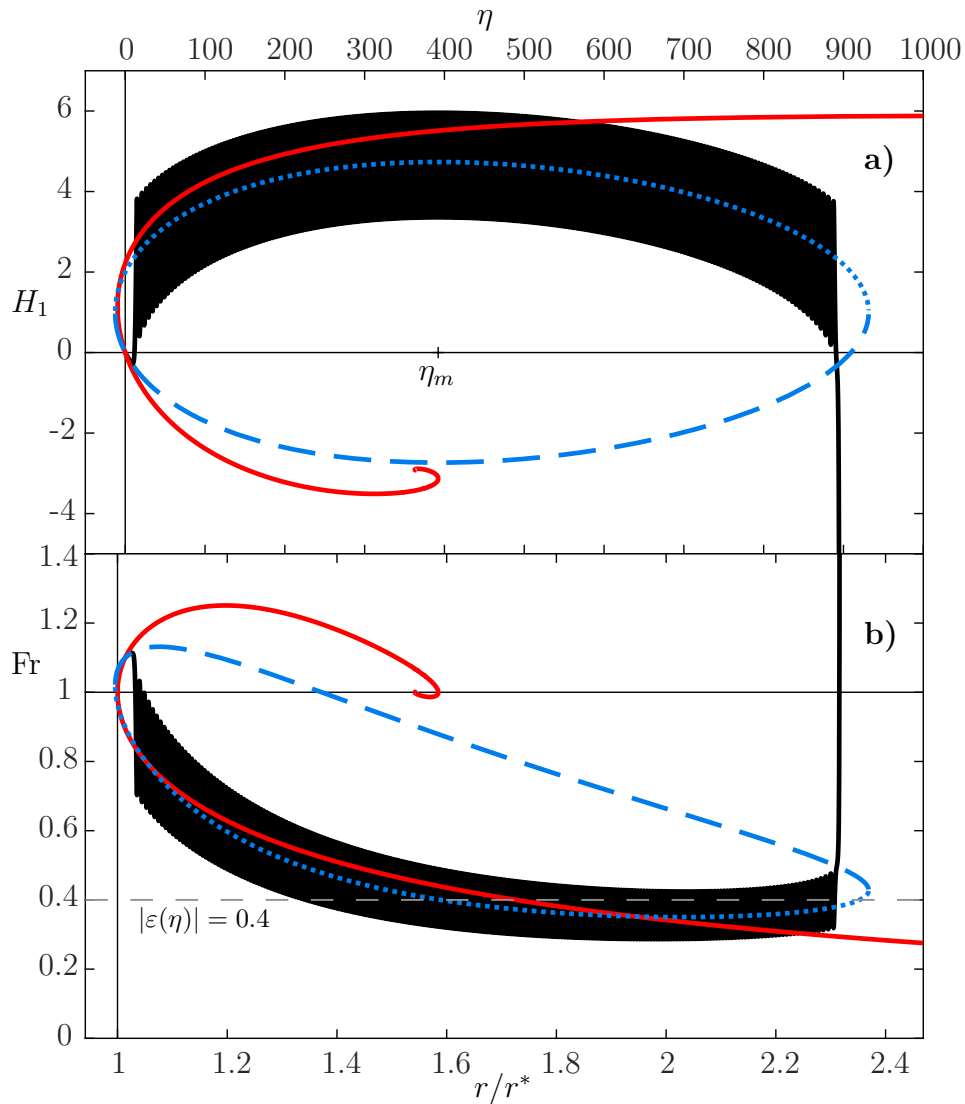


Figure 8.5: Behaviour of an undular hydraulic jump in turbulent axisymmetric flow with  $R_r = O(\varepsilon^{-5/2})$  at large radii;  $\varepsilon = 0.067$  ( $Fr_r = 1.1$ ),  $\tilde{R} = 0.8$ ,  $B = 2.4$ , i.e.  $C = -1.39$ ,  $\eta_m = 392$ . a) Non-dimensional surface elevation,  $H_1$ , b) Local Froude number,  $Fr$ . Black: Numerical solution of the extended KdV equation (8.10) for initial conditions according to (8.13) with  $n = 5/2$ , i.e.  $H_1(0) = 0$ ,  $H_{1,\eta}(0) = -3.87 \cdot 10^{-2}$ ,  $H_{1,\eta\eta}(0) = 1.50 \cdot 10^{-3}$ . Red: Full hydraulic approximation according to (6.9). Blue dashed and dotted: Super- and subcritical branch, respectively, of the hydraulic approximation of the extended KdV equation, (8.13a).

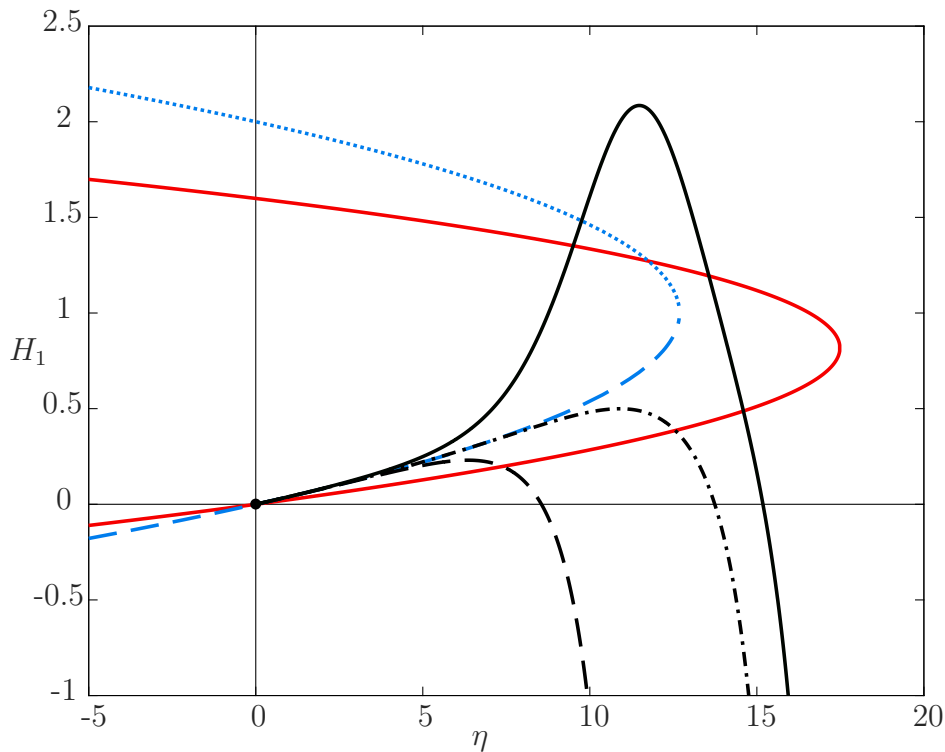


Figure 8.6: Numerical solutions of the extended KdV equation (8.10) with  $n = 5/2$ , for  $\varepsilon = 0.08$  ( $\text{Fr}_r = 1.12$ ),  $\tilde{R} = 1.71$ ,  $B = 3$ , i.e.  $C = 2.5$ . Initial conditions:  $H_1(0) = 0$ ,  $H_{1,\eta}(0) = 3.91 \cdot 10^{-2}$ ; black dashed:  $H_{1,\eta\eta}(0) = 1.53 \cdot 10^{-3}$ , black dash-dotted:  $H_{1,\eta\eta}(0) = 1.83 \cdot 10^{-3}$ , black solid:  $H_{1,\eta\eta}(0) = 2.29 \cdot 10^{-3}$ . Red: Full hydraulic approximation according to (6.9). Blue dashed and dotted: Super- and subcritical branch, respectively, of the hydraulic approximation of the extended KdV equation, (8.13a).

dash-dotted curve. Increasing  $H_{1,\eta\eta}(0)$  by as much as 50%, a single wave crest develops with immediate breakdown afterwards. Note that for  $C > 0$ , the extended KdV equation (8.10) with a negative right-hand side is of a very similar form as in the case of near-critical open-channel flow over a horizontal bottom, cf. (2.35). Thus, the solutions are similar, and regardless of the value of  $\text{Fr}_r$ , extremely large initial curvatures are necessary to obtain undulations at all, cf. Fig. 2.4.

The analysis of the results for  $C \leq 0$  shows that  $C < 0$  corresponds to a reference state in the region where the effect due to axisymmetric flow is dominant, which enhances the development of undular jumps as in the case of inviscid axisymmetric flow, cf. Sec. 7.3.1. However, as  $\eta$  increases the solution of the extended KdV equation (8.10)

	Fig. 8.4	Fig. 8.5	Fig. 8.7	Fig. 8.8
$Fr_r$	1.12	1.10	1.10	1.20
$Fr_{\tau,r}$	$3.20 \cdot 10^{-2}$	$2.67 \cdot 10^{-2}$	$3.22 \cdot 10^{-2}$	$8.29 \cdot 10^{-2}$
$R_r$	$4.14 \cdot 10^2$	$6.97 \cdot 10^2$	$4.95 \cdot 10^2$	$7.31 \cdot 10^1$
$Re_r$	$6.64 \cdot 10^4$	$4.56 \cdot 10^4$	$5.61 \cdot 10^4$	$4.02 \cdot 10^4$
$Re_{\tau,r}$	$1.90 \cdot 10^3$	$1.11 \cdot 10^3$	$1.64 \cdot 10^3$	$2.77 \cdot 10^3$
$\bar{h}_r$	7.10 cm	5.60 cm	6.42 cm	4.85 cm
$r_r$	34.66 m	50.39 m	41.03 m	3.24 m
$\bar{u}_r$	0.94 m/s	0.82 m/s	0.87 m/s	0.83 m/s

Table 8.1: Non-dimensional and dimensional reference values of the Figs. 8.4, 8.5, 8.7, corresponding to  $Q = 2.3 \text{ m}^3/\text{s}$  and  $\nu = 10^{-6} \text{ m}^2/\text{s}$ . The values for Fig. 8.8 correspond to  $Q = 0.13 \text{ m}^3/\text{s}$ .

reaches the region  $\eta > \eta_m$  of dominant friction effects, which ultimately force a breakdown, see Figs. 8.4 and 8.5. For  $C > 0$ , the reference state is located in the region where the dominant friction effects tend to suppress the development of an undular jump as in the case of turbulent open-channel flow over horizontal bottoms, cf. Sec. 2.4.3.

### 8.3.2 Undular jumps at a reference radius of $O(\varepsilon^{-2})$

From a smaller reference radius of  $O(\varepsilon^{-2})$  follows that for  $\eta = 0$  the two extension terms on the right-hand side of the extended KdV equation (8.10) are of different orders of magnitude. This implies that according to (8.14) for any combination of  $\tilde{R}$  and  $B$ , the reference state is located upstream of  $\eta_m$ , in the region where the effect due to axisymmetric flow is dominant and promotes the development of undular jumps. In Fig. 8.7a) and b) a solution of (8.10) with  $n = 2$  is shown as black curve in terms of  $H_1$  and  $Fr$ , respectively. The black curve in Fig. 8.7b) stays close to the limit of near-critical flow indicated by the horizontal dashed line, showing the solution's uniform validity over a large distance from the reference state.

The characteristics of the black curves are the same as in the case of  $R_r = O(\varepsilon^{-5/2})$ . Past the transition from super- to subcritical flow, the extended KdV equation's solution oscillates around the blue dotted subcritical branch of (8.13a). With increasing distance from the reference state, the effect of axisymmetric flow decays, and friction becomes

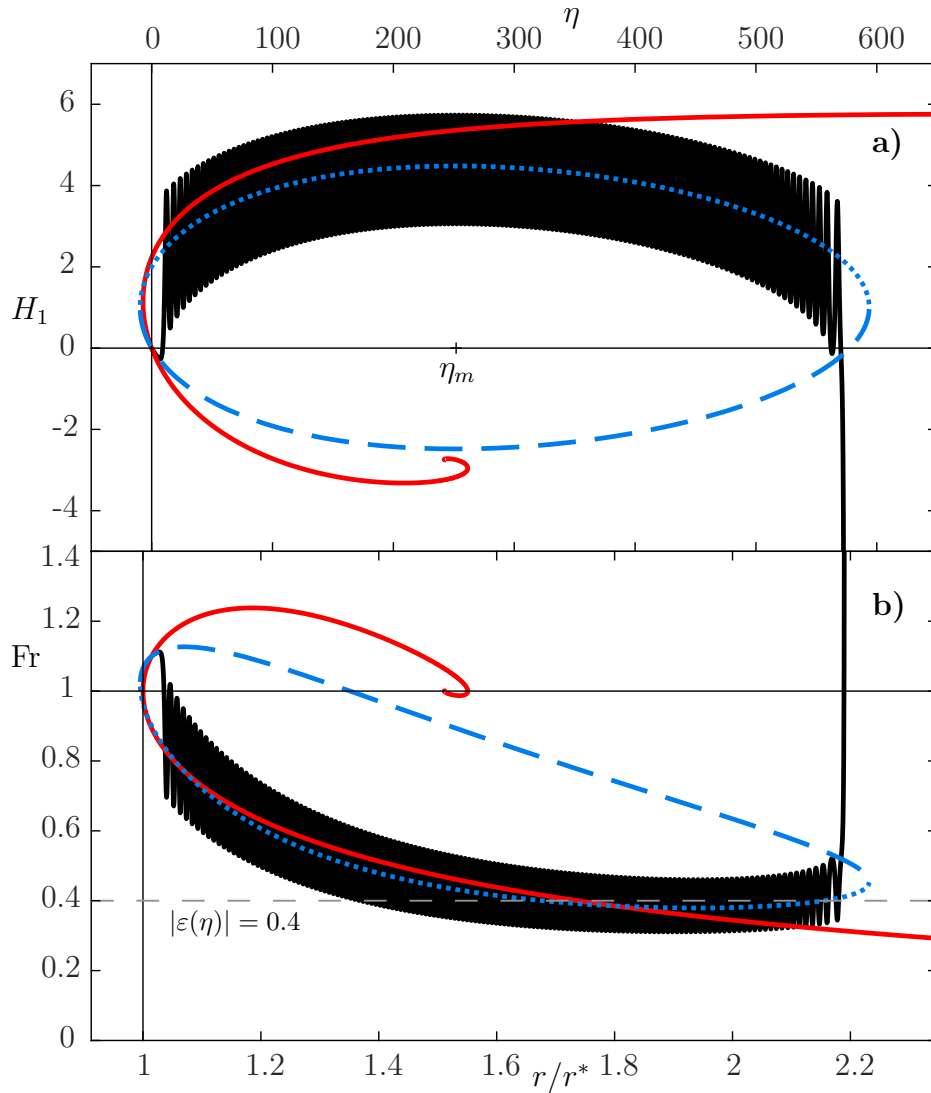


Figure 8.7: Behaviour of an undular hydraulic jump in turbulent axisymmetric flow with  $R_r = O(\varepsilon^{-2})$  at large radii;  $\varepsilon = 0.067$  ( $\text{Fr}_r = 1.1$ ),  $\tilde{R} = 2.2$ ,  $B = 3.5$ , i.e.  $C = -1.31$ ,  $\eta_m = 252$ . a) Non-dimensional surface elevation,  $H_1$ , b) Local Froude number,  $\text{Fr}$ . Black: Numerical solution of the extended KdV equation (8.10) for initial conditions according to (8.13) with  $n = 2$ , i.e.  $H_1(0) = 0$ ,  $H_{1,\eta}(0) = -5.11 \cdot 10^{-2}$ ,  $H_{1,\eta\eta}(0) = 2.61 \cdot 10^{-3}$ . Red: Full hydraulic approximation according to (6.9). Blue dashed and dotted: Super- and subcritical branch, respectively, of the hydraulic approximation of the extended KdV equation, (8.13a).

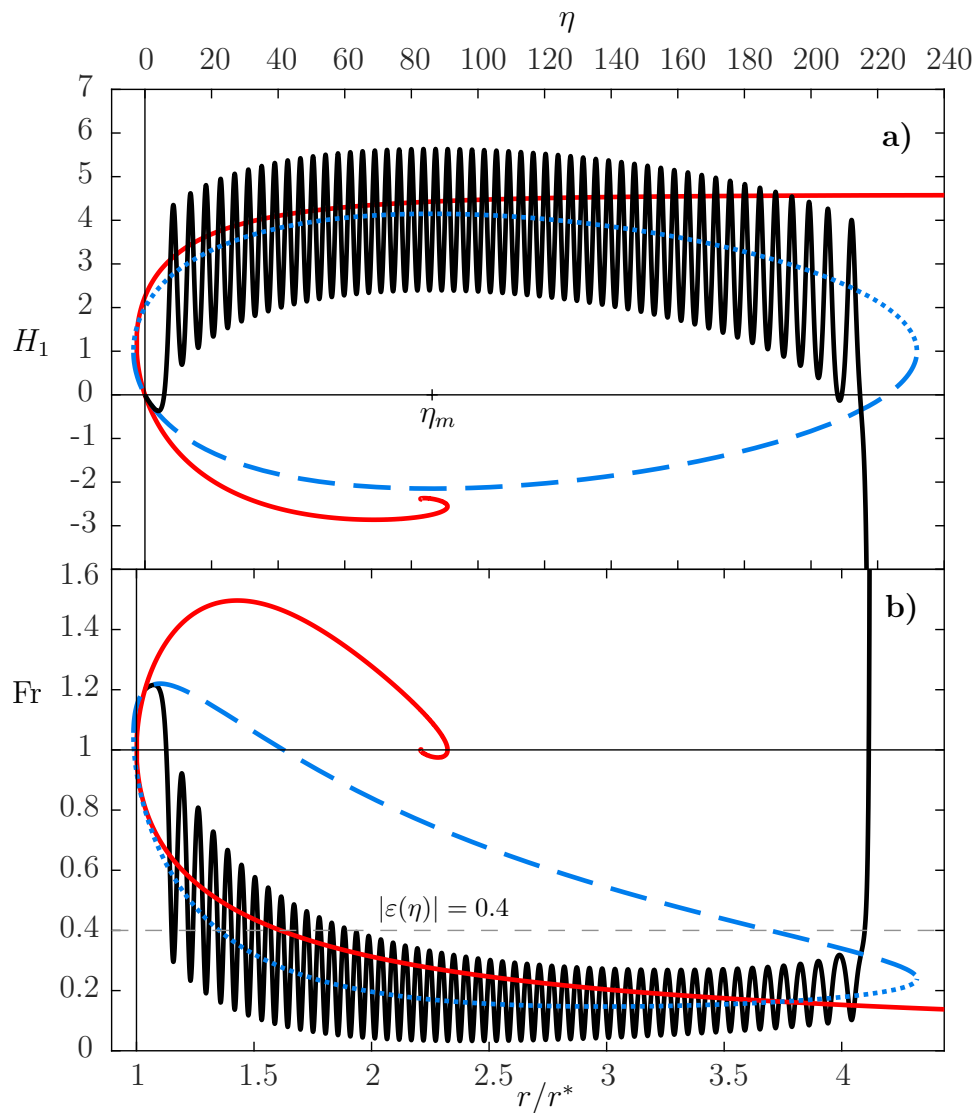


Figure 8.8: Behaviour of an undular hydraulic jump in turbulent axisymmetric flow with  $R_r = O(\varepsilon^{-2})$  at large radii;  $\varepsilon = 0.13$  ( $Fr_r = 1.2$ ),  $\tilde{R} = 1.3$ ,  $B = 2.9$ , i.e.  $C = -1.48$ ,  $\eta_m = 86$ . a) Non-dimensional surface elevation,  $H_1$ , b) Local Froude number,  $Fr$ . Black: Numerical solution of the extended KdV equation (8.10) for initial conditions according to (8.13) with  $n = 2$ , i.e.  $H_1(0) = 0$ ,  $H_{1,\eta}(0) = -0.14$ ,  $H_{1,\eta\eta}(0) = 1.93 \cdot 10^{-2}$ . Red: Full hydraulic approximation according to (6.9). Blue dashed and dotted: Super- and subcritical branch, respectively, of the hydraulic approximation of the extended KdV equation, (8.13a).

dominant, eventually leading to a breakdown.

The relatively small Froude number  $Fr_r = 1.1$  used in Fig. 8.7 requires a large discharge to obtain a large Reynolds number in the reference state. Therefore, the reference values in the third column of Table 8.1 are given for  $Q = 2.3 \text{ m}^3/\text{s}$ , but a reference radius of about 40 m appears unfeasible for practical applications. However, by increasing the reference Froude number to  $Fr_r = 1.2$ , a much smaller discharge  $Q = 0.13 \text{ m}^3/\text{s}$  is sufficient to maintain a large Reynolds number but  $r_r$  is significantly reduced to a realistic value of  $r_r = 3.24 \text{ m}$ , see the last column in Table 8.1. The corresponding solution of the extended KdV equation (8.10) is shown as black curve in Fig. 8.8.

In Fig. 8.8 the perturbation parameter in the reference state is doubled with respect to Fig. 8.7. As a consequence, already the first wave violates the previously introduced validity limit  $|\varepsilon(\eta)| = 0.4$ , see the horizontal dashed line in Fig. 8.8b). Nevertheless, this case shows that undular solutions are possible for parameters corresponding to reference values that are close to the estimated values ( $r_r \approx 2 \div 3 \text{ m}$ ) of the observation shown in Fig. 5.1. The large supercritical region upstream of the jump, visible in the photograph, seems to be caused by the slightly inclined street. Thus, it cannot be represented by the present version of the extended KdV equation, (8.10), derived for horizontal bottoms. The critical radius, below which no free-surface flow is possible, is  $r^* = 3.13 \text{ m}$  in Fig. 8.8 and  $r^* = 40.44 \text{ m}$  in Fig. 8.7. Thus, a vertically impinging jet, often considered as the source of the flow, seems unrealistic in the present case. However, a large circular slit nozzle may be an appropriate way to realise the flow, cf. [31].

### 8.3.3 Comparison between undular hydraulic jumps in turbulent and inviscid axisymmetric flow

In the present theory of undular jumps in turbulent axisymmetric flow over horizontal bottoms, the effect of friction is assumed to be small, i.e.  $Fr_{\tau,r}^2 = O(\varepsilon^3)$ , which stems from the analysis of plane turbulent flow over horizontal bottoms in Sec. 2.2. With increasing distance from the reference state, the effect of friction accumulates and gains dominance. In comparison to the theory for turbulent flow, the theory of undular jumps in inviscid axisymmetric flow in Ch. 7 corresponds to  $Fr_{\tau,r}^2 = O(\varepsilon^{7/2})$  or smaller. The

inspection of the equations then shows that friction effects are too small to appear in the analysis of terms up to order  $\varepsilon^2$ . The difference between the solutions of both theories shall be explored for  $R_r = O(\varepsilon^{-5/2})$  in the following. However, for  $R_r = O(\varepsilon^{-2})$  the results may be adopted qualitatively.

In Fig. 8.9 the black curve shows a solution of the extended KdV equation for turbulent flow, (8.10), with  $n = 5/2$ . The initial conditions are chosen to be in accord with the supercritical branch of the hydraulic approximation (8.13a). For comparison, the same initial conditions and identical parameter values of  $\varepsilon$  and  $\tilde{R}$  are used to solve the extended KdV equation of inviscid flow, (7.14), with  $n = 5/2$ , shown as orange curve. The orange curve in Fig. 8.9 develops into an undular jump almost one entire wavelength before the black curve. For the orange curve, the driving force for the

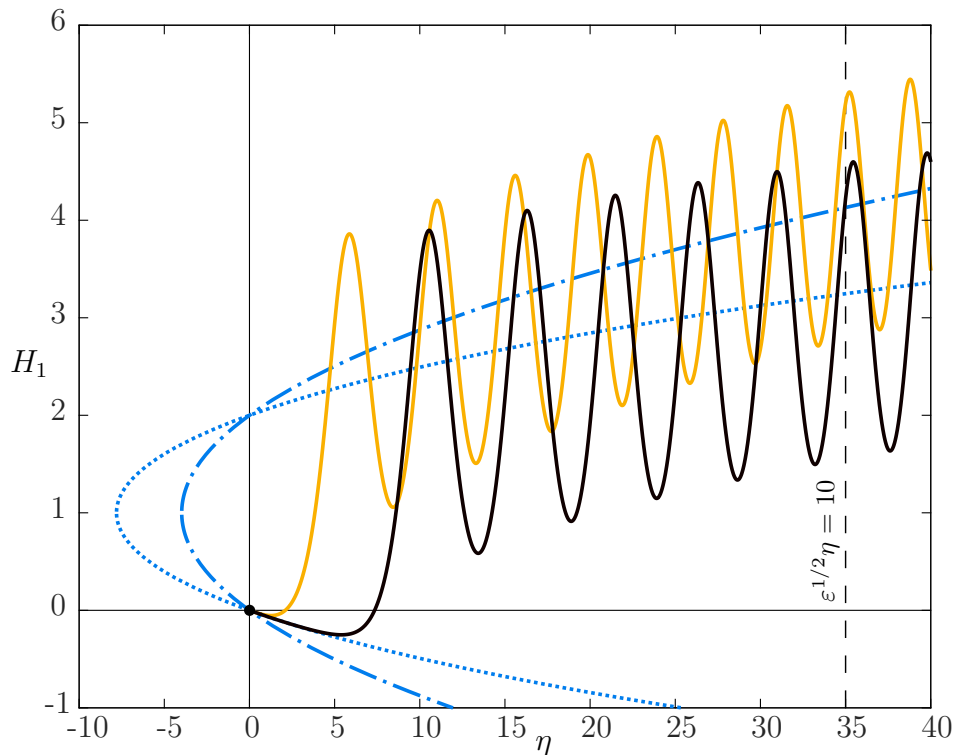


Figure 8.9: Comparison between undular jump solutions of the extended KdV equation of turbulent (black) and inviscid (orange) axisymmetric flow with  $n = 5/2$ , i.e. (8.10) and (7.14), respectively;  $\varepsilon = 0.08$  ( $Fr_r = 1.12$ ),  $\tilde{R} = 0.75$ ,  $B = 2$ . Initial conditions:  $H_1(0) = 0$ ,  $H_{1,\eta}(0) = -6.29 \cdot 10^{-2}$ ,  $H_{1,\eta\eta}(0) = 3.95 \cdot 10^{-3}$ . Blue dotted: Hydraulic approximation of the extended KdV equation (8.10), i.e. (8.13a). Blue dash-dotted: Near-critical hydraulic approximation (6.7).

development of an undular jump is the effect due to axisymmetric flow. The small effect of friction taken into account by the black solution seems to delay the transition from super- to subcritical flow. Moreover, the wavelength is slightly increased by the presence of friction, as can be observed by comparing the distance between successive wave crests of both curves. The orange and black curves both oscillate around the corresponding blue subcritical branch of the hydraulic approximation, (6.7) and (8.13a), respectively. Since these two subcritical branches are of different forms, the orange and black curves diverge as  $\eta$  increases. However, recalling the validity condition,  $\varepsilon^{1/2}\eta = O(1)$ , for the theory of inviscid axisymmetric flow with  $R_r = O(\varepsilon^{-5/2})$ , restricts the comparison to a

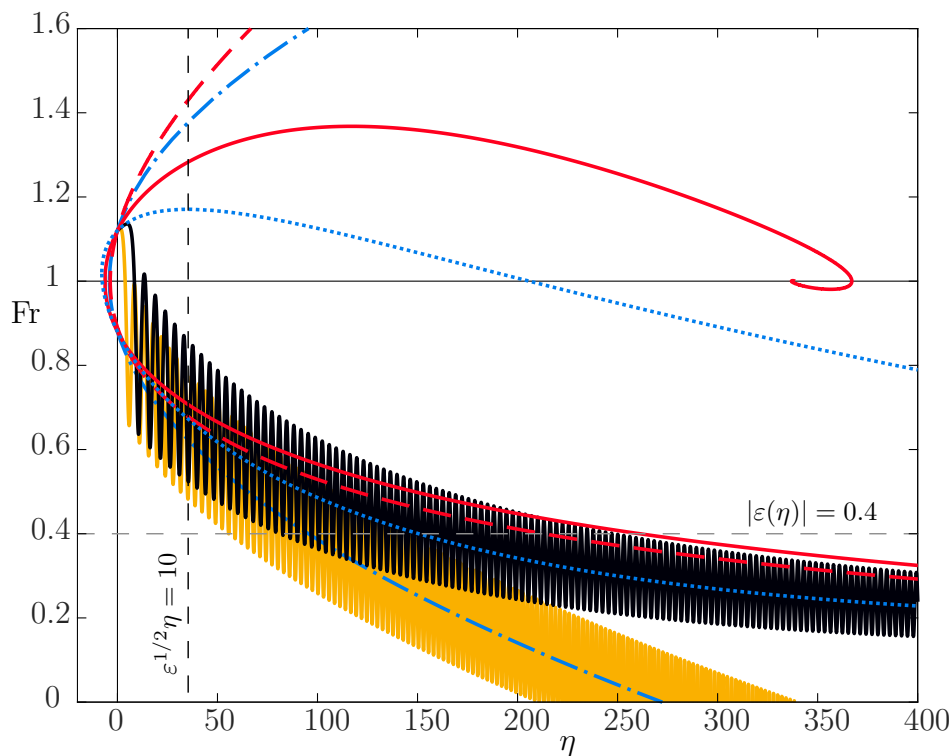


Figure 8.10: Behaviour of the flow at large radii in terms of  $Fr$ . Numerical solution of the extended KdV equation of turbulent (black) and inviscid (orange) axisymmetric flow with  $R_r = O(\varepsilon^{-5/2})$ , i.e. (8.10) and (7.14), respectively;  $\varepsilon = 0.08$  ( $Fr_r = 1.12$ ),  $\tilde{R} = 0.75$ ,  $B = 2$ . Initial conditions:  $H_1(0) = 0$ ,  $H_{1,\eta}(0) = -6.29 \cdot 10^{-2}$ ,  $H_{1,\eta\eta}(0) = 3.95 \cdot 10^{-3}$ . Red solid and dashed: Full hydraulic approximation according to (6.9) and (6.6), respectively. Blue dotted: Hydraulic approximation of the extended KdV equation (8.10), i.e. (8.13a). Blue dash-dotted: Near-critical hydraulic approximation (6.7).

region of moderate distance from the reference state. The validity limit is indicated by the black vertical dashed lines in Figs. 8.9 and 8.10.

In Fig. 8.10 the black and orange solutions of Fig. 8.9 are shown at large radii in terms of the local Froude number, referring to the mutual reference state at  $\eta = 0$ . Due to the skewed scales of the abscissa and the ordinate, individual oscillations are hardly distinguishable. The solutions of the extended KdV equations appear as thick black and orange bars. The red solid and dashed curve depicts the solution of the full hydraulic approximation according to (6.9) and (6.6), respectively. Even though the orange curve is not valid for large  $\eta$ , it is still interesting to compare it with the black solution of the extended KdV equation (8.10), which was derived as a uniformly valid differential equation. While minor deviations between the two curves are observed within the orange curve's validity region (vertical dashed line), a severe discrepancy occurs farther downstream. In particular, the substantial divergence between the orange curve and the red dashed full hydraulic approximation is striking, while the black curve follows the trend of the red full hydraulic approximation for turbulent flow even beyond the validity limit (horizontal dashed line). This comparison shows that in the vicinity of the reference state, friction is of minor relevance, whereas downstream of this region, the effect of friction slowly accumulates and has to be taken into account.

# Chapter 9

## Near-critical turbulent axisymmetric sink flow

### 9.1 Problem formulation and asymptotic analysis

The investigation of near-critical turbulent sink flow over a horizontal bottom is a coherent continuation of the analysis of source flow in the preceding chapter. In turbulent sink flow, the radial flow direction is towards the axis, see Fig. 9.1. As a consequence, the governing equations of turbulent source flow (8.2), (8.3) can be adopted by simply changing the signs of the velocity component in radial direction,  $\bar{U}$ , and the Reynolds shear stress,  $\overline{U'W'}$ . The same holds for the boundary conditions (8.4), (8.5) and the matching conditions subject to which the governing equations will be solved. Therefore, analogue to Ch. 8, the conditions (2.5–2.8) are prescribed by substituting  $X$  with  $R$ ,  $Y$  with  $Z$ ,  $V$  with  $W$ , and changing the signs of  $\bar{U}$  and the Reynolds shear stress.

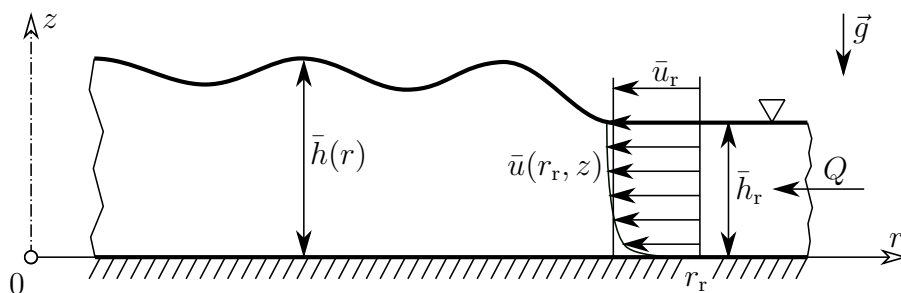


Figure 9.1: The stationary undular hydraulic jump in turbulent sink flow over a horizontal bottom. Flow from right to left.

The asymptotic analysis is performed analogue to Sec. 8.2 with only a few results affected by the changing signs. The leading order of the Reynolds shear stress becomes

$$(\overline{U'W'})_0 = -Z + 1 + \Delta \overline{U'W'}(Z), \quad (9.1)$$

and the first-order result of the vertical velocity component reads

$$W_1 = -H_{1,\eta} Z. \quad (9.2)$$

All other results throughout the analysis remain unchanged. The analysis of the second-order equations results in a solvability condition, obtained from the equation of motion in the radial direction and the kinematic boundary condition. In both these equations, the appearing vertical velocity component  $W_2$  has a different sign with respect to source flow. However, the effect cancels such that the solvability condition is unaffected. Thus, the extended KdV equation (8.10) of Sec. 8.2, which is valid for both  $R_r = O(\varepsilon^{-5/2})$  and  $R_r = O(\varepsilon^{-2})$ , is recovered as final result also for turbulent sink flow. Moreover, all other results, (8.10–8.16), of Sec. 8.2 can be applied.

## 9.2 Results and discussion

The extended KdV equation (8.10) may be solved numerically as an initial value problem with standard methods, using the commercial software Matlab R2018b. Solutions are obtained with the function `ode45`, a relative error tolerance of  $10^{-4}$ , an absolute error tolerance of  $10^{-8}$ , and a maximum step size of  $10^{-4}$ . In contrast to source flow, the computational domain  $[0, \eta_{\text{end}}]$  is to be defined with a negative end value  $\eta_{\text{end}} < 0$ .

In Fig. 9.2a) and b) a numerical solution of (8.10) for turbulent sink flow with  $R_r = O(\varepsilon^{-5/2})$  is shown as black line in terms of the free-surface elevation  $H_1$  and the local Froude number  $Fr$ , respectively. The flow direction is from right to left. The prescribed initial conditions are in accord with the blue dashed supercritical branch of the hydraulic approximation of the extended KdV equation, (8.13a). The parameters  $\varepsilon$ ,  $B$  and in particular the value of  $C$ , which was defined in (8.16), are chosen to be identical as in Fig. 8.6, where in the case of source flow,  $C > 0$  led to no undular solutions of the extended KdV equation. However, for the development of an undular hydraulic jump in sink flow, the opposite flow direction not only permits but requires  $C > 0$ , which in this case corresponds to a reference state upstream of  $\eta_m$ , see Fig. 9.3a). This means

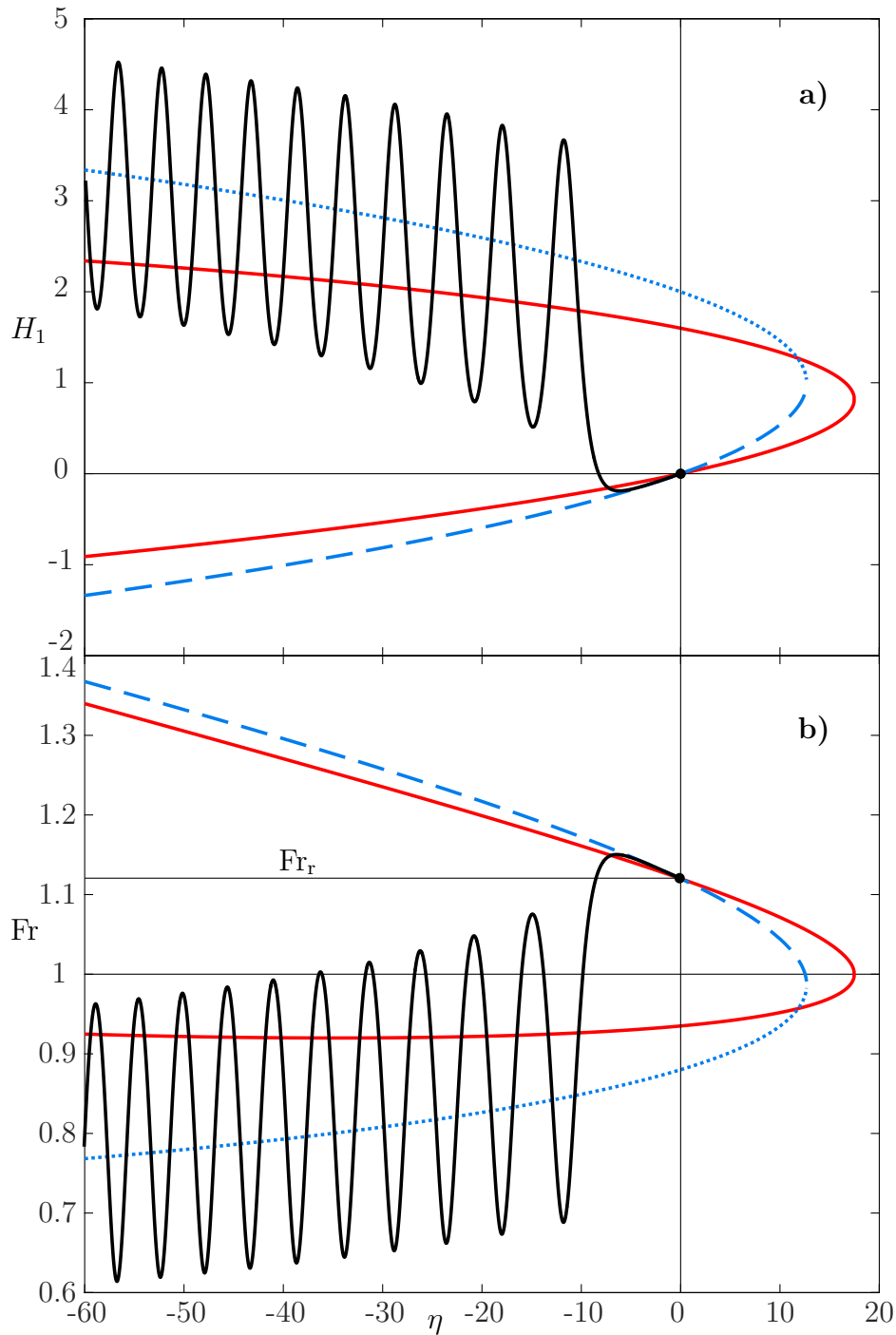


Figure 9.2: Initial behaviour of an undular jump in turbulent sink flow with  $R_r = O(\varepsilon^{-5/2})$ . Flow from right to left;  $\varepsilon = 0.08$  ( $Fr_r = 1.12$ ),  $\tilde{R} = 1.71$ ,  $B = 3$ , i.e.  $C = 2.5$ . a) Non-dimensional surface elevation,  $H_1$ , b) Local Froude number,  $Fr$ . Black: Numerical solution of the extended KdV equation (8.10) for initial conditions according to (8.13), i.e.  $H_1(0) = 0$ ,  $H_{1,\eta}(0) = 3.91 \cdot 10^{-2}$ ,  $H_{1,\eta\eta}(0) = 1.53 \cdot 10^{-3}$ . Red: Full hydraulic approximation according to (6.9). Blue dashed and dotted: Super- and subcritical branch, respectively, of the hydraulic approximation of the extended KdV equation, (8.13a).

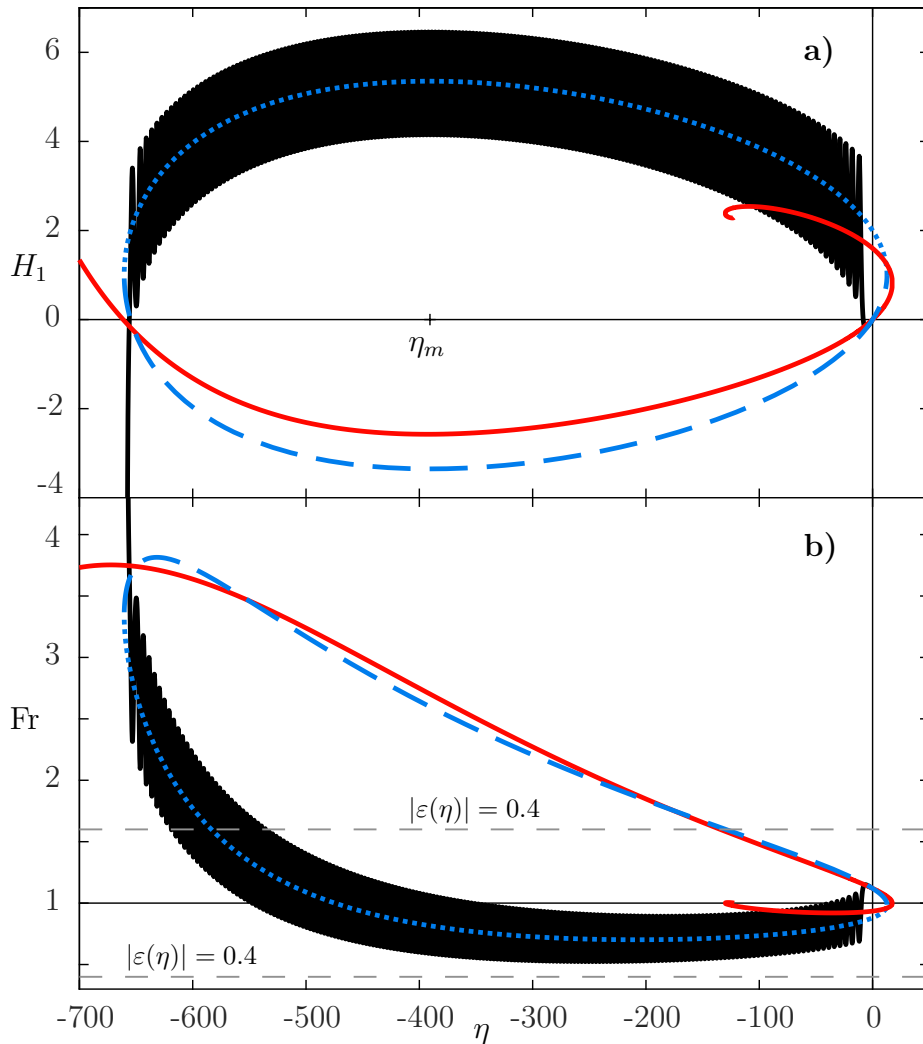


Figure 9.3: Behaviour of an undular jump in turbulent sink flow with  $R_r = O(\varepsilon^{-5/2})$  far downstream of the reference state. Flow from right to left;  $\varepsilon = 0.08$  ( $Fr_r = 1.12$ ),  $\tilde{R} = 1.71$ ,  $B = 3$ , i.e.  $C = 2.5$ . a) Non-dimensional surface elevation,  $H_1$ , b) Local Froude number,  $Fr$ . Black: Numerical solution of the extended KdV equation (8.10) for initial conditions according to (8.13), i.e.  $H_1(0) = 0$ ,  $H_{1,\eta}(0) = 3.91 \cdot 10^{-2}$ ,  $H_{1,\eta\eta}(0) = 1.53 \cdot 10^{-3}$ . Red: Full hydraulic approximation according to (6.9). Blue dashed and dotted: Super- and sub-critical branch, respectively, of the hydraulic approximation of the extended KdV equation, (8.13a).

that, for instance, the parameter configuration with  $C < 0$  for which undular source flow solutions of (8.10) are shown in Fig. 8.3 will lead to an immediate breakdown of the solution of (8.10) in the case of sink flow. In Fig. 9.2 the undular solution of the extended KdV equation reaches a fully subcritical state after about five undulations.

Figure 9.3 shows the solutions of Fig. 9.2 at large distances from the reference state. Due to the strongly skewed scales of the abscissa and the ordinate, the solution of (8.10) appears as a thick black bar rather than as multiple oscillations. Interestingly, the flow remains well within the limits of near-critical flow, indicated by the horizontal dashed lines, for a considerable distance from the reference state. At  $\eta \approx -354$ , the flow becomes again supercritical. While the free-surface elevation according to Fig. 9.3a) changes only slightly, the converging flow causes acceleration, and thus a rapidly rising local Froude number eventually violates the assumption of near-critical flow. The black curve oscillates around the blue dotted branch of the hydraulic approximation, (8.13a), until a breakdown at  $\eta \approx -660$  occurs, which may be interpreted as supercritical overflow into a plug hole, cf. [45]. Similar to turbulent source flow, the characteristic behaviour of a sink flow solution of the extended KdV equation (8.10) with  $R_r = O(\varepsilon^{-2})$  does not change with respect to the sink flow solution with  $R_r = O(\varepsilon^{-5/2})$  shown in Figs. 9.2 and 9.3. Results with  $R_r = O(\varepsilon^{-2})$  will thus not be discussed individually.

In Figs. 9.2 and 9.3 the parameters  $\text{Fr}_r = 1.12$ ,  $B = 3$ ,  $\tilde{R} = 1.71$  were used. These parameters together with a discharge  $Q = 3.5 \text{ m}^3/\text{s}$  yield the reference values  $\bar{h}_r = 6.04 \text{ cm}$ ,  $r_r = 67.2 \text{ m}$ ,  $\bar{u}_r = 0.86 \text{ m/s}$ , and  $\text{Re}_r = 5.2 \cdot 10^4$ ,  $\text{Re}_{\tau,r} = 1.8 \cdot 10^3$ . The breakdown occurs at a radius of  $r \approx 20.2 \text{ m}$  with  $\text{Re} = 1.7 \cdot 10^5$ . Like in turbulent source flow, the large radii are caused by the small reference Froude number, which requires a large discharge to obtain large values of  $\text{Re}_r$  and  $\text{Re}_{\tau,r}$ . For comparison, with the same values of  $B$  and  $\tilde{R}$ , but  $\text{Fr}_r = 1.2$ , a discharge of  $Q = 0.5 \text{ m}^3/\text{s}$  suffices to obtain  $\bar{h}_r = 4.98 \text{ cm}$ ,  $r_r = 12.0 \text{ m}$ ,  $\bar{u}_r = 0.84 \text{ m/s}$ ,  $\text{Re}_r = 4.2 \cdot 10^4$ ,  $\text{Re}_{\tau,r} = 2.9 \cdot 10^3$ . The breakdown occurs at a radius of  $r \approx 3.5 \text{ m}$  with  $\text{Re} = 1.4 \cdot 10^5$ .

It is interesting to note that whereas undular hydraulic jumps are possible in both turbulent and inviscid source flow, this is not true for sink flow. From the universal relation for the local Froude number, (6.6), shown as a dashed curve in Fig. 6.2, follows that in inviscid flow, a near-critical state exists only in the vicinity of the critical radius  $r^*$  below which no free-surface flow is possible. Thus, in the case of inviscid axisymmetric flow, undular hydraulic jumps can only originate from source flow.

# Chapter 10

## Conclusions of Part II

In this part of the thesis, undular hydraulic jumps in steady axisymmetric free-surface flow over a horizontal bottom were investigated. The jump was assumed to originate at a relatively large non-dimensional reference radius  $R_r$  from the centre of the cylindrical coordinate system. Particularly the two cases  $R_r = O(\varepsilon^{-5/2})$  and  $R_r = O(\varepsilon^{-2})$  with  $\varepsilon \ll 1$  were examined.

The asymptotic analysis of *turbulent* axisymmetric source flow in the limit of very large Reynolds numbers and Froude numbers close to the critical value 1 could be kept free of turbulence modelling due to a specific coupling of the two limiting processes. The analysis's main result is a new version of an extended KdV equation, that is, (8.10), describing the free-surface elevation. Remarkably, the homogeneous part of (8.10) is identical to the classical KdV equation for inviscid plane flow. The two extension terms, however, represent the effect of friction and the effect due to axisymmetric flow according to (2.36) and (8.11), respectively. By restricting the extension terms' parameters to a specific regime, (8.10) was derived as a uniformly valid differential equation describing the free surface over a wide reach from the reference state. However, the overflow at the plate's edge far downstream cannot be expected to be accurately represented by the breakdown of the extended KdV equation's solution.

Numerical solutions of the extended KdV equation (8.10) were analysed in terms of the free-surface elevation and in terms of the local Froude number. Undular jump solutions are obtained if the effect of axisymmetric flow dominates the effect of friction in the reference state. With increasing distance from the reference state, friction effects accumulate and eventually force the solution's breakdown. However, by choosing the

reference state in the region of dominant friction, the development of an undular jump is suppressed. The comparison of numerical solutions of (8.10) for both  $R_r = O(\varepsilon^{-5/2})$  and  $R_r = O(\varepsilon^{-2})$  revealed a sensitive dependence on the parameters describing the flow in the reference state, i.e. the Froude number  $Fr_r$ , the friction Froude number  $Fr_{\tau,r}$ , and  $R_r$ . On the one hand, maintaining near-critical flow from the reference state until the solution's breakdown is only possible if  $Fr_r$  is very close to 1. On the other hand, relatively large reference Froude numbers (e.g.  $Fr_r = 1.2$ ) are necessary to obtain undular solutions with parameters corresponding to reasonably small reference radii in the order of a few metres.

Furthermore, *inviscid* axisymmetric source flow was analysed in the limit of Froude numbers close to the critical value 1. It turned out that the velocity profile can be chosen freely via a function of integration  $c_1(Z)$ , provided  $c_1(Z) = O(1)$ . The velocity profile does not affect the final result for the surface elevation, i.e. an extended KdV equation, (7.14), with a constant extension representing the effect due to axisymmetric flow. The validity of the results is limited to non-dimensional distances from the reference radius up to  $\eta = O(\varepsilon^{-1/2})$  and  $\eta = O(1)$  for  $R_r = O(\varepsilon^{-5/2})$  and  $R_r = O(\varepsilon^{-2})$ , respectively.

Numerical solutions of (7.14) showed that – in contrast to inviscid plane flow – undular hydraulic jumps are possible in inviscid axisymmetric flow. Moreover, the supercritical branch of the hydraulic approximation is prone to develop into an undular jump. A comparison between solutions of the extended KdV equation for turbulent and inviscid flow showed that friction is indeed of minor relevance within the latter's validity region. However, to accurately describe the flow over a wide reach, friction must be taken into account. While for the analysis of turbulent flow  $Fr_{\tau,r}^2 = O(\varepsilon^3)$  was assumed, the consideration of inviscid flow corresponds to  $Fr_{\tau,r}^2 = O(\varepsilon^{7/2})$  or smaller, such that friction effects do not appear in the analysis.

An asymptotic analysis of near-critical turbulent *sink* flow was performed analogue to the analysis of turbulent source flow. Interestingly, the resulting extended KdV equation for the free-surface elevation is identical to the case of turbulent source flow, i.e. (8.10). However, the opposite flow direction has a significant impact as the undular jump solution of (8.10) inherently remains near-critical for a considerable distance from the reference state. The continuous acceleration of the flow towards the centre causes an undular transition from sub- to supercritical flow before the solution breaks down far downstream.

# Appendix A

## Algebraic properties of the polynomial $p(H_1; R, S)$

The following algebraic relations are adopted from [27], p. 24. The polynomial defined in (2.24), i.e.

$$p(H_1; R, S) := -H_1^3 + 3H_1^2 + 6RH_1 + S, \quad (\text{A.1})$$

may be written in terms of its ordered roots  $h_1(R, S) \leq h_2(R, S) \leq h_3(R, S)$  as

$$p(H_1; R, S) = (H_1 - h_1)(H_1 - h_2)(h_3 - H_1). \quad (\text{A.2})$$

Whether the roots are real and independent of each other is determined by the discriminant  $\bar{D}$ , cf. [1], p. 17,

$$\bar{D}(R, S) = (1 + 3R + 3S)^2 - (1 - 2R)^3, \quad (\text{A.3})$$

or

$$\bar{D}(h_1, h_2, h_3) = -[(h_1 - h_2)(h_1 - h_3)(h_2 - h_3)]^2/108. \quad (\text{A.4})$$

The three roots are real if  $\bar{D} \leq 0$  and independent of each other if  $\bar{D} < 0$ . In the case of real roots, the following relations hold:

$$h_1 + h_2 + h_3 = 3, \quad (\text{A.5})$$

$$1/h_1 + 1/h_2 + 1/h_3 = -R/S, \quad (\text{A.6})$$

$$h_1 h_2 h_3 = 6S, \quad (\text{A.7})$$

or alternatively

$$R = [h_2^2 + h_2h_3 + h_3^2 - 3(h_2 + h_3)]/6, \quad (\text{A.8})$$

$$S = (3 - h_2 - h_3)h_2h_3/6. \quad (\text{A.9})$$

The inverse of (A.8) and (A.9) read

$$h_1 = 1 - 2\sqrt{|1 + 2R|} \cos [(\varphi - (\text{sgn} + 1)\pi/2)/3], \quad (\text{A.10})$$

$$h_2 = 1 - 2\text{sgn}\sqrt{|1 + 2R|} \cos [(\varphi + \pi)/3], \quad (\text{A.11})$$

$$h_3 = 1 + 2\sqrt{|1 + 2R|} \cos [(\varphi + (\text{sgn} - 1)\pi/2)/3], \quad (\text{A.12})$$

with the definitions

$$\text{sgn} := \text{sign}(1 + 3R + 3S), \quad (\text{A.13})$$

$$\cos \varphi := |1 + 3R + 3S|/|1 + 2R|^{3/2} > 0. \quad (\text{A.14})$$

# Bibliography

- [1] Abramowitz, M. and Stegun, I. A. *Handbook of mathematical functions*. New York: Dover Publications, 1972.
- [2] Bohr, T., Dimon, P., and Putkaradze, V. “Shallow-water approach to the circular hydraulic jump”. *Journal of Fluid Mechanics* 254 (1993), 635–648.  
DOI: 10.1017/S0022112093002289.
- [3] Bohr, T., Ellegaard, C., Hansen, A. E., and Haaning, A. “Hydraulic jumps, flow separation and wave breaking: an experimental study”. *Physica B: Condensed Matter* 228 (1996), 1–10.  
DOI: 10.1016/s0921-4526(96)00373-0.
- [4] Bowles, R. I. and Smith, F. T. “The standing hydraulic jump: theory, computations and comparisons with experiments”. *Journal of Fluid Mechanics* 242 (1992), 145–168.  
DOI: 10.1017/s0022112092002313.
- [5] Brocchini, M. and Peregrine, D. “The dynamics of strong turbulence at free surfaces. Part 1. Description”. *Journal of Fluid Mechanics* 449 (2001), 225–254.  
DOI: 10.1017/s0022112001006012.
- [6] Brocchini, M. and Peregrine, D. “The dynamics of strong turbulence at free surfaces. Part 2. Free-surface boundary conditions”. *Journal of Fluid Mechanics* 449 (2001), 255–290.  
DOI: 10.1017/s0022112001006024.
- [7] Bush, J. W. M. and Aristoff, J. M. “The influence of surface tension on the circular hydraulic jump”. *Journal of Fluid Mechanics* 489 (2003), 229–238.  
DOI: 10.1017/s0022112003005159.

- [8] Bush, J. W. M., Aristoff, J. M., and Hosoi, A. E. “An experimental investigation of the stability of the circular hydraulic jump”. *Journal of Fluid Mechanics* 558 (2006), 33–52.  
DOI: 10.1017/s0022112006009839.
- [9] Castro-Orgaz, O. and Hager, W. H. *Non-Hydrostatic Free Surface Flows*. Springer, 2017.  
DOI: 10.1007/978-3-319-47971-2.
- [10] Chanson, H. “Current knowledge in hydraulic jumps and related phenomena. A survey of experimental results”. *European Journal of Mechanics B/Fluids* 28 (2009), 191–210.  
DOI: doi:10.1016/j.euromechflu.2008.06.004.
- [11] Chanson, H. *Hydraulics of Open Channel Flow: An Introduction*. 2nd ed. Oxford Burlington: Elsevier Butterworth-Heinemann, 2004.
- [12] Chanson, H. “Physical modelling of the flow field in an undular tidal bore”. *Journal of Hydraulic Research* 43 (2005), 234–244.  
DOI: <https://doi.org/10.1080/00221680509500118>.
- [13] Chanson, H. and Montes, J. S. “Characteristics of undular hydraulic jumps: Experimental apparatus and flow patterns”. *Journal of Hydraulic Engineering* 121 (1995), 129–144.  
DOI: 10.1061/(asce)0733-9429(1995)121:2(129).
- [14] Chow, V. T. *Open-Channel Hydraulics*. New York: McGraw-Hill, 1959.
- [15] Craik, A. D. D., Latham, R. C., Fawkes, M. J., and Gribbon, P. W. F. “The circular hydraulic jump”. *Journal of Fluid Mechanics* 112 (1981), 347–362.  
DOI: 10.1017/s002211208100044x.
- [16] Dasgupta, R. and Govindarajan, R. “Nonsimilar solutions of the viscous shallow water equations governing weak hydraulic jumps”. *Physics of Fluids* 22 (2010), 112108.  
DOI: 10.1063/1.3488009.
- [17] Drazin, P. G. and Johnson, R. S. *Solitons: An Introduction*. Cambridge: Cambridge University Press, 1989.  
DOI: 10.1017/cbo9781139172059.

- [18] Ellegaard, C., Hansen, A. E., Haaning, A., Hansen, K., Marcussen, A., Bohr, T., Hansen, J. L., and Watanabe, S. “Creating corners in kitchen sinks”. *Nature* 392 (1998), 767–768.  
DOI: 10.1038/33820.
- [19] Fernandez-Feria, R., Sanmiguel-Rojas, E., and Benilov, E. S. “On the origin and structure of a stationary circular hydraulic jump”. *Physics of Fluids* 31 (2019), 072104.  
DOI: 10.1063/1.5109247.
- [20] Gersten, K. and Herwig, H. *Strömungsmechanik. Grundlagen der Impuls-, Wärme- und Stoffübertragung aus asymptotischer Sicht*. Wiesbaden: Vieweg, 1992.  
DOI: 10.1007/978-3-322-93970-8.
- [21] Gotoh, H., Yasuda, Y., and Ohtsu, I. “Effect of channel slope on flow characteristics of undular hydraulic jumps”. *River Basin Management III*. Ed. by Brebbia, C. A. Vol. 83. WIT Transactions on Ecology and the Environment. Wessex: WIT Press, 2005, 33–43.  
DOI: 10.2208/journalam.7.953.
- [22] Grillhofer, W. and Schneider, W. “The undular hydraulic jump in turbulent open channel flow at large Reynolds numbers”. *Physics of Fluids* 15 (2003), 730–735.  
DOI: 10.1063/1.1538249.
- [23] Henderson, F. M. *Open Channel Flow*. New York: Macmillan Publishing, 1966.
- [24] Higuera, F. J. “The hydraulic jump in a viscous laminar flow”. *Journal of Fluid Mechanics* 274 (1994), 69–92.  
DOI: 10.1017/s0022112094002041.
- [25] Idelchik, I. E. *Handbook of Hydraulic Resistance*. 4th ed. Redding, CT: Begell House, 2008.
- [26] Ishigai, S., Nakanishi, S., Mizuno, M., and Imamura, T. “Heat transfer of the impinging round water jet in the interference zone of film flow along the wall”. *Bulletin of JSME* 20 (1977), 85–92.  
DOI: 10.1299/jsme1958.20.85.
- [27] Jurisits, R. “Wellige Wassersprünge bei nicht voll ausgebildeter turbulenter Zuströmung”. PhD thesis. Vienna, Austria: TU Wien, 2012.

- [28] Jurisits, R. and Schneider, W. “Undular hydraulic jumps arising in non-developed turbulent flows”. *Acta Mechanica* 223 (2012), 1723–1738.  
DOI: 10.1007/s00707-012-0666-4.
- [29] Jurisits, R., Schneider, W., and Bae, Y. S. “A multiple-scales solution of the undular hydraulic jump problem”. *Proceedings in Applied Mathematics and Mechanics* 7 (2007), 4120007–4120008.  
DOI: 10.1002/pamm.200700755.
- [30] Kasimov, A. R. “A stationary circular hydraulic jump, the limits of its existence and its gasdynamic analogue”. *Journal of Fluid Mechanics* 601 (2008), 189–198.  
DOI: 10.1017/s0022112008000773.
- [31] Lawson, J. D. and Phillips, B. C. “Circular hydraulic jump”. *Journal of hydraulic engineering* 109 (1983), 505–518.  
DOI: 10.1061/(asce)0733-9429(1983)109:4(505).
- [32] Liu, X. and Lienhard, J. H. “The hydraulic jump in circular jet impingement and in other thin liquid films”. *Experiments in Fluids* 15 (1993), 108–116.  
DOI: 10.1007/bf00190950.
- [33] Mathur, M., Dasgupta, R., Selvi, N. R., John, N. S., Kulkarni, G. U., and Govindarajan, R. “Gravity-free hydraulic jumps and metal femtoliter cups”. *Physical Review Letters* 98 (2007), 164502.  
DOI: 10.1103/physrevlett.98.164502.
- [34] Milne-Thomson, L. M. *Theoretical Hydrodynamics*. 5th ed. Hampshire London: Macmillan Education, 1986.
- [35] Montes, J. S. and Chanson, H. “Characteristics of undular hydraulic jumps: experiments and analysis”. *Journal of Hydraulic Engineering* 124 (1998), 192–205.  
DOI: 10.1061/(asce)0733-9429(1998)124:2(192).
- [36] Murschenhofer, D. and Schneider, W. “Asymptotic analysis of the undular hydraulic jump over vanishing bottom slope”. *Proceedings of the 14th International Conference on Heat Transfer, Fluid Mechanics and Thermodynamics (HEFAT2019)*. Ed. by Meyer, J. P. Wicklow, 2019, 217–222.

- [37] Murschenhofer, D. and Schneider, W. “Multiple scales analysis of the undular hydraulic jump over horizontal surfaces”. *Proceedings in Applied Mathematics and Mechanics* 19 (2019), e201900051.  
DOI: 10.1002/pamm.201900051.
- [38] Ohtsu, I., Yasuda, Y., and Gotoh, H. “Characteristics of undular jumps in rectangular channels”. *Proceedings of the 26th IAHR Congress (HYDRA 2000)*. Ed. by Telford, T. Vol. 1. 1C14. London, 1995, 450–455.
- [39] Ohtsu, I., Yasuda, Y., and Gotoh, H. “Flow conditions of undular hydraulic jumps in horizontal rectangular channels”. *Journal of Hydraulic Engineering* 129 (2003), 948–955.  
DOI: 10.1061/(ASCE)0733-9429(2003)129:12(948).
- [40] Ohtsu, I., Yasuda, Y., and Gotoh, H. “Hydraulic condition for undular-jump formations”. *Journal of Hydraulic Research* 39 (2001), 203–209.  
DOI: 10.1080/00221680109499821.
- [41] Pope, S. B. *Turbulent flows*. Cambridge: Cambridge University Press, 2000.  
DOI: 10.1017/cbo9780511840531.
- [42] Rayleigh, L. “On the theory of long waves and bores”. *Proceedings of the Royal Society of London. Series A, Containing Papers of a Mathematical and Physical Character* 90 (1914), 324–328.
- [43] Reinauer, R. and Hager, W. H. “Non-breaking undular hydraulic jump”. *Journal of Hydraulic Research* 33 (1995), 683–698.  
DOI: 10.1080/00221689509498564.
- [44] Rostami, F., Yazdi, S. R. S., Said, M. A. M., and Shahrokhi, M. “Numerical simulation of undular jumps on graveled bed using volume of fluid method”. *Water Science and Technology* 66 (2012), 909–917.  
DOI: 10.2166/wst.2012.213.
- [45] Scheichl, B., Bowles, R., and Pasiadis, G. “Developed liquid film passing a trailing edge under the action of gravity and capillarity”. *Journal of Fluid Mechanics* 850 (2018), 924–953.  
DOI: 10.1017/jfm.2018.464.

- [46] Scheichl, B. and Bowles, R. I. “On transcritical states in viscous flow passing the edge of a horizontal plate”. *Proceedings in Applied Mathematics and Mechanics* 17 (2017), 663–664.  
DOI: 10.1002/pamm.201710300.
- [47] Schlichting, H. and Gersten, K. *Boundary-Layer Theory*. 9th ed. Berlin Heidelberg: Springer, 2017.  
DOI: 10.1007/978-3-662-52919-5.
- [48] Schneider, W. *Mathematische Methoden der Strömungsmechanik*. Braunschweig: Vieweg, 1978.  
DOI: 10.1007/978-3-322-83943-5.
- [49] Schneider, W. “Oblique stationary solitary waves in turbulent free-surface flow”. submitted to *Physics of Fluids*. 2021.
- [50] Schneider, W., Jurisits, R., and Bae, Y. S. “An asymptotic iteration method for the numerical analysis of near-critical free-surface flows”. *International Journal of Heat and Fluid Flow* 31 (2010), 1119–1124.  
DOI: 10.1016/j.ijheatfluidflow.2010.07.004.
- [51] Steinrück, H. “Multiple scales analysis of the steady-state Korteweg-de Vries equation perturbed by a damping term”. *Zeitung für Angewandte Mathematik und Mechanik* 85 (2005), 114–121.  
DOI: 10.1002/zamm.200310162.
- [52] Steinrück, H. “Multiple Scales Analysis of the Turbulent Undular Hydraulic Jump”. *Asymptotic Methods in Fluid Mechanics: Survey and Recent Advances*. Ed. by Steinrück, H. Vol. 523. CISM Courses and Lectures. Wien New York: Springer, 2010, 197–219.  
DOI: 10.1007/978-3-7091-0408-8\_6.
- [53] Steinrück, H., Schneider, W., and Grillhofer, W. “A multiple scales analysis of the undular hydraulic jump in turbulent open channel flow”. *Fluid Dynamics Research* 33 (2003), 41–55.  
DOI: 10.1016/S0169-5983(03)00041-8.

- [54] Tani, I. “Water jump in the boundary layer”. *Journal of the Physical Society of Japan* 4 (1949), 212–215.  
DOI: 10.1143/jpsj.4.212.
- [55] Thorpe, S. A. and Kavcic, I. “The circular internal hydraulic jump”. *Journal of Fluid Mechanics* 610 (2008), 99–129.  
DOI: 10.1017/s0022112008002553.
- [56] Valiani, A. and Caleffi, V. “Free Surface Axially Symmetric Flows and Radial Hydraulic Jumps”. *Journal of Hydraulic Engineering* 142 (2016), 06015025.  
DOI: 10.1061/(ASCE)HY.1943-7900.00011104.
- [57] VDI-Gesellschaft Verfahrenstechnik und Chemieingenieurwesen, ed. *VDI Heat Atlas*. 2nd ed. Berlin Heidelberg: Springer, 2010.  
DOI: 10.1007/978-3-540-77877-6.
- [58] Watson, E. J. “The radial spread of a liquid jet over a horizontal plane”. *Journal of Fluid Mechanics* 20 (1964), 481–499.  
DOI: 10.1017/s0022112064001367.
- [59] Yokoi, K. and Xiao, F. “Relationships between a roller and a dynamic pressure distribution in circular hydraulic jumps”. *Physical Review E* 61 (2000), R1016.  
DOI: 10.1103/physreve.61.r1016.

# Curriculum vitae

29/08/1989	born in Vienna (Austria)
09/2004 – 06/2009	HTL Wiener Neustadt (Austria), Electrical Engineering/IT
22/06/2009	School leaving examination at HTL Wiener Neustadt, with distinction
10/2009 – 11/2013	TU Wien, Bachelor's programme, Mechanical Engineering
01/2010 – 09/2010	Community service, Red Cross Wiener Neustadt
02/2012 – 06/2013	Project assistant and design engineer at the Safety & Security Department, AIT Austrian Institute of Technology, Vienna
07/11/2013	Bachelor examination at TU Wien
12/2013 – 05/2014	Internship at the Institute of Space Propulsion, DLR German Aerospace Center, Lampoldshausen (Germany)
10/2014 – 07/2017	TU Wien, Master's programme, Mechanical Engineering
02/2015 – 07/2017	Project assistant at the Christian Doppler Laboratory for Model Based Calibration, Institute of Mechanics and Mechatronics, TU Wien
03/2016 – 07/2016	Politecnico di Milano (Italy), semester abroad, Aeronautical Engineering
12/07/2017	Diploma examination at TU Wien, with distinction Master's thesis: „A real-time capable quasi-2D PEM fuel cell model“, supervised by Ao.Prof. Dr. Stefan Braun and Prof. Dr. Stefan Jakubek
11/2017 –	Project assistant in the AIC research group, Institute of Fluid Mechanics and Heat Transfer, TU Wien



Die approbierte gedruckte Originalversion dieser Dissertation ist an der TU Wien Bibliothek verfügbar.  
The approved original version of this doctoral thesis is available in print at TU Wien Bibliothek.